Imaging, Mechanics, Construction, and Sonification of Three-Dimensional Spider Webs

by

Isabelle Su

Diplôme d'Ingenieur, Ecole Spéciale des Travaux Publics (2015)

M.Eng., Massachusetts Institute of Technology (2015)

Submitted to the Department of Civil and Environmental Engineering
in partial fulfillment of the requirements for the degree of

Doctor of Philosophy in the field of Structures and Materials

at the

Massachusetts Institute of Technology

June 2021

© Massachusetts Institute of Technology 2021. All rights reserved.

Author .....
Department of Civil and Environmental Engineering
February 25, 2021

Certified by .....
Markus J. Buehler
Professor of Civil and Environmental Engineering
Thesis Supervisor

Accepted by .....
Colette L. Heald
Professor of Civil and Environmental Engineering
Chair, Graduate Program Committee

Imaging, Mechanics, Construction, and Sonification of Three-Dimensional Spider Webs

by

Isabelle Su

Submitted to the Department of Civil and Environmental Engineering
on February 25, 2021, in partial fulfillment of the
requirements for the degree of
Doctor of Philosophy in the field of Structures and Materials

Abstract

Spiders, silks and webs have adapted, survived, and prospered in most ecosystems for millions of years, despite being subjected to environmental and human pressures. They are the proof of an evolutionary success, in part due to the exceptional mechanical and biological properties of their silks but also the various web geometries they can build, from simplistic T-webs, to typical 2D orb webs, to complex 3D webs. Silk's microscale thickness and the highly complex spatial network are significant challenges towards quantifying and visualizing the intricate architectures, mechanics, and construction of 3D webs. In this work, we aim to provide a consistent and automated non-destructive in-situ experimental and computational framework for quantifying and validating what has been observed in nature. A better understanding of the biological and mechanical performance of the 3D spider webs could inspire sustainable high-performance fiber networks and complex assembly strategies.

Our framework begins with the first automatic imaging method for quantifying 3D spider web geometries. We use image processing on high-resolution images of slices of the web illuminated by a sliding sheet laser to automatically quantify and model the web. Using the web model and coarse-grain bead-spring particle dynamic simulations, we investigate the important role of the interplay between nonlinear behavior of dragline silk and the complex and redundant structure of the web in the mechanical and functional performance of the web. We investigate and quantify the structure and mechanics of a 3D spider web at varying stages of construction. This is accomplished by imaging, modelling and simulations throughout the web-building process to capture changes in the natural web geometry and the mechanical properties. Finally, we introduce a novel method for visualizing complex 3D spider web using sonification, a visualization method through sound. We developed an intuitive, interactive, and immersive sonification platform that, by translating the complex 3D fiber network architecture into sound, can be used for 3D spider web data and creative exploration.

Thesis Supervisor: Markus J. Buehler
Title: Professor of Civil and Environmental Engineering

Acknowledgments

First and foremost, I would like to express my appreciation and gratitude to my advisor, Professor Markus J. Buehler, who supported, guided, and encouraged me during the past years. He is the reason I decided to pursue a PhD. I attended a talk on spiders and musical webs at the MIT Museum with artist Tomás Saraceno and Prof. Markus Buehler. I was inspired and became fascinated with spiders, silk, webs, and understanding how we can learn from complex natural architectures. I thank Markus for providing the many insightful advice about my research, ideas, presentation, and future career.

I would also like to thank the rest of my thesis committee: Professors Admir Masic, Benedetto Marelli, and Evan Ziporyn for their insightful comments, suggestions, and questions. I am very fortunate to have such a wonderful thesis committee.

I would like to thank my collaborators at MIT. This includes Zhao, for the guidance. I thank the Studio Tomás Saraceno team, which includes Tomás Saraceno, who inspired the spider web work, Ally and Roland for their recommendations. I want also want to thank the Spider's Canvas/Arachnodrone band: Evan Ziporyn, Christine Southworth, and Ian Hattwick. Working and rehearsing with them was not only fun but also a great learning experience. I would also like to thank my UROPs: Neosha, Marcos, Lucy, and Ian.

Thank you to my lab mates at the Laboratory for Atomistic and Molecular Mechanics: Anna, Chun Teh, Diego, Eesha Flavia, Fran, Gang Seob, Grace, Jonny, Kai G, Kai J, Mario, Sabrina, Shengfei, Yiwen, Zhao, Zhenze

I would like to thank the friends I met at MIT: Laélia, Martin, Elise, Anne, Rim, Sam T, Ben, Devony, Sam R, Justin M, Justin C, James, Murat, Affi...

I must also thank Steve, for his incredible patience. I am very lucky to have you in my life. A special thanks to our dog Ginger for the necessary emotional support.

Finally, I would like to express my greatest thanks and appreciation to my family for their support and the continuous encouragement all the way from France and China. This accomplishment would not have been possible without them.

Research funded by ONR (N00014-19-1-2375, N00014-16-1-2333), ARO (W911NF1920098),

AFOSR MURI (FA9550-15-1-0514), NIH (HH4977), NASA (PO# 7000000843Studio), Tomás Saraceno GmbH, MIT's Center for Art, Science and Technology (CAST), the Mellon Foundation, AY19-20 MathWorks Engineering Fellowship. Their support is greatly appreciated.

List of Publications

I am the author of all the work presented in this thesis. Research was conducted in the Department of Civil and Environmental Engineering at the Massachusetts Institute of Technology. Parts of the work presented here has been published or is in preparation for publication. The following publication are listed in chronological order

- Gu GX, **Su I**, Sharma S, Voros JL, Qin Z, Buehler MJ: "Three-dimensional-printing of bio-inspired composites." *J Biomech Eng* 2016, 138:21006.
- **Su I**, Buehler MJ: "Nanomechanics of silk: The fundamentals of a strong, tough and versatile material." *Nanotechnology* 2016, 27:302001.
- **Su I**, Buehler MJ: "Spider silk: Dynamic mechanics." *Nat Mater* 2016, 15:1054–1055.
- **Su I**, Qin Z, Saraceno T, Krell A, Mühlethaler R, Bisshop A, Buehler MJ: "Imaging and analysis of a three-dimensional spider web architecture." *J R Soc Interface* 2018, 15.
- **Su I**, Jung GS, Narayanan N, Buehler MJ: "Perspectives on 3D printing of self-assembling materials and structures." *Curr Opin Biomed Eng* 2020,
- **Su I**, Buehler MJ: "Mesomechanics of a Three-Dimensional Spider Web." *J Mech Phys Solids* 2020,
- **Su I**, Qin Z, Bisshop A, Mühlethaler R, Saraceno T, Ziporyn E, Buehler MJ: "Sonification of a 3D Spider Web and Reconstitution into Musical Composition using Granular Synthesis." *Comput Music J.* 2021 (accepted)
- **Su I**, Hattwick I, Southworth C, Ziporyn E, Bisshop A, Mühlethaler R, Saraceno T, Buehler MJ: "Interactive exploration of a hierarchical spider web structure with sound." *J Multimodal User Interfaces.* (revision)
- **Su I**, Narayanan N, Logrono MA, Bisshop A, Mühlethaler R, Saraceno T, Buehler MJ: "In-situ Three-Dimensional Spider Web Construction and Mechanics." Proc Natl Acad Sci (submitted)

Contents

List of Figures

List of Tables

List of Media

- V4-1 - Construction.mp4
- M5-1 - Dense web melody_x.wav
- M5-2 - Dense web melody_y.wav
- M5-3 - Dense web melody_z.wav
- M5-4 - Porous web melody_x.wav
- M5-5 - Porous web melody_y.wav
- M5-6 - Porous web melody_z.wav
- V5-1 - Dense web video_x.mp4
- V5-2 - Dense web video_y.mp4
- V5-3 - Dense web video_z.mp4
- V5-4 - Porous web video_x.mp4
- V5-5 - Porous web video_y.mp4
- V5-6 - Porous web video_z.mp4
- V6-1_SpidersCanvas_PalaisDeTokyo_Excerpt3.mp4
- V6-2_SpidersCanvas_MITtheatre.mp4
- V6-3_FieldofView.mp4
- V6-4_HearingDistance.mp4
- V6-5_VRdemo.mp4

Chapter 1

Introduction

Parts of the review presented in this chapter have been/will be published in:

- **Su I**, Buehler MJ: "Nanomechanics of silk: The fundamentals of a strong, tough and versatile material." *Nanotechnology* 2016, 27:302001.
- **Su I**, Qin Z, Saraceno T, Krell A, Mühlethaler R, Bisshop A, Buehler MJ: "Imaging and analysis of a three-dimensional spider web architecture." *J R Soc Interface* 2018, 15.
- **Su I**, Jung GS, Narayanan N, Buehler MJ: "Perspectives on 3D printing of self-assembling materials and structures." *Curr Opin Biomed Eng* 2020,
- **Su I**, Buehler MJ: "Mesomechanics of a Three-Dimensional Spider Web." *J Mech Phys Solids* 2020,
- **Su I**, Qin Z, Bisshop A, Mühlethaler R, Saraceno T, Ziporyn E, Buehler MJ: "Sonification of a 3D Spider Web and Reconstitution into Musical Composition using Granular Synthesis." *Comput Music J.* 2021 (accepted)
- **Su I**, Hattwick I, Southworth C, Ziporyn E, Bisshop A, Mühlethaler R, Saraceno T, Buehler MJ: "Interactive exploration of a hierarchical spider web structure with sound." *J Multimodal User Interfaces.* (revision)

- **Su I**, Narayanan N, Logrono MA, Bisshop A, Mühlethaler R, Saraceno T, Buehler MJ: "In-situ Three-Dimensional Spider Web Construction and Mechanics." Proc Natl Acad Sci (submitted)

1.1 Background

1.1.1 Spiders, Silks, and Webs

Spiders, silks, and webs are abundant in most ecosystems, showing that they are a dramatic evolutionary success. They have been prospering and surviving for millions of years, because they were able to adapt to their environment extremely well [12]. The superior mechanical and biological properties of silks and various silk-based webs have inspired many applications in biomedicine [13], art [14], structural engineering [15], electronics [16], and optics [17]. Spiders can spin up to seven different types of silks, each with a specific function. For example, stiff dragline silks are used for scaffolding, and extensible and sticky viscid silks are used to catch prey on an orb web. Spiders also construct a variety of webs spanning from simple T-webs, to typical two-dimensional (2D) vertical orb webs, to complex three-dimensional (3D) spider webs such as cobwebs, funnel, or sheet webs [5]. Silk is biodegradable and biocompatible, which make it excellent for biomedical applications such as tissue engineering and drug delivery [13]. Silk's and webs' superior strength, extensibility, and toughness originate from a hierarchical structure ranging from protein scale to fibers to macro-scale spider webs. Figure 1-1 describes the hierarchical organization of spider silk. At the molecular scale, silk is a sequence of amino acids that dictates the folding mechanism and the final molecular structure. Polyalanine-rich regions fold into β-strands bonded by hydrogen bonds which form β-sheets. They are stacked into stiff β-sheet nanocrystals which are embedded in a disordered semi-amorphous phase derived from the folding of glycine-rich protein [18, 1, 19, 20]. This semi-amorphous phase constitutes the majority of silk and consists of disordered secondary structures. Along the fiber axis, the distribution of crystalline regions is heterogeneous [21]. Up a level of scale, the silk nanocomposites form a network that is nanoconfined into fibrils. The fibrils are bundled together into a fiber of a few micrometers to finally form webs [18, 1, 19, 20]. Silk is strong because of the stiff β-sheet

nanocrystals resulting from protein folding, and extensible thanks to the hidden length of a disorganized amorphous phase, where the core molecular structure is controlled by weak hydrogen bonds [1, 19, 20]. Adopting a bottom-up approach, spider silk is a remarkable material that provides a template for upscaling nanoscale and molecular properties to the macro-scale.

The robustness of 2D vertical orb webs results from the nonlinear material behavior of the radial threads (dragline silk) which helps to localize the deformation and ruptures caused by a point load (prey or debris) [6], and from the distribution of thickness of the fibers that may allow sacrificial failure of thin spiral threads [22]. In addition to the effect of the nonlinear mechanics of silk, the geometry of the spider web, which defines how the individual silk fibers are connected and how they are anchored to substrates, plays an important role in carrying out its biological functions such as housing, protection and prey capture. Biologists suggest that spiders needed a 3D barrier to protect themselves from predators [23, 24, 25]. In the case of sheet webs and cobwebs, the geometric regularity and the use of capture silk are reduced, which lead them to capture prey differently compared to aerial orb webs [23, 26]. For example, it has been observed that cobwebs catch ambulatory prey by catapulting the prey inside the scaffolding of the web, in contrast to the orb webs that capture prey by dissipating the energy of the prey stuck to the web's spiral threads [23]. 3D webs are energetically costly [26, 27] and are often more permanent structures [23, 28], requiring silk fibers that can withstand prolonged and repetitive stresses [23, 29]. Therefore, no weak viscid silk can be included [23, 30]. These ecological observations of the differences between 2D and 3D webs highlight the importance of the interplay between the biological function and the structural features of 3D spider webs, a subject that has remained elusive. A better understanding of the biological and mechanical performance of the 3D spider webs could inspire sustainable high-performance fiber networks and complex assembly strategies.

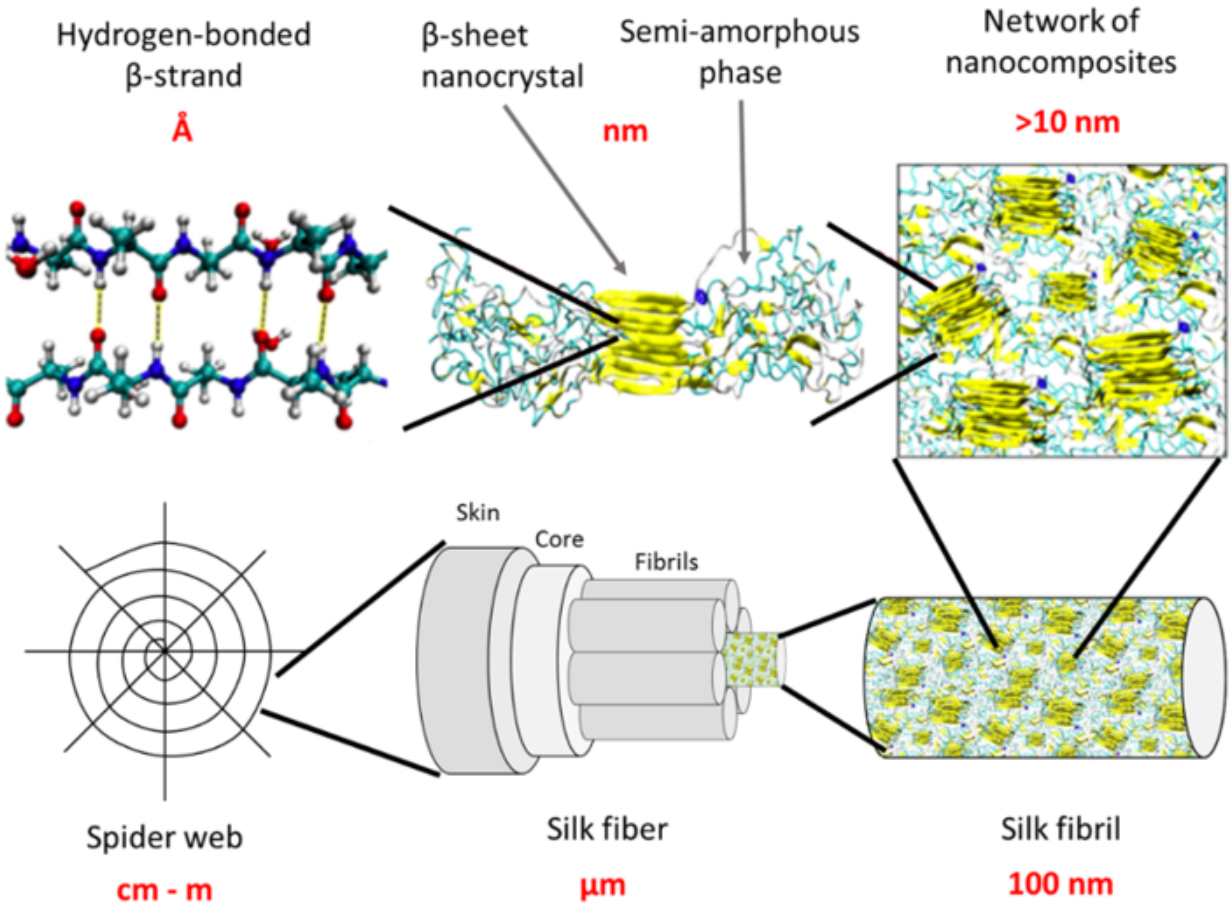

Figure 1-1: Schematic depiction of the hierarchical structure of spider silk, from hydrogen bonded chains to spider web structures, featuring multiple length-scales in which structural organization is found (from protein secondary structures to macroscopic geometries) [1, 2, 3]. The three images in the top panel were reprinted (adapted) from [1] with permission from Springer Nature.

1.1.2 Spider Webs Imaging

In order to fully understand the structure–function relationship of 3D webs, the intricate architecture of 3D webs needs to be precisely revealed. Because of the complex irregular 3D network and the micro-scale thickness of the silk fibers, there is no existing imaging toolkit that allows direct quantification of the topology of web structures. Indeed, the extremely thin silk fibers (approx. 1 μm [11]) are only visible to human eyes under appropriate lighting conditions and angles [27]. Although it is possible to distinguish the fibers and visualize the webs by spraying water [31] for example, this method is not suitable for precise imaging because it applies unknown loads that can generate deformation, such as contraction of up to 50% from water [11]. Non-invasive imaging techniques such as CT (computed tomogra-

phy) scans or ultrasound imaging do not work for webs because the fibers are too thin to be captured [14, 32]. A confocal microscope could describe the web's architecture, but only partially for a small size sample with very close observation for its 2D projection [32, 33]. Micro-CT machines have enough resolution and capability for 3D imaging, but their sizes are limited to small samples that are not suitable for capturing an entire spider web [34].

For a tens-of-centimeter-scale 3D spider web, the Spider Web Scan (SWS) laser-supported tomographic method was recently proposed, developed by Studio Tomás Saraceno (STS) with the collaboration of Peter Jäger (Senckenberg Institut) and the Photogrammetric Institute at the TU Darmstadt. The SWS approach consists of illuminating one plane of the spider web, housed in a clear Perspex box, using a red sheet laser to capture stereoscopic image pairs and then repeating this process along the length of the web. The use of stereo cameras allowed for sharper and more precise images of fibers. STS developed this method and used it to capture the architecture of a 3D spider web (*Latrodectus mactans*) in a non-automated way [14, 35, 36, 37, 38]. One of the shortcomings of this method is that it was tedious to move the laser and take an image for each imaging event in a step-wise fashion. Moreover, the web geometry that was derived lacked certain elements, as the gap size between each scan was too large (5 mm) [14, 39] and lacked an automated functionality that made image-processing labor intensive. These structures were not sufficient to be directly translated into a computer model of the web. Similarly, 3D webs had been scanned with infrared cameras that captured slices of the web illuminated by a sliding infrared sheet laser [40]. However, infrared cameras often have a lower resolution (640 $\times$ 480 pixels) than commercial visible light cameras (5184 $\times$ 3456 pixels). In a low-resolution image, regions of dense fibers could become indistinguishable. As a result, this method was used to approximate the topology of a 3D spider web structure with missing elements, but was capable of tracking spider movements during web construction [40]. We need more systematic methods to quantify the complex geometry of 3D spider webs in an automated way.

1.1.3 Spider Web Mechanics

Spiders and webs can be found almost everywhere: in urban environments, in the

corner of houses, between windows, behind doors, but also outside in nature on bushes, tree branches, across rivers, and others. Spider webs' scaffolding that are attached to moving foundations, such as tree branches moving with wind or sliding windows are constantly subject to stretching. However, even with those natural stretching conditions, spider webs are effective in retaining their functionality of catching prey and protecting spiders from predators while minimizing and repairing defects. Most research has been focused on 2D orb webs [5]. 2D orb webs are composed of stiff radial threads and extensible spiral threads, and they are quickly repairable [41] so they can withstand a few defects.

Spiders usually destroy and recycle their silk by consuming it and rebuild orb webs overnight, so if webs are stretched to complete destruction, spiders would just build a new one the next day and webs are still able to function [41]. On the other hand, 3D spider webs have a more complex architecture that is challenging to visualize because of the thin silk fibers. 3D webs are more permanent structures so they need to be robust to stay functional under defects [23]. Understanding the extreme behavior of 3D spider web under uniaxial stretching could lead to high-performance and resilient porous fiber network composites. Spider silk fiber stretching has been extensively studied, from stiff dragline silk, to extensible viscid silk [42], or natural-spun silk to forced-spun silk [43]. However, little is known about the stretching of macro-scale spider webs, and in particular 3D spider webs.

The web architecture dictates prey-catching mechanisms. For instance, 2D orb webs catch prey by dissipating the energy of impact with radial, spiral and aerodynamic drag [44], while 3D webs, such as cobwebs and sheet webs, rely on catapulting ambulatory prey that get stuck on a pretensioned sticky thread inside the web where the spider is located [23] or prey bouncing in the 3D barrier to reach the sheet where the spider waits [25], respectively. While social behavior is common in bees, ants, and termites, it is rare among spiders [45]. Social foraging spiders rely on colonial or cooperative foraging which allows them to successfully capture larger and more prey, as prey are caught after bouncing off several webs successively [46]. 2D webs are more efficient in catching and retaining prey than 3D webs; however they need more energy to maintain as spiders need to renew their webs every day [47, 48, 26]. The differences of web maintenance energy results in different web defense mechanisms. Indeed,

even though 2D webs are faster to build and more efficient, they do not protect the spiders from predators, as they are often positioned in the center of the web where they measure web vibrations [49]. Biologists have suggested the 3D barrier on webs evolved as a defense mechanism against wasp predators [24, 25]. Understanding the natural prey catching and predator defense mechanisms of spiders could inspire lightweight and efficient fiber network filters and safety nets, with customizable functions such as blocking, redirecting and/or penetrating of projectiles of different sizes and impact speeds.

1.1.4 Spider Web Construction

Spiders are among nature's engineers: they design, build, use, and maintain high-performance and lightweight silk webs. Not only do they produce, build, and tune highly functional silks and large-scale web structures, they also monitor, repair, and recycle webs. Spiders use vibrational information to locate and identify potential mates, prey, predators, and defects on their webs [49, 50, 51, 52]. Webs avoid catastrophic failure because the interplay, between the nonlinear behavior of dragline silk and complex spider web architecture, localizes defects, making quick repairs possible [6]. This makes the complex of spider, silk, and web a self-sufficient, self-monitored, and self-repairable system. This system can inspire sustainable and high-performance complex new materials, structural designs, and construction procedures [53]. Spiders build web structures several times their size with very few external supports, using only silk fibers. Comparing them to traditional construction at the human scale, such a large structure would require bulky scaffolding, large construction equipment, and many workers. Understanding the construction stages of a spider web could lead to more efficient and sustainable construction.

Gaining such understanding can begin by analyzing the 2D orb web geometry and construction process by facing a camera to the plane of the web. Orb webs are composed of stiff dragline silk radial threads and extensible and sticky viscid silk spiral threads. Orb web construction starts with the spider building the frame of the web after exploring the site. Orb-weaver spiders build the hub with radial threads and then place the spiral threads using spiral scaffolding as a guide. Compared to 2D orb webs, 3D spider webs are more com-

plicated to describe because of their complex fiber architecture and their nanoscale fibers. Yablonina [40] approximated a 3D spider web architecture using infrared cameras and a sliding laser and investigated the importance of supporting threads, reinforcing threads, and joints between threads by recording spider movement during web construction. Arachnologists have studied 3D spider web construction through meticulous behavioral observations and video recordings. Jörger and Eberhard [54] characterized three stages of the construction of *Achaearanea tesselata* spider webs: exploration, construction of anchor lines and tangle web, and alternating construction of sheet and tangle webs. Other species follow a similar web construction process. For example *Tidarren sisyphoides* spiders explore the surroundings, anchor the retreat, build the web scaffolding, and then construct the dome-shaped sheet, horizontal sheet, and upper tangle web [31]. *Steatoda triangulosa* comb-footed spiders explore, and then build a 3D supporting structure and gumfooted lines that connect the 3D structure and the substrate [55]. Web construction observations have already inspired new automation methods [40] and algorithms [56] for fiber network construction.

1.1.5 Spider Web sonification for visualization

Sonification, a subset of the field of auditory display research, is a technique for representing data through sound [57, 58], which can be applied in numerous domains such as seismology, interfaces for visually impaired people or biomedical applications [58]. Sonification facilitates the interpretation of data, especially in large and complex datasets and where conventional visualization methods are unable to comprehend certain features of the data [59]. Sonifying data is very useful for interpreting complex temporal data, as human auditory perception is more sensitive to temporal characteristics, and sonification can be combined with visualization to enhance data representation [59]. It can be difficult to comprehend 3D structures from only one perspective; for instance, we tend to use both eyes to visualize perspective, and to rotate or zoom a 3D physical model to extract all of the 3D information [58]. Similar to visual perception, auditory perception can grasp a more comprehensive "picture" of complex data via several sonic perspectives, which translates to several sonification mappings [58]. Spider web sonification is the transformation of spatial spider web topology

data into an audio signal: changing the parameters or the rules of the sonification provides different sonic views [58]. For our study, we couple visual and auditory views to deepen our perception and understanding of 3D spider web architectures. With sonification, we aim to visualize through sound the complex structure of the web.

Giesa et al. [60] and Cranford and Buehler [2] introduced the concept that spider silks and webs have a hierarchical organization and functions analogous to those operative in Western classical music of the 18th and 19th century [61]. They have demonstrated how silk and other biological materials are analogous to music using hierarchical ontology logs (ologs), based on the mathematical concept of category theory and abstraction. For instance, the polypeptides born from the bonding amino acids can be seen as equivalent to the stacking and interference of sound waves. The protein secondary structure and strengthening mechanism of silk proteins, such as β-sheet nanocrystals, are comparable to musical notes and chords, respectively. The robustness and damage localization of spider webs by failure of sacrificial fibers [6] is analogous to the harmonic function which remains unaffected by the removal of a single musical chord [60]. The tonal coherence and functionality are unaffected by the removal of certain chords from a sequence [60, 62]. Wong et al. [61] have applied these analogies by composing melodies that reflect how protein sequence affects the formation of synthetic, engineered protein silk fibers that consist of *de novo* proteins. For their specific set of rules, they have shown that more lyrical (more conjunct, shapelier, and gentler) melodies led to a successful formation of fibers [61]. Spider webs are also connected to musicality through biotremology, the field of research exploring vibrational communication across substrates such as silk and spider webs [63, 64]. Spiders are extremely sensitive to vibrations and use the sonic properties of their webs to communicate, locate prey and predators, gather information on their environment and sense mates [49, 65]. Similar to a player and a musical instrument, spiders can tune and play with their webs to communicate, forage and provide protection. This relationship between spider webs, silk and music has been artistically explored by Saraceno, using biotremological insights to create material spider web-based instruments [66]. Sonification of 3D spider webs can be used for intuitive and holistic data and creative exploration.

1.2 Thesis Overview

1.2.1 Research Objective

Spiders have survived and prospered for millions of years. Spiders' evolutionary success is in part due to the superior mechanical and biological properties of their silks and high-performance webs. While silks and 2D orb webs have been extensively studied, little is known on the structure and mechanics of 3D spider webs. The micro-scale size of the silk fibers and the complex 3D fiber structure makes them difficult to visualize and comprehend. There is a need to quantify and understand what arachnologists have observed in order to derive important applicable insights.

The objective of this research is to use experimental and computational methods to quantify and validate what has been observed in nature. These methods will provide a basis for understanding 3D spider web architectures, mechanics, construction, and visualizations. Understanding the role of the interplay between silk mechanics and 3D web structure in spiders, silks and webs' evolutionary fitness could lead to high-performance and lightweight fiber network composites for structural, material, biomedical, and sustainable construction engineering.

This research will provide an important tool for learning insights not only on the spider web architecture, mechanics and construction, but also the spider web life cycle that can be improved and adapted for human applications. Indeed, spiders, silks and webs make a system that is a self-sufficient, self-monitored, and self-reparable that could inspire more sustainable and high-performance complex structures.

1.2.2 Research Approach

While 2D spider webs and silk fibers have been extensively studied, little is known about the structure, mechanics, construction, and visualization of 3D spider web, even though they are commonly found in nature. Most research on 3D spider webs has been carried through meticulous observations by arachnologists. In this work, we focus on quantifying 3D spider web structures and mechanics and designing innovative and intuitive ways

to visualize complex spider web data through sight and sound. This is a pioneering effort as no existing 3D spider web in-situ imaging, mechanical simulations, or sonification exist.

Our framework begins with the first automatic imaging method for quantifying 3D spider web geometries (Chapter 2). Due to these existing 3D spider web imaging limitations, we have developed a new systematic and rigorous toolkit, inspired by the SWS approach [39], to directly capture the geometry of the 3D architecture of the spider web and generate a computer model automatically, in a fast, convenient, and more precise way. We will use this method to reveal the structure of 3D spider webs and investigate the relation between architecture, material, and performance of numerous 3D spider webs, and the role of this interplay in completing the functions of the web. Understanding 3D spider webs could contribute to structural and material optimization for bioinspired composite material design.

Based on the 3D spider web geometry traced in Chapter 2, we report a combination of experimental data with computational methods, especially focused on meso–scale bead-spring particle dynamics simulations, to investigate key mechanical features of spider web structure-property relationships of webs at different scales, providing a systematic exploration of what is observed in nature. We specifically study the stretching and projectile impact behavior of a *Cyrtophora citricola* spider web, composed of a high fiber density tent region confined between porous tangle web regions (Chapter 3).

We use and upgrade our experimental imaging method for capturing 3D spider webs at different stage of construction. We investigate the mechanical behavior of the different construction stages of a *Tidarren sisyphoides* spider web and determine whether the web can carry out its biological functions during construction (Chapter 4).

Using our 3D spider web model, it is possible to visualize the structure; however, adding sonification would bring another perspective for comprehending the model and natural spider webs, and identifying key web features. We use parameter-mapping combined with animations to sonify a 3D spider web. The listener can determine the fiber lengths, connectivity and web porosity, depending on the virtual location of the listener in the spider web (Chapter 5).

Finally, we use model-based sonification and the analogy between spider webs and

music. We introduce a novel interactive tool for exploring complex fiber networks that can also be used as a virtual musical instrument for live performances and creative art installations. The user is immersed in a virtual 3D spider web environment, travels through the web, and hears the fibers that are in their field of view. This data exploration and manipulation tool can be used for numerous and versatile 3D network applications beyond spider web topologies, such as social, transportation, or neural networks [67], just to mention a few. It is also a creative platform with built-in parametrizing freedom for artists to create, tune, and perform unique musical pieces from spider web data (Chapter 6).

1.2.3 Thesis Organization

This thesis is organized as follows:

Chapter 1: General background, motivation, research objectives and approach.

Chapter 2: An automatic method for imaging and quantifying a 3D spider web.

Chapter 3: An investigation of the mechanics and functions of a 3D spider web.

Chapter 4: Application of our imaging methods and mechanical simulations to investigate a 3D spider web geometry and mechanics under different stages of construction

Chapter 5: Using parameter mapping sonification for visualizing a 3D spider web through sound

Chapter 6: Interactive model-based sonification for exploring a 3D spider web architecture

Chapter 7: Summary of the findings, contributions, and impact of this thesis. Future research directions are presented.

Chapter 2

Imaging and Analysis of a Three-Dimensional Spider Web Architecture

This research and review presented in this chapter have been published in:

- **Su I**, Qin Z, Saraceno T, Krell A, Mühlethaler R, Bisshop A, Buehler MJ: "Imaging and analysis of a three-dimensional spider web architecture." *J R Soc Interface* 2018, 15.

2.1 Introduction

Spiders (order Araneae) are extremely abundant in most ecosystems on the planet as a result of their evolutionary success, making up more than 49,000 different species [68] that have existed for over 380 million years [69, 12, 70]. Indeed, spiders have survived and proliferated in diverse environments due to the adaptive skills made possible because of their silk [69]. Spiders can spin up to eight different types of silk that have different properties and functions, such as flexibility and stickiness of viscid silk to catch prey, or strength and stiffness of dragline silk for making the frame of the web or as a safety line [11, 6, 69, 23]. Silk structures spun by spiders play a significant role in their survival. The web architectures are

abundant and varied: from primal trapdoor subterranean burrows [12], minimalist silken T webs, triangular webs or vertical geometrical orb webs, and more complex 3D webs such as tangle, funnel, cobweb, and complex orb webs [69, 23]. Although orb weaver spiders account for only 10% of spider species [23], vertical orb webs have received disproportionate attention. Extensive research has been done on the mechanics of silk and of the vertical orb web, the typically 2D web built from stiff radial silk and from extensible and sticky spiral threads to catch aerial prey [6]. Biologists have suggested that 3D silk barriers on webs evolved to protect spiders from predators, such as mud-dauber wasps. 3D webs have a more complex geometry and different foraging and defensive mechanisms. Understanding the mechanics of 3D webs could lead to web-inspired high-performance, long-span, and lightweight fiber network applications.

We aim to provide the first framework to investigate quantitatively the geometry, mechanisms, construction, and sonification of 3D spider web that can be used consistently and systematically to understand and validate what has been observed in nature. To investigate the role of the interplay between silk fibers and complex 3D web architecture, in the mechanical and biological functions of the 3D web, we first need to quantify such geometry. The topology of a 3D spider web is difficult to trace because of the micro-scale thickness of spider silk and the large and complex structure of the 3D network. Indeed, the fibers are so thin, the web structure can only be seen with the naked eye under certain lighting and angles of view. For a tens-of-centimeter-scale 3D spider web with microsize fibers, the most recent attempt to capture 3D spider web geometry was led by Studio Tomás Saraceno (STS) with the collaboration of Peter Jäger (Senckenberg Institut) and the Photogrammetric Institute at the TU Darmstadt. They developed the Spider Web Scan (SWS) a laser-supported tomographic method that consists of illuminating slices of a 3D web (built inside a Perspex box) with a red sheet laser, taking stereoscopic images, and manually linking the fiber network together to obtain the web topology. While this method works, it is time-consuming, labor-intensive, and subject to more human error.

These existing limitations led us to develop a new systematic experimental and computational method, inspired by the SWS approach, to quantify and model 3D spider web

geometries directly from a natural web. We designed the experimental set-up of a spider web laser scanning machine that capture high-resolution images of slices of the web illuminated by a sliding sheet laser. We use image processing methods to study the scanned fibers and analyze the intricate architecture of spider webs through a 3D model derived from the processed scans. Our results provide a template for automatic, fast, convenient tracing and analysis of natural 3D webs. Incorporating silk mechanics into the complex web architecture, we can deepen our understanding of spider web ecological and evolutionary fitness. This future effort could lead to 3D spider web-inspired structures such as high-performance lightweight long-span structures, safety nets, or the designs of fiber-reinforced composite materials.

2.2 Materials and Methods

2.2.1 Spider Web Construction

The spider built its web in a rectangular frame over a few days (Figure 2-1A). Spiders build webs in low lit environments, often using branches, rocks, and corners as support [69]. To build intact spider webs in controlled conditions, we built a rectangular 35.6 $\times$ 35.6 $\times$ 24.4 cm frame (Figure 2-1A), adapted from the Spider Web Frame (SWF) method developed by STS [71]. We constructed the frame using carbon fiber tubes of 3.175 mm diameter. To connect the tubes, we built a tripod made of 0.889 mm diameter spring-back stainless steel wire. For each connection: we bent three wires to 90° to connect the perpendicular tubes. We added glue at the corners to strengthen connections. The frame is reusable, dismountable, and was assembled from readily available components. The materials used for the frame were purchased from McMaster-Carr [72]. To prevent the spiders from escaping, we purchased large storage containers and filled them with water to surround the frame (Figure 2-1A). Depending on the size of the spider, we needed to increase the ratio of the size of the container to the size of the frame because some spiders could still escape by jumping out of the container. We purchased spiders via Bugs In Cyberspace [73]. The spiders built their initial web structures over a few days but kept modifying them over time, waiting to catch prey in their webs. Spiders can survive without eating for weeks but need water which occurs

naturally on the web as dew [74]. We fed the spiders, moths, flies and other insects. The spider web used for scanning was a tent-web built by the *Cyrtophora citricola* spider.

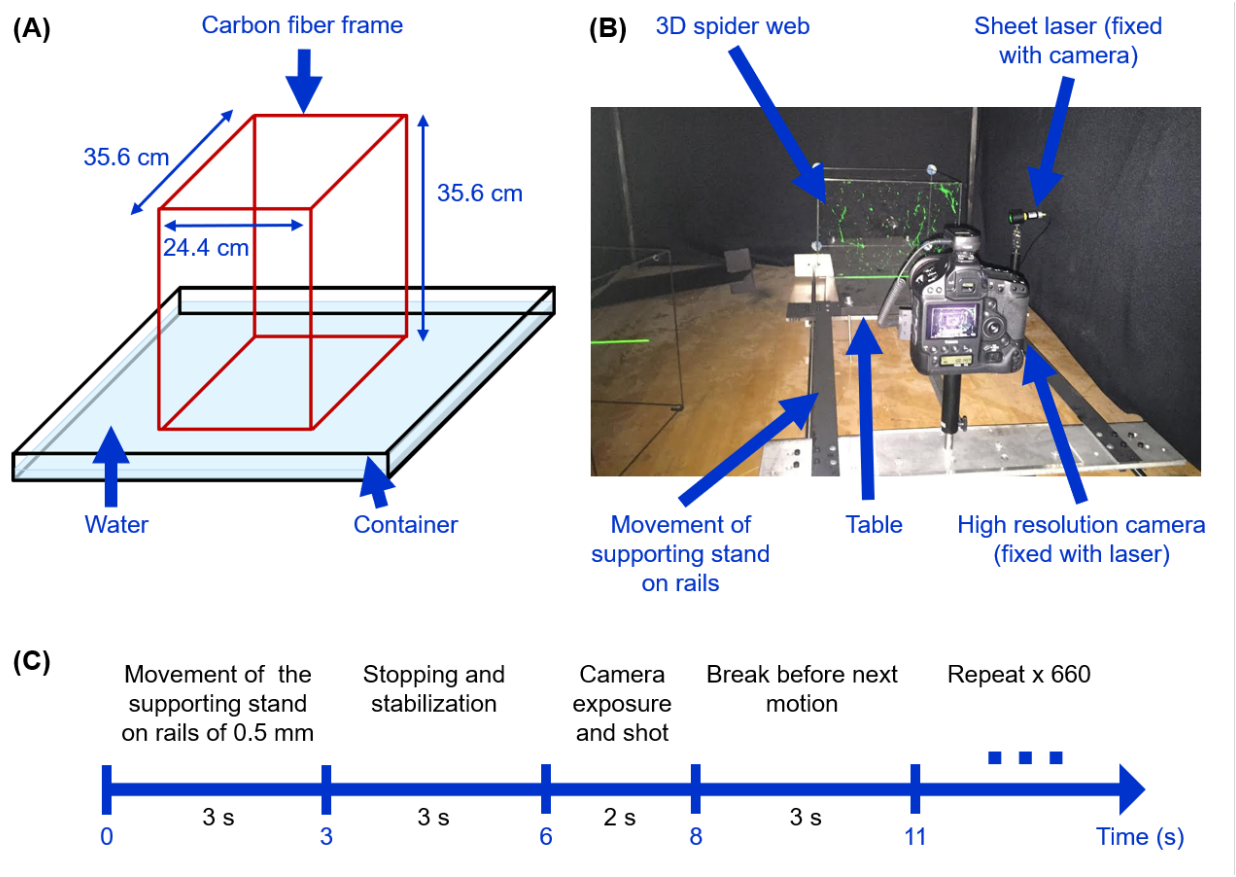

Figure 2-1: Experimental set-up. **(A)** Schematic of the rectangular 35.6 × 35.6 × 24.4 cm frame where the spider spun its web. The frame was placed in a container filled with water so that the spider did not escape. **(B)** Laser scanner set-up. The frame with the spider web was placed on the supporting stand which moved on rails along the depth (z) direction of the spider web. On the moving supporting stand, a sheet laser that lit up slices of the web and a high-resolution camera were fixed. The camera was always focused on the laser plane. **(C)** Scanning steps. The supporting stand moved 0.5 mm every 11 s for 3 s. It stopped to allow equilibration of the laser and camera for 3 s. The camera took a scan of a slice of the web after a 2 s exposure. The next motion started 3 s after the scan. This process was repeated 660 times to scan the full web.

2.2.2 Set-up of the Moving Rail and the Supporting Stand

The camera and sheet laser moved along a moving rail (Figure 2-1B). The moving rail consists of supporting stand that moves linearly along the depth of the spider web. The camera and the sheet laser are permanently fixed on the supporting stand. Moving together during scanning, the camera was always in focus to the plane of the sheet laser, which led

to clear images of the slices of the web. We chose to fix the spider web and slide the camera and sheet laser to avoid vibrations of the frame and its web. The movement and speed of the moving rail were controlled using Mach3 [75] software. Details of the construction of the moving rail is described in [5].

2.2.3 Laser Scanning Process

The camera captured images of 2D slices of the web illuminated by the green sheet laser when the supporting stand is stationary (Figure 2-1B,C). Once the spider had finished its web in the carbon frame, we placed the frame containing the web on a raised table in the middle of the supporting stand of the moving rail machine. We used a green (532 nm) sheet laser with a width of 1 mm to illuminate each 2D plane of the 3D web. We selected this specific wavelength because the charge-coupled device (CCD) in commercial cameras are typically two times more sensitive to green than red or blue. We fixed a single high-resolution EOS-1D X Canon camera to the supporting stand so that the plane lit up by the laser was perpendicular to the axis of the camera. This set-up was simpler and cheaper for gathering and processing scans than the manual SWS set-up that required two cameras [39]. The camera was equipped with a Canon 24-70 mm f/4 L EF IS USM lens with an aperture of f/22, that was positioned 61 cm away from the sheet laser. Each scanning step was composed of four stages: (i) the movement of the moving rail (together with the camera and the sheet laser) of 0.5 mm for 3 s; (ii) the stopping and stabilization of the moving rail for 3 s; (iii) the shutter action and exposure time of the camera for 2 s; (iv) a break before the next motion for 3 s. The camera shots were timed with a Vello Wireless Shutterboss timer remote, which differed from the timer of the system used for the moving rail (Mach3 [75]). As a result, we used a 3 s pause between snapshots to ensure that the shutter action and exposure time were synchronized and did not occur during the movement of the rail between images. By repeating this scanning step, we managed to obtain a series of snapshots that each included a slice of the web structure. Here, we considered only one direction of displacement and speed. We chose to slide the frame every 11 s, to allow time for camera exposure, image capture, sliding of the frame and stabilization, which was equal to the time-lapse period of

the camera. Figure 2-1B shows the laser scanning set-up and figure 2-1C the timeline of the workflow. The scans were shot in a dark room to obtain clear images of the fibers. The web was scanned using 660 images every 0.5 mm, which was sufficient to visualize the fiber architecture. The resolution was 5184 pixels $\times$ 3456 pixels $\times$ 24 BPP (bits per pixel). After scanning, we observed that the web exhibited a very dense region ("tent" web) and porous regions with distinguishable fibers.

2.2.4 Image Processing

We used image processing to transform 2D color images into a 3D skeletonized binary image (Figure 2-3). As the fibers were very thin, the laser light was scattered, which made the fibers look thicker and increased the noise of the image. This scattering also induced the fibers that were close to the laser plane to be illuminated and captured by the camera. The images required processing to decrease the noise and determine the coordinates of the fibers in the laser plane. The image processing aims to transform a color picture into a simpler binary image without losing any spatial information. This is equivalent to transforming a 3D matrix (color) into a simplified 2D matrix of 0 and 1 (black and white). To reduce computational time, we divided the entire spider web structure into 100 samples that were analyzed independently and subsequently assembled to make the full web. For describing our approach, we considered a representative 76.2 mm cubic volume obtained from the porous region that was composed of 160 images each containing 1001 $\times$ 1001 pixels, such that each pixel corresponds to 76 μm. First, the color channels of the images were split into three greyscale images: red, blue, and green. In every image, the fibers that were cut directly by the laser plane appeared white, while the fibers that were close to the laser plane appeared green. To reduce the noise of the green color and keep only the white colored fibers, the minimum values of the greyscale images of the blue and red color channels were merged, as white is composed of all three colors (Figure 2-2). Each red-blue greyscale image was filtered with a Gaussian blur with a standard deviation of 1.

The intensity values of the images were adjusted to increase contrast. Finally, the greyscale images were transformed into binary images by applying a normalized threshold of

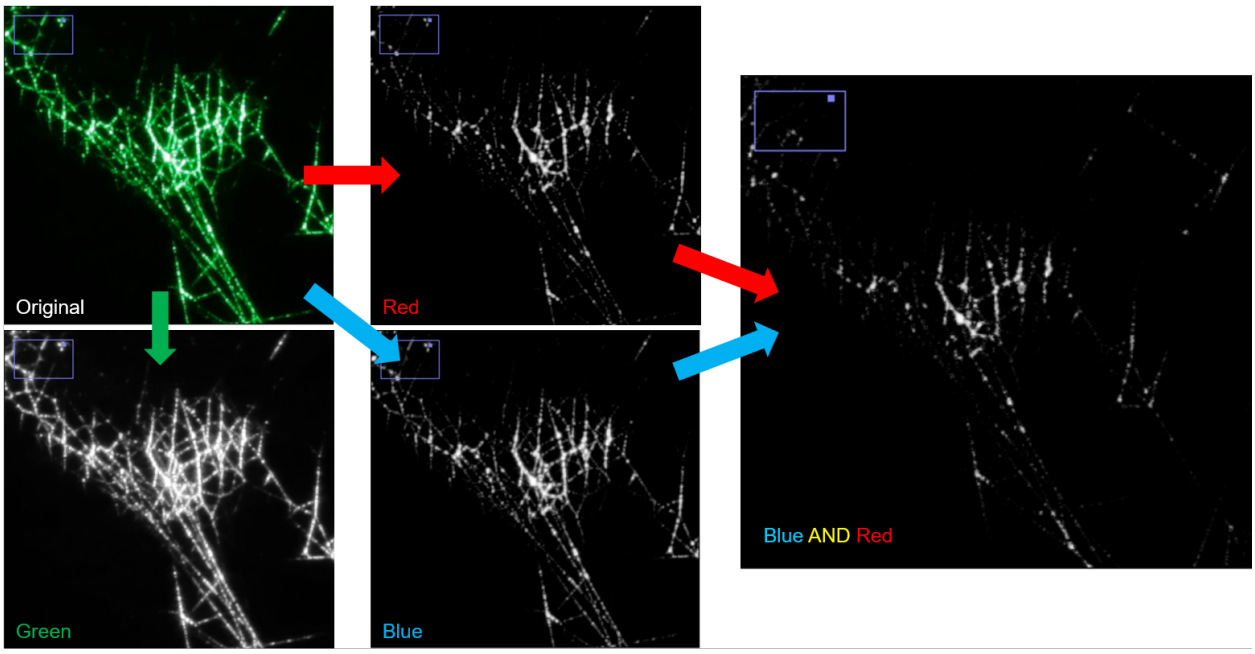

Figure 2-2: Color channel split image processing. Three greyscale images (red, green, blue) were split from the original color picture. The blue and red images were combined by taking the lowest value of each

0.75 which we had chosen after testing on numerous images. The binary images were stacked together into a 3D matrix of 1 and 0, with 1 a white pixel and 0 a black pixel. The fibers were represented by white pixels and the background in black. For this small sample of the web, the resulting 3D image was composed of 643 374 white voxels. Voxels are the 3D equivalent of 2D pixels which represent cubic elements in 3D space. We dilated the 3D image to create a new image of 1,873,187 white voxels. Dilation is an image processing operation that enlarges objects in a 3D image by adding voxels to their boundaries, which allowed us to increase the continuity of the images in the depth (z) direction as images were stacked. The dilated image (Figure 2-4A(i)) had been skeletonized (Figure 2-4A(ii)) using an algorithm adapted from [76] so that the thickness of fibers became 1 voxel (Figure 2-3), reducing the total number of white voxels to 40,775. The skeletonized process sometimes created additional branches due to noise during scanning and the non-uniformity of the thickness of the fibers that were removed in a later step. This image processing, summarized in Figure 2-3, was able to transform 160 color 2D images into a set of points of about 40,000 points. The image processing was performed with MATLAB and its image processing toolbox [77].

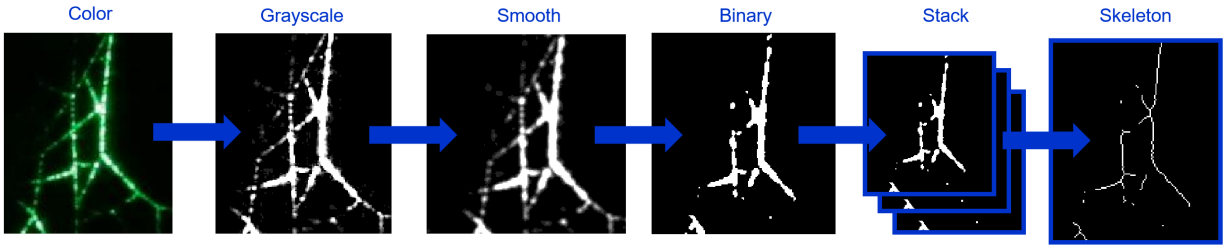

Figure 2-3: Image processing steps from the original color image to the 3D image skeleton. The original color image was transformed into a greyscale image using the minimum values of the red and blue color channels. This greyscale image was smoothed to erase the sharp edges using Gaussian blur with a standard deviation of 1, which was binarized with a threshold of 0.75. All the binary images were stacked together to make a 3D image which was skeletonized. The thickness of the fibers was one voxel.

2.2.5 Image-to-line Algorithm

We derived a straight-line fiber network from the processed 3D image (Figure 2-4A). Web fibers were in tension due to supercontraction that had occurred after construction, meaning that the fibers were not sagging and we could consider them as straight lines. The line-finding algorithm aims to transform a skeletonized image (Figure 2-4A(ii)) into a list of nodes, which are the extremity points of lines, and a list of pairs of indices. Each pair gives the node indices of the first and last points of the line. For this part of the analysis, we measured distances in "units", with one unit in the xy plane equivalent to 76 μm (pixel size), and one unit in the depth (z) direction equivalent to 0.5 mm (gap size between slices). First, we looked for the connection and free-end voxels of the skeleton using an algorithm adapted from [76]. The connection voxels were those that linked at least three skeleton branches while the free-end voxels were part of branches that were linked to only one other voxel (Figure 2-4A(iii)). These extremity points were used to identify a network of straight-line segments (Figure 2-4A(iv)). To delete the noise of this network that remained after the image had been skeletonized, short lines that had one free-end extremity and a length shorter than 20 units were deleted (Figure 2-4A(v)). We categorized the remaining segments into two types: (1) segment in which at least one extremity was connected to only one other segment, (2) all other segments in which extremities were either connected to two or more other segments or no segment. The category (1) segments were linked together to make a polyline composed of smaller segments, and these polylines were transformed into straight lines by linking their

extremities (Figure 2-4A(vi)). At the end of this step, all segments were category (2) and represented one complete fiber. Figure 2-4A illustrates these steps.

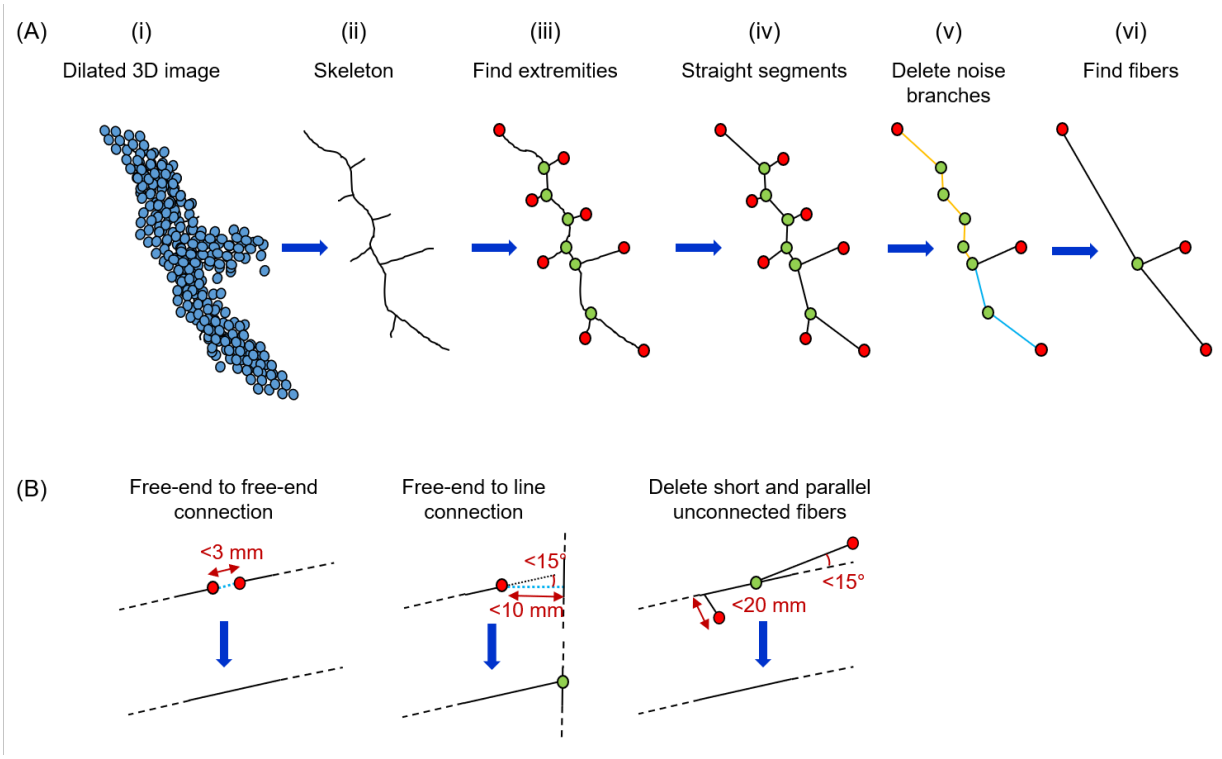

Figure 2-4: Schematic of the image-to-fiber network process. **(A)** From the image processed dilated 3D image to a straight line fiber network. (i) The dilated 3D image was (ii) skeletonized, making the fibers 1 voxel thick. (iii) The segments of the skeleton were defined by their extremities and (iv) transformed into straight line segments. (v) The noise line segments generated by the non-uniformity of fiber thickness were deleted. Finally, (vi) the adjacent line segments, making a polyline, were regrouped into one line segment describing one fiber. **(B)** Verification and cleaning process. Fibers whose free-end extremities were closer than 3 mm were combined into one fiber. If a fiber's free-end extremity was closer than 10 mm to another fiber and if the extension segment that linked the free end to the line was almost parallel (angle smaller than 15°), then the free-end fibers was extended and connected. The free-end fibers were shorter than 20 mm or almost parallel to other fibers were deleted.

2.2.6 Verification and Cleaning of the Network

We obtained a 3D fiber network model (Figures 2-5 and 2-6) after linking the fibers, fixing them to the frame or deleting them (Figure 2-4B). After obtaining a preliminary fiber network, we verified its consistency by checking that all the fibers were connected to at least two other fibers or attached to the boundary of the sample. We also identified the fibers that had at least one free-end extremity and were closer than 20 units from the boundary

of the sample, and considered them as unconnected lines which belonged to fibers in an adjacent section of the web or as fibers fixed to the frame. We also identified the anchor threads (fibers fixed to the frame), which were the fibers that had one extremity end close (less than 20 units) to the frame position. The fiber network model was scaled to its original dimensions, by multiplying the xy coordinates with the pixel size, and the z coordinates with the scanning gap size. We connected the remaining free-end lines if the distance between the free ends was within 3 mm, or if a segment extending between their free ends was shorter than 10 mm and almost parallel (angle smaller than 15°). The last step of the process was to clean the web from any remaining unconnected fibers that were artifacts from image processing by deleting unconnected fibers that were parallel to other fibers or shorter than 20 mm in length. These conditions for cleaning up the fiber network were found iteratively through the analysis of many samples within the overall web structure, and may need to be adjusted if scanning and imaging conditions were changed. Following this methodology, we obtained a fiber network that was described by a list of nodes (endpoint of the fibers) and a list of pairs of nodes that represented the endpoints of the fiber. Figure 2-4B illustrates these steps. Figure 2-5 shows the result of the 3D spider web model. By repeating this process on all the samples composing the entire web, we automatically generated, for the first time, the architecture of the spider web for porous regions or tangle webs (Figure 2-6). This network forms the basis for meso-scale bead-spring models, which we can use to study the response of a realistic web structure to mechanical loads.

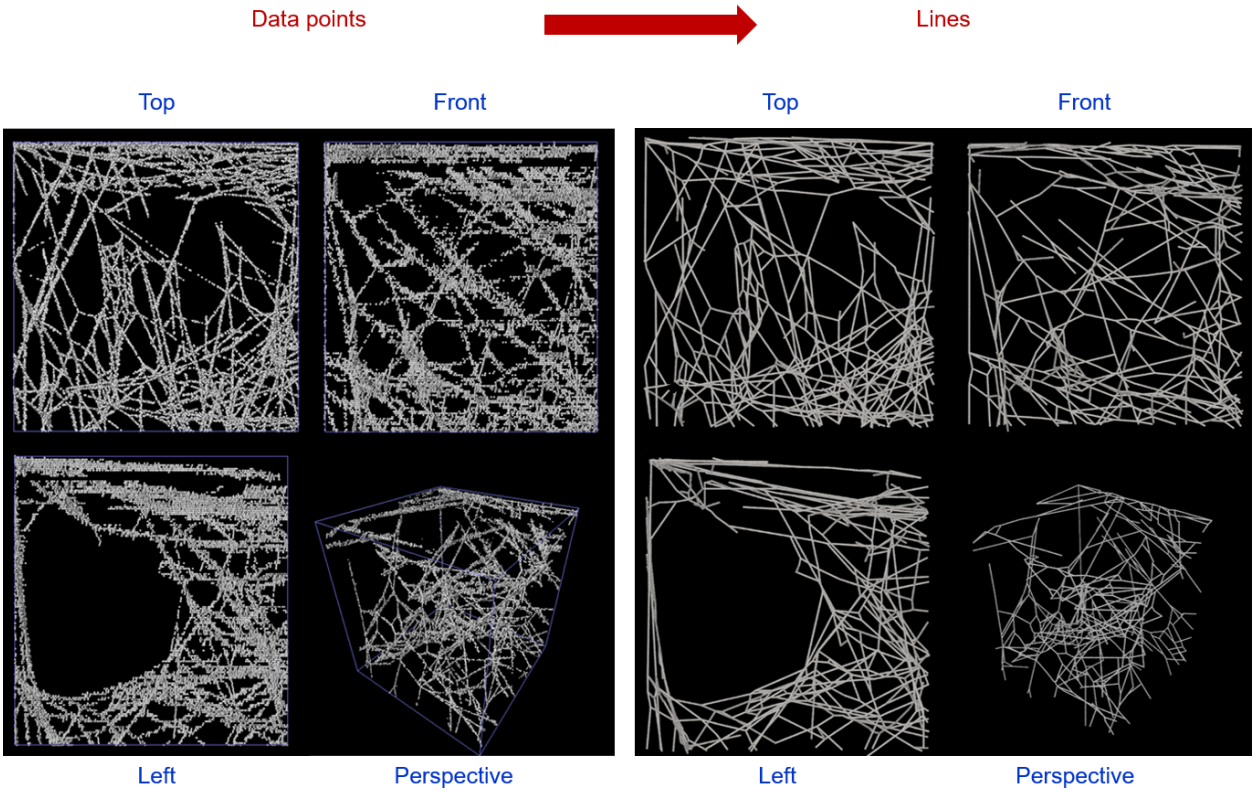

Figure 2-5: From data points to spider web network. Top view: plane of the scan. Front and left views: perpendicular to the scanned plane. (Left) Data points of the 3D image. (Right) Spider web fiber network. The fibers were connected and followed the path of the fiber data points on the left.

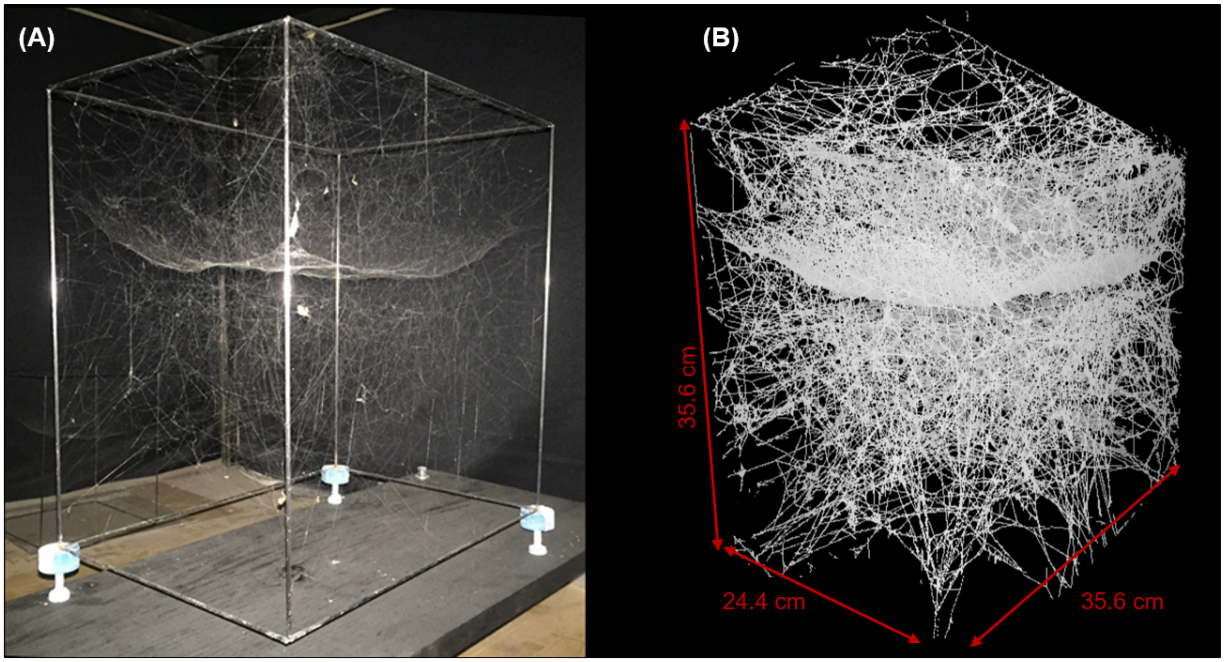

Figure 2-6: Comparison between the 3D spider web and its 3D network model. **(A)** Picture of the 3D spider web spun by a *Cyrtophora citricola* spider. **(B)** 3D spider web model architecture on VMD (Visual Molecular Dynamics) [4]. Full web assembled from 100 cube samples (76.2 × 76.2 × 76.2 mm). Complex tangle webs at the top and bottom part of the structure and very dense tent web in the middle.

2.2.7 Bead–spring Model

We used the model derived from scanning and image processing algorithms to map its topology to a meso-scale bead-spring model of the web. This bead-spring model can be used to carry out molecular dynamic simulations and investigate the mechanics of the 3D spider web. A similar approach was used to investigate the implication of silk's nonlinear behavior in orb webs [6]. This mesoscopic "bead-spring" method consisted of approximating silk fibers as straight chains of beads, with an equilibrium spacing that could be selected based on the distance between scanning slices (0.5 mm). For example, to describe the stress-strain behavior of silk, we used behaviors from previous experimental and numerical studies on spider dragline silk [6] that were assigned to the spring connecting adjacent beads. This model is an invaluable tool to investigate the impact of silk material behavior and 3D fiber architecture on the overall functions of the web.

2.2.8 Limitations

The laser scanning and line-finding algorithms are fully automatic, however, there are some intermediate steps that require manual intervention, such as placing the frame and its web on the scanning table, initiating the acquisition of laser scanning images, and importing the images into a computer for processing. This automatic laser scanning process and image processing cannot currently capture individual fibers within the localized dense regions that create the "tent" of the *Cyrtophora citricola* web. In these tent regions, the fibers were too densely packed together to be distinguished by image processing. However, we noticed that the dense region had regular features such as parallel threads leading to an open hub. To complete the web, we could replace the dense region with this regular thread geometry. This work is the first method proposed for automated scanning and modeling of 3D web networks, and we limited our imaging process to scanning in only one direction. We chose to scan in the depth direction (z-axis) because it allowed us to observe the high-density "tent" region and the individual fibers that compose it. Scanning a different axis (x or y), would make it even more difficult to capture distinct fibers in the tent region. The use of images from only one direction was sufficient to construct the entire web because our laser-sliding gap of

0.5 mm was smaller than the distances between fibers in the porous regions of the web, so that all of the fibers were distinguishable and continuous. This set-up could be improved by implementing two-directional scanning of the web using two perpendicular sets of cameras and sheet lasers. Multi-directional scanning could increase the precision of fiber connectivity and eliminate the need to rotate the frame to allow scanning in different directions, thereby reducing the risk of damaging the web.

2.3 Results and Discussion

From the *Cyrtophora citricola* 3D spider web model, we quantified features of its topology. We focused on porous cube web regions, where we could precisely measure the topology, in contrast to dense tent-like regions of the web. The porous web region selected made up 72% of the volume of the spider web frame (30,923 cm^3). It was composed of 80,350 fibers, with lengths varying from 150 μm to 56 mm in length as shown in Figure 2-7A. The total length of the porous web, i.e. all fibers combined, was 244 m for a box volume of 21,397 cm^3, which was averaged to a length-to-volume ratio of 11.3 mm/cm^3. For an *Araneus diadematus* spider 2D orb web, the combined length of radial and spiral threads was about 12.9 m for a 30×30×5 cm frame, averaged to 2.9 mm/cm^3 [78]. The 3D web's length-to-volume ratio was about four times higher than that of the 2D web, which could explain the longer web construction time. The average fiber length in the 3D web was 3.0 mm which was comparable to the 2.3 mm mesh spacing (distance between each spiral turn) for 2D webs [78]. Considering a fiber thickness of 4.34 μm [79] for the *Cyrtophora citricola* 3D spider web, the total fiber volume was of 3 mm^3. This web weighed 4.7 mg, calculated using silk's density of 1.3 g/cm^3 [80], from which we derived a web density of 2.2×10^{-7} g/cm^3.

We defined the connectivity of the web as the number of fibers to which one node is connected. Figure 2-7C illustrates different connectivity nodes. Figure 2-7B shows the distribution of connectivity in the web. We observed that most nodes were connected to three other fibers, with a maximum connectivity of 9. The high connectivity nodes originated from the noise of the images after scanning. Nodes of connectivity 1 were only connected to one

fiber, which made the fiber a free-end fiber, some of which were artifacts created during the construction of the model, whereas others represented actual free-end dangling fibers or fibers connected to the frame. There were no connectivity 2 nodes because all the fibers were straight. Omitting connectivity 1 nodes, we observed that the connectivity distribution of our spider web fiber network followed the power law of a scale-free network: $P(k) \sim k^{-\gamma}$ [81], with k the connectivity of the node, and γ=5.9. A scale-free network was observed in numerous fields such as biology (e.g. cellular metabolic networks), social interactions (e.g. spreading of ideas on social networks) or World Wide Web (e.g. web pages links) [81, 82]. Compared to random networks, scale-free networks showed higher robustness under accidental failure [50]. This is consistent with the function of spider webs which have a low sensitivity to flaws and defects, a well-known concept for 2D webs that avoid catastrophic failure through sacrificial failure of a limited number of fibers [11, 6].

This new automatic laser scanning method for tracing the complex topology of 3D spider webs can lead to new critical insights into the functions of spider webs [38, 83]. We now have a powerful tool to understand how the properties of silk and the geometry of a 3D web influence the functions of catching prey and providing protection. Previous research showed how the interplay between mechanical properties of silk fibers and the structure of 2D aerial orb webs influences the prey capture function of the web. The radial threads –made of strong and nonlinearly elastic dragline silk –are structural, while the spiral threads –made of viscid silk –are very extensible and tough. The silk type arrangement combined with the distribution of thicknesses leads to a web that is robust against distributed load (wind) and localized load (impact of prey), avoiding catastrophic failure [6, 22]. However, this interplay between structural and material properties and its influence on the web function has yet to be investigated in 3D spider webs.

Biologists observed that starved black widow (*Latrodectus hesperus*) spiders built cobwebs that are optimized for catching prey, while well-fed spiders built webs that offered better protection against predators [84][52]. The architecture of the web defines its functions [84]. Moreover, the 3D web is a relatively permanent structure [23, 28]; it needs to be robust and to be able to preserve its functions in the event of structural defects. This raises some

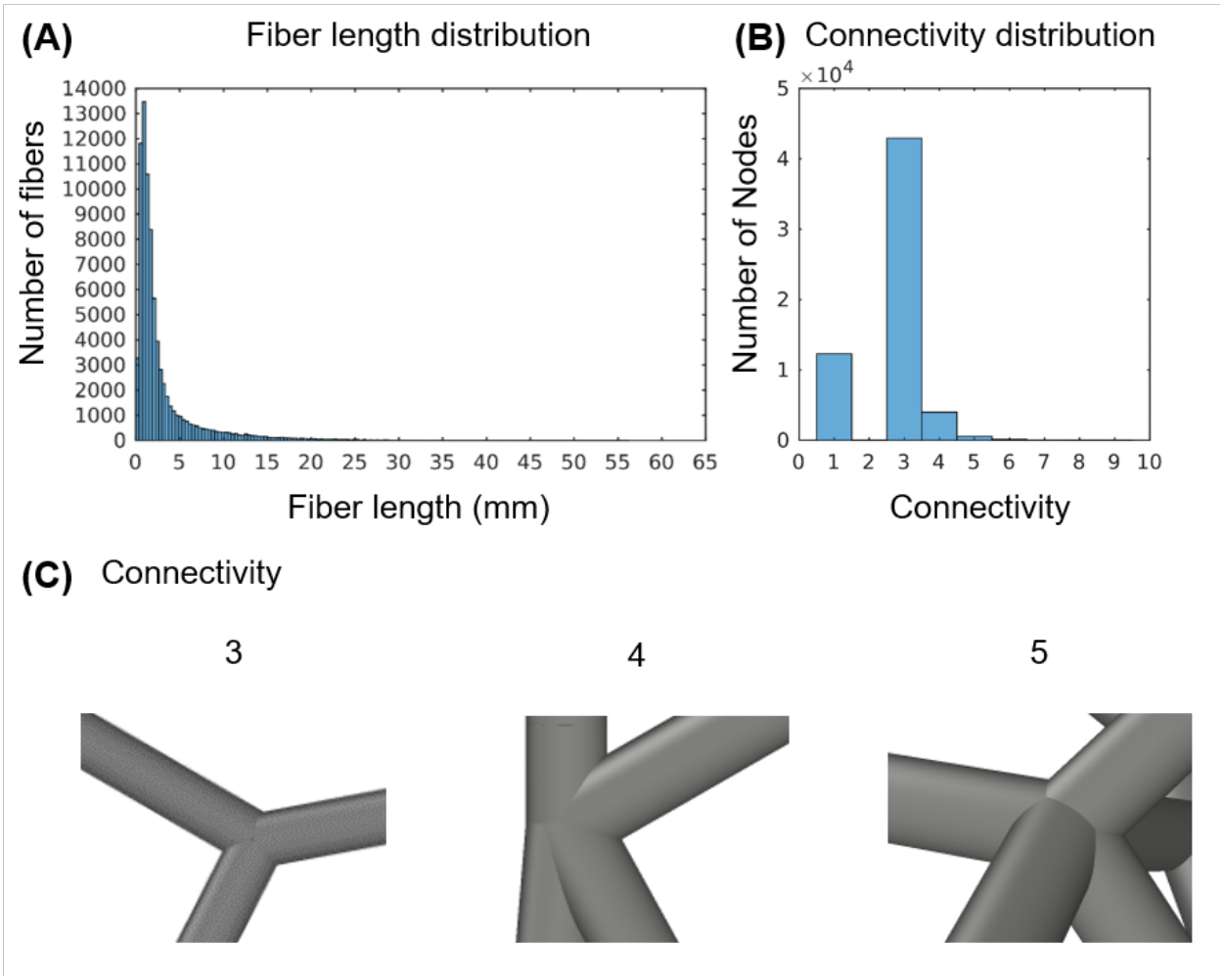

Figure 2-7: **(A)** Fiber length distribution histogram showing that 84% of the fibers were shorter than 5 mm. Lengths varied from 150 μm to 56 mm with an average of 3.0 mm. **(B)** Connectivity distribution histogram showing that most of the nodes (72%) connected three fibers. The nodes of connectivity 1 represented the free-end dangling fibers, the fibers connected to the frame and actual broken fibers. Omitting connectivity 1 nodes, the connectivity distribution followed the power law of a scale-free network. **(C)** Visualization of nodes of connectivity 3, 4 and 5 from the 3D spider web network model.

critical questions regarding the function, silk fiber material and web structure of the 3D web: how does the geometry of 3D web architecture and its silk properties help the web to carry out its functions? How do structural defects influence these functions? How does supercontraction of the fibers change the structure, and impact the web's functionality? Combining the 3D topology of the web and using computational methods, such as meso-scale molecular dynamic simulations will allow a better understanding and validation of observations reported in biological experiments. Models and simulations allow us to carry

out non-destructive experiments on tunable webs. For example, future use of this spider web model, obtained by our automatic scanning method, could include the study of prey trapping mechanisms; investigations of the efficiency of web prey capture via "bouncing" and entanglement; and to determine how long prey is retained. We can also use our model to explore the protection and robustness functions of the web, by applying predator impact or wind load, and determining whether the web fails catastrophically or whether this failure is only localized, and to detect whether the damaged web retains its functions.

While we were able to observe the complexity of the spider web architecture in both the physical web and our model in Figure 2-6, we could not follow the web-building process from the completed web structure. Using this optimized automatic laser scanning method during stages of the construction of the web will lead to important insights into the "smart construction" process of complex 3D spider webs. Spiders build webs that are commonly several times their body size, with some exceptions such as the Darwin's bark spider (*Caerostris darwini*) that are capable of building webs that span rivers [85]. The size of a spider web scaled up to human scale would be similar to the height of a multi-story building. While humans need bulky scaffolding or at least a crane to construct such a building, the spider only uses its silk. Previous studies recorded the construction patterns of 3D web-building spiders, in particular, theridiid spiders [31, 86, 55]. The construction stages for *Tidarren sisyphoides* species include the exploration phase, anchorage of the retreat (for example, a leaf), scaffolding, and construction of the sheet and tangle webs [31]. Benjamin and Zschokke [86, 55] used automated methods with infrared cameras, to precisely track spider movement and web construction patterns to understand their effect on spider and web evolution. Similarly, they observed that gumfoot-web construction is organized and stereotyped; its stages consist of the set-up of the retreat, exploration, scaffolding of the supporting structure and attaching gumfoot lines [86, 55]. Gumfoot threads are silk fibers that are glued with viscid silk to the bottom substrate. They detach and catapult prey toward the spider inside the web [23, 86, 55]. These spiders build their web structure and gumfoot threads continuously over days [86, 55]. We can use our scanning and image processing method to derive precise topologies of webs at intermediate stages, and investigate their mechanical behavior using

modeling and simulations, which we can compare to biological observations [86, 55]. The structural mechanics of these web-building stages and temporary web architectures remain elusive. For example, it would be interesting to know whether the scaffolding fibers have functions other than as a tool for construction: are the scaffold fibers retained in the permanent structure to signal the presence of an intruder? Are these fibers structural, and necessary for maintaining the completed spider web? Do these fibers contribute to the prey capture or protective functions of the web? Or, are these fibers recycled after the spider no longer needs scaffolding? Spiders have the blueprints of their webs and silk in their genes, which have been tuned for millions of years and have contributed to spiders' ecological success [70, 87]. Learning from their invaluable experience, this model can be used to focus on the mechanics and architecture of temporary web structures to understand the function of each stage of web construction. This can lead to applications for web-building-inspired innovative methods to build 3D fiber network architectures.

A further application of this automatic web tracing method is its use in designing innovative and high-performance 3D spider web-inspired fiber networks for structural and material applications. Using the spider web model, we can explore different spider web-inspired architectures and material distributions to tune the fiber network for specific functions; such as impact resilience or reinforcement. As most spiders are solitary, it is difficult to mass-produce spider silk through spider farming [88], requiring the use of bioinspired or engineered material in fiber network structures. However, synthetic fibers are not as strong, tough and extensible as dragline silk [18, 89, 90]: replacing the silk in the spider web structure with bioengineered materials may reduce its unique functionality. The architecture and material distribution of the network should be adapted to the material change. We can develop a computational–experimental approach to build web-inspired fiber network structures, by using modeling and simulations to predict the properties of the structure and experimental testing on 3D-printed prototypes to validate the simulations. New insights from 3D web-inspired architectures and engineered materials could lead to numerous applications, such as improving robust fiber network with redundancies, vibration propagation, or safety/fishing nets. For instance, adding a tangle web-like structure on top of a safety net could help to

redirect and decelerate falling objects into the bottom of the net.

2.4 Conclusions

The study reported here presents a new method to trace 3D spider webs in an automatic, rapid and precise way. Our method improved on previous manual laser scanning methods developed by STS by introducing increased sensitivity through a green light laser, resulting in improved image resolution, and automation of the scanning process. Furthermore, we introduced a new image processing component to precisely map the real web architecture to a meso-scale model. This new method to trace the topology of 3D spider webs can lead to critical insights into the functions of spider webs. Using the model as a basis for meso-scale bead–spring models of the entire web, we can study the interplay between silk fiber mechanics and fiber network architecture and how it influences the functions of the web. The laser scanning process can be used to follow the stages of web-building construction, and understand their functionality. Furthermore, this fiber network model can be used as a tool to deepen our understanding of spider web evolutionary fitness, which can be used to design innovative 3D spider web-inspired structures.

Chapter 3

Mesomechanics of a Three-Dimensional Spider Web

This research and review presented in this chapter have been published in:

- **Su I**, Buehler MJ: "Mesomechanics of a Three-Dimensional Spider Web." *J Mech Phys Solids* 2020,

3.1 Introduction

Spiders and webs can be found in most habitats, whether in the nature or in urban environments. 3D webs are considered permanent compared to 2D orb webs, which are rebuild everyday. As permanent structures, they need to be robust and resilient, and remain functional while being subject to environmental pressures and threats such as stretching from moving attachment supports or impact from prey, predators, and debris.

In this chapter, we aim to understand how the interplay between the nonlinear behavior of dragline silk and the complex 3D spider web architecture influences the functions of 3D spider webs. In particular, we focus on the mechanical and biological properties of a 3D *Cyrtophora citricola* spider web under stretching and projectile impact. The *Cyrtophora citricola* spider web is composed of a dense sheet region surrounded by tangle webs. We create the model of the 3D spider web, the geometry of which was quantified in Chapter 2, for

meso-scale bead-spring particle dynamic simulations. We present and discuss the stretching and projectile impact behavior of 3D spider structures of different densities. We explore future applications of spider web inspired composites for stretching and projectile impact. A deeper understanding of the role of silk and web structure in the evolutionary fitness of spiders, silks, and webs could lead to 3D web-inspired fiber network composites for structural and material applications

3.2 Models and Methods

3.2.1 3D Spider Web Model

In this study, we use the *Cyrtophora citricola* 3D spider web model that has been previously quantified in Chapter 2 to investigate the mechanical behavior of the 3D spider web using meso-scale simulations. This particular spider web is composed of a high fiber density region sandwiched in between two lower density tangle web regions. The tangle region on top of the tent is denser in fibers than the lower tangle region (Figure 3-1A). The original physical 3D web was obtained by letting the *Cyrtophora citricola* spider build its web freely in a rectangular frame over a few days. The frame, composed of carbon fiber tubes, was placed in a water container, so the spider cannot escape and has to build a web in a restricted space [5]. Under these artificial conditions, the spider built a web architecture similar to *Cyrtophora citricola* spider webs found in nature, with a horizontally aligned tent surrounded by a 3D tangle silk barrier [91, 92]. We divide this large spider web (35.6 $\times$ 35.6 $\times$ 24.4 cm) in smaller cubic samples (76 mm $\times$ 76 mm $\times$ 76 mm) (Figure 3-1C), in order to decrease simulation time and investigate the effect of silk density on the web's mechanical response. Figure 3-1B is a histogram showing the distribution of the number of web samples with web density. The web sample densities range from 9.9 $\times$ 10^{-5} kg/m^3 to 6.0 $\times$ 10^{-4} kg/m^3 (Figure 3-1B). Most of the spider web is composed of porous tangle fiber regions.

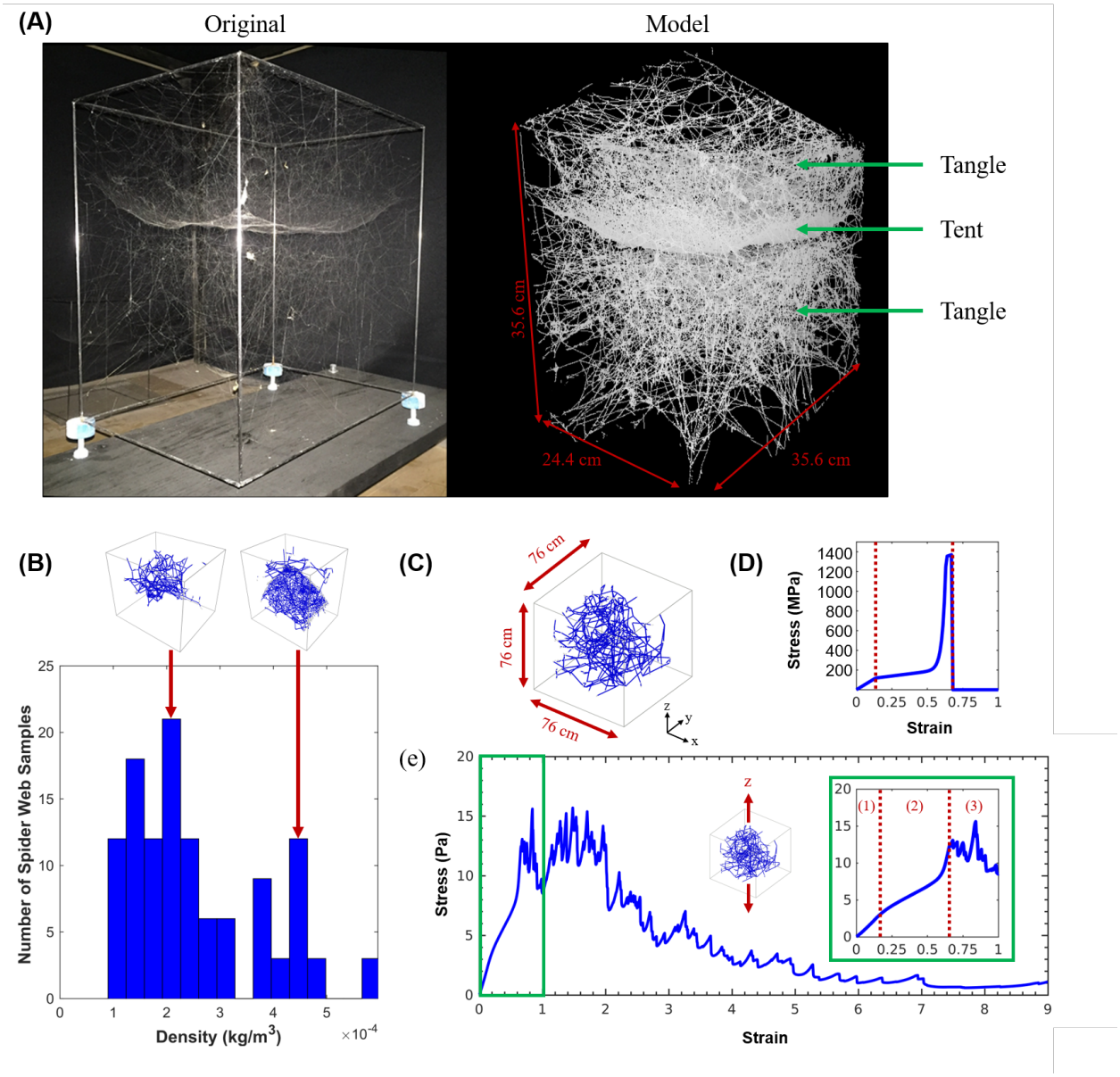

Figure 3-1: **(A)** Overall web geometry used in this study, as reported in earlier work [5]. **(B)** Histogram of the distribution of web sample densities making the large-scale spider web. Most of the web samples belong to the tangle regions of the web. **(C)** Meso-scale bead-spring web sample model. **(D)** Stress-strain curve of an atomistically derived dragline silk parameterized from [6, 7, 8]. **(E)** Stress-strain curve of a web sample (density: 2.6×10^{-4} kg/m^3) uniaxially stretched along the z-axis. In the green frame, the stress-strain curve for strains below 1. We observe three regimes: (1) linear elastic behavior, (2) nonlinear stiffening until the first fiber failure, and (3) continuous fiber failure.

3.2.2 Computational Model of Silk and Spider Web

For each spider web sample, we create a meso-scale bead-spring model for parti-

cle dynamic simulations using LAMMPS (Large-scale Atomic/Molecular Massively Parallel Simulator) [93]. The 3D spider web network data is represented through a list of node coordinates (fiber connections) and a list of pairs of linked nodes (fibers) (Chapter 2). The fibers are modeled as a chain of beads separated by springs that follow the mechanical properties of atomistically derived dragline silk parameterized from [6, 7, 8]. We assume that all the fibers making the *Cyrtophora citricola* spider webs are dragline silks because the webs are non-adhesive (no viscid silk) [91], and also because 3D spider webs are permanent structures that need silks that age better and that can withstand repetitive and prolonged stresses [23]. Each bead represents a segment of dragline silk fiber of length $r_0 = 1$ mm, the equilibrium distance between 2 beads, diameter d = 4.3 μm, which is an average of the *Cyrtophora citricola* silk diameters measured in [79] and density $\rho_{silk} = 1.3$ g/cm^3, the density of silk [94]. The equilibrium distance of the spring between beads is $r_0 = 1$ mm. The modeled silk follows a nonlinear behavior composed of four regimes: linear until yielding, entropic unfolding, exponential stiffening, and stick-slip plateau until failure [6]. The parameters and method for this stress-strain behavior can be found in [6] (Figure 3-1D). We use an angular spring between consecutive silk segments to describe the bending stiffness of silk threads. Silk's bending stiffness is given by [95]: $K_B = E\pi d^4/(128\ r_0)$, with E = 875.9 MPa the initial stiffness, d the diameter of silk and r_0 the equilibrium distance. We consider the silk threads to be under tension, and consequently straight: the angle between neighboring springs is 180°. We include damping effects caused by the energy dissipation of silk threads moving in the air. As silk's threads are thin, we use Stokes' law to define drag force given by [95]: $f_{drag} = -6\pi\mu R\nu$, where $\mu = 1.86 \times 10^{-5}$ Pa·s is the air viscosity at room temperature, R the radius of mesoscopic sphere equivalent to the silk segment. ν is the relative velocity of the silk bead in air. Spring bonds are broken when the strain is greater than the ultimate breaking strain $\varepsilon_{break} = 0.6725$. We define two types of beads: boundary and free beads. Boundary beads are fixed during the simulation; they are the ends of silk fiber attached to the boundary frame or the ends of silk attached to the boundary of the web sample cube. Free beads are free to move and have the properties of silk. The models and simulation scripts were prepared using MATLAB [77].

We use meso–scale bead-spring model for transitioning from the nano-scale properties to the meso and macro-scale behavior. The silk fibers properties are parametrized from atomistically derived dragline silk that has been derived from silk protein simulation at the nano-scale [6, 7, 8]. The limits of this method are that dragline silk properties used are an approximation, even though if follows the natural dragline silk properties. Similarly, we assume that all the fibers have the same diameter and same properties, while in nature, many factors could affect those geometrical and mechanical properties. For example, silk diameter and mechanical properties depend on the spinning speed, size, weight of the spider [96]. One way to improve the model would be to include properties of each fiber in the model. The diameter and mechanical properties of each fiber would need to be measured, for example using, polarized light microscopy [96] and non-invasive, non-destructive Brillouin light scattering [97], respectively.

3.2.3 Spider Web Stretching Simulation

We select 38 web samples of different densities, and apply uniaxial stretching in x, y and z directions at a rate of 10 m/s, resulting in 114 simulations. The webs are stretched up to 900% and the simulation timestep is 1×10^{-7} s. The simulations output web stresses and web strain in the direction of stretching. The visual representations were rendered using OVITO (Open Visualization Tool) [98], with stress or strain fiber color coding.

3.2.4 Spider Web under Projectile Impact Simulation

We select eight web samples of different densities ranging from 0.95×10^{-4} kg/m^3 to 4.5×10^{-4} kg/m^3 : five belong to the tangle region and three belong to the tent region of the large-scale web (Figure 3-2A). For each web sample, two different sphere projectiles are thrown in the center of the web at eleven different speeds and two directions, along the z-axis, resulting in 352 simulations. The sphere projectiles represent natural projectiles that a spider is subjected to, such as a prey and predators. We choose to model a fly and a mud-dauber wasp as a prey and predator projectile, respectively. We choose to use the flies as prey to propel into the web because, house flies and fruit flies are commonly found in nature.

We choose the predator projectile to be a mud-dauber wasps because Blackledge et al. [24] have suggested that mud-dauber wasps, the primary predators of the orbicularian spiders, had a role in the development of the third dimensional barrier as a defense mechanism. Furthermore, Blamires et al. [25] have also demonstrated that webs with an additional 3D fiber barrier enhanced prey foraging as well as increased protection from predatory wasps. The fly and mud-dauber wasp modeled projectiles have for diameter 7 mm and 25 mm and weights 4.7 mg and 133 mg, respectively (Figure 3-2B). Insect weights were derived from their lengths using the model described in [99]. The size of the projectiles are within the range of insects caught in *Cyrtophora citricola* web colonies [48]. The flying speeds of house and fruit flies vary between 1.8 and 3.05 m/s and between 0.49 and 1.37 m/s, respectively and the flying speeds of the wasps' Order (Hymenoptera) varies between 0.19 and 15.7 m/s [100]. Taking an average of the reported flying speeds, we estimate the natural speeds of flies and mud-dauber wasps to be 2 and 5 m/s. To capture the wide range of flying speeds, the projectiles are thrown in the web at 11 different velocities ranging from 0.5 m/s to 20 m/s. Little is known on the flying speed of insects [100]. Flying speeds greatly depend on the unique biological properties of an insect, such as health, size, and gender, it also depend on environmental conditions such as humidity and wind speed [100]. We investigate a wide range of impact velocities that includes all the possible flying speeds of the modeled insects. Furthermore, the range of velocities chosen includes the flying velocities of hangingflies (0.97 m/s) and deer flies (1.72 m/s) entering an orb web, which have been recorded in [101]. The simulations output the position and velocity of the projectile inside the web as well as the fiber stresses and strains.

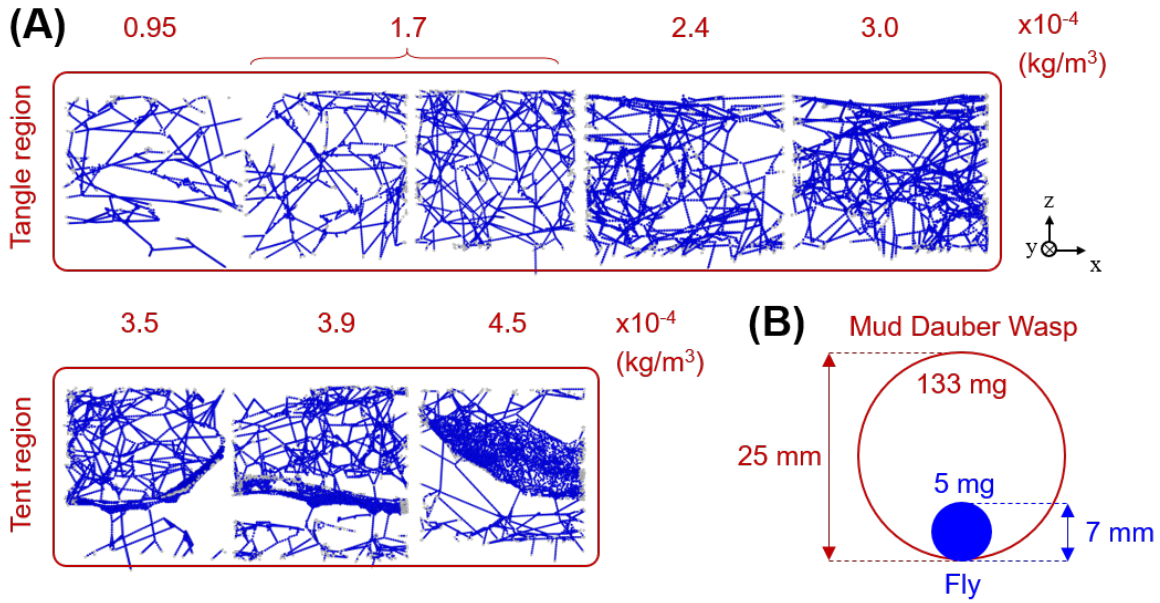

Figure 3-2: **(A)**Web samples selected to undergo projectile impact simulations. **(B)** Schematic of the insect projectiles.

3.3 Results and Discussion

3.3.1 Spider Web under Stretching

We first investigate the role of fiber density in the mechanical performance of 3D spider webs under uniaxial stretching. Figure 3-3 shows the composite stress-strain curves of three different density web samples in uniaxial stretching in x, y and z directions. For all cases, the webs follow three regimes: (1) linear elastic behavior, (2) nonlinear stiffening until the first fiber failure and (3) continuous fiber failures (Figure 3-1E). The web's strain at yielding and at the first fiber failure is similar to the strain of the single silk fiber (Figure 3-1D). Each stress fluctuation (in the third regime) is attributed to one or several fibers bearing most of the load, which is why the composite stress-strain curve of the web matches the stress strain curve of a single fiber. Indeed, each spike correspond to a single fiber breaking, which is followed by a nonlinear stiffening behavior of another fiber that results in a spike showing that this fiber broke and followed by progressive fiber failures. The webs do not fail catastrophically thanks to the fibers working together and web redundancy: most of the load is carried by one fiber, which breaks when it reaches maximum stress, distributing

the load to the other fibers.

The strength of the web increases with density, because the load is distributed in more fibers. For example, the dense web region (Figure 3-3C) is more than twice as strong as the low density webs (Figure 3-3A,B). For the tangle regions (Figure 3-3A,B), web strength is not sensitive to stretching direction (x, y, and z). However, for the dense tent region (Figure 3-3C), it is much stronger in the x and y directions than the z direction because the tent of the web is oriented along the x-y plane, so more fibers bear the stretching load. For this particular web geometry, the strength in the x-axis is higher than in the y-axis because of the physical location of this specific sample in the large-scale web. One side of the web sample (y) has no boundary fibers as this sample is not connected to any other samples or web frame.

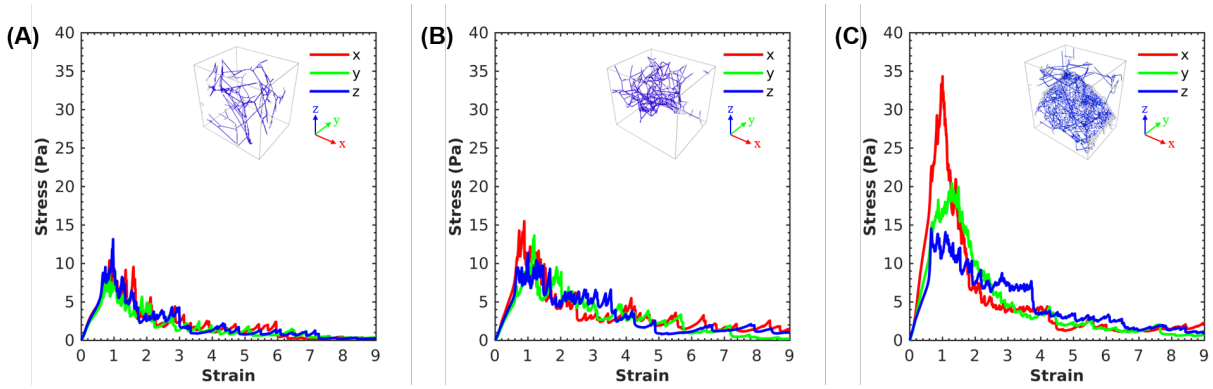

Figure 3-3: Stress-strain curves of 3 different density web samples in uniaxial stretching in x, y and z directions. Density: **(A)** 1.4×10^{-4} kg/m^3 , **(B)** 1.8×10^{-4} kg/m^3 , **(C)** 4.4×10^{-4} kg/m^3

Figure 3-4 is a visual representation of stress (Figure 3-4A) and strain (Figure 3-4B) fiber distribution in a web sample belonging to the tangle region being uniaxially stretched in the z-axis (Figure 3-3B). From 0% to 200% web strain, most of the fibers are dark blue, meaning the fibers have a very low stress, and are far from breaking strength. For 100% and 200%, we can clearly discern the fibers being loaded (colored in green to red). This validates what has been observed in the stress-strain curves (Figure 3-3), that only a few fibers bear the load of web stretching. Figure 3-4B shows the fiber strain distribution in the web under stretching. We observe that at 20% web strain, only a few fibers are loaded and they have a strain of about 20% which is the same as the web strain. This is the reason why the web's strain at yielding is similar to the strain of a single fiber, as described in the

stress-strain behavior of webs. For 100% and 200% web strain, we see that numerous fibers have a strain above 30%, even though they have a low stress (Figure 3-4A). This discrepancy between fiber strains (Figure 3-4B) and fiber stresses (Figure 3-4A) is due to the nonlinear behavior of dragline silk. Indeed, dragline silk fiber has a nonlinear behavior composed of a slow increase of stress with high strain due to homogeneous stretching and unfolding of the semi-amorphous phase, a high increase of stress until fiber failure due to the load transfer to the stiff β-sheet crystals, at the nano-scale [6]. In the *Cyrtophora citricola* spider web models and simulations, all the fibers follow dragline silk behavior. In nature, dragline silk is also used to build the frame and the radial threads of orb webs. Even though fibers are stretched during web stretching, only a few fibers reach a high stress and contributes to web strength. At high web strain, not all the fibers are stretched and many fibers are unloaded (colored in blue). The loose fibers are either fibers that have already broken or fibers that are unaffected by web stretching because of the redundancy of the web structure. At 100% web strain, most of the web structure is unbroken, which would allow the spider web to remain functional. Under uniaxial stretching 3D spider webs avoid catastrophic structural failure by allowing sequential failure of fibers which is due to the interplay between the redundancy of the complex spider web and the unique nonlinear behavior of spider dragline silk. 3D spider webs are robust and resilient, as they avoid major structural collapse allowing the web to retain its functions and the spider to repair the few defects.

The variation of strength and toughness with web density is summarized in Figure 3-5. Web strength and toughness increase with density. We fit the variation strength and toughness with density with the equations:

$$\sigma = 15.05e^{685.4d} - 20.28e^{-7878d} \tag{3.1}$$

$$T = -64.31e^{-8140d} - 37.29e^{360d} \tag{3.2}$$

With σ web strength, T web toughness, and d web density ranging between 1.0×10^{-4} kg/m^3 and 5.0×10^{-4} kg/m^3. We observe a higher increase of strength and especially toughness with a small increase of web density from 1.0×10^{-4} kg/m^3 to 2.0×10^{-4} kg/m^3.

Within this web density range, adding a small amount of silk fibers will considerably increase web toughness and strength. The plateau after the initial increase of strength and toughness is in part due to the averaging of strength and toughness values in the x, y and z directions. Indeed, for the higher web densities, the web samples include a high-density silk tent oriented in the x-y plane, which have lower strength and toughness in the z-direction. Another reason for the plateaus is that when web density increases, it is the weakest region that dictates the strain localization and overall material performance, which is why we see the rate of increase of strength and toughness diminish. Taking inspiration from natural 3D spider web complex structures and their high rate of increase of strength and toughness for lower densities could lead to tougher and stronger lightweight fiber network composites.

Thanks to the 3D spider web imaging and modeling methods previously developed in Chapter 2, we used simulations to derive the relation between strength and toughness with web density of a natural *Cyrtophora citricola* 3D spider web. This relation was determined using meso–scale bead-spring simulations on a spider web built in a threat-free environment (no predators and no environmental threats) with the assumptions that all the silk fibers had the same diameter and mechanical properties. However, in nature, the silk properties and web structure will depend on the energetic state of the spider and selective environmental pressures [27]. For example, Blackledge and Zevenbergen [27] have observed that fed *Latrodectus hesperus* spiders would spin silk twice as thick as starved spiders but also reassigned silk in the web for protection rather than prey foraging. Spiders' adaptive skills are directly reflected in their web structure. An ideal web would depend on the environmental conditions such as support availability, wind load, humidity, debris impact but also the web functions that depends on the energetic state of the spider. Future studies on the effect of environment and spider health on web geometry, strength and toughness would lead to new insight for designing adaptive and more efficient complex fiber architectures.

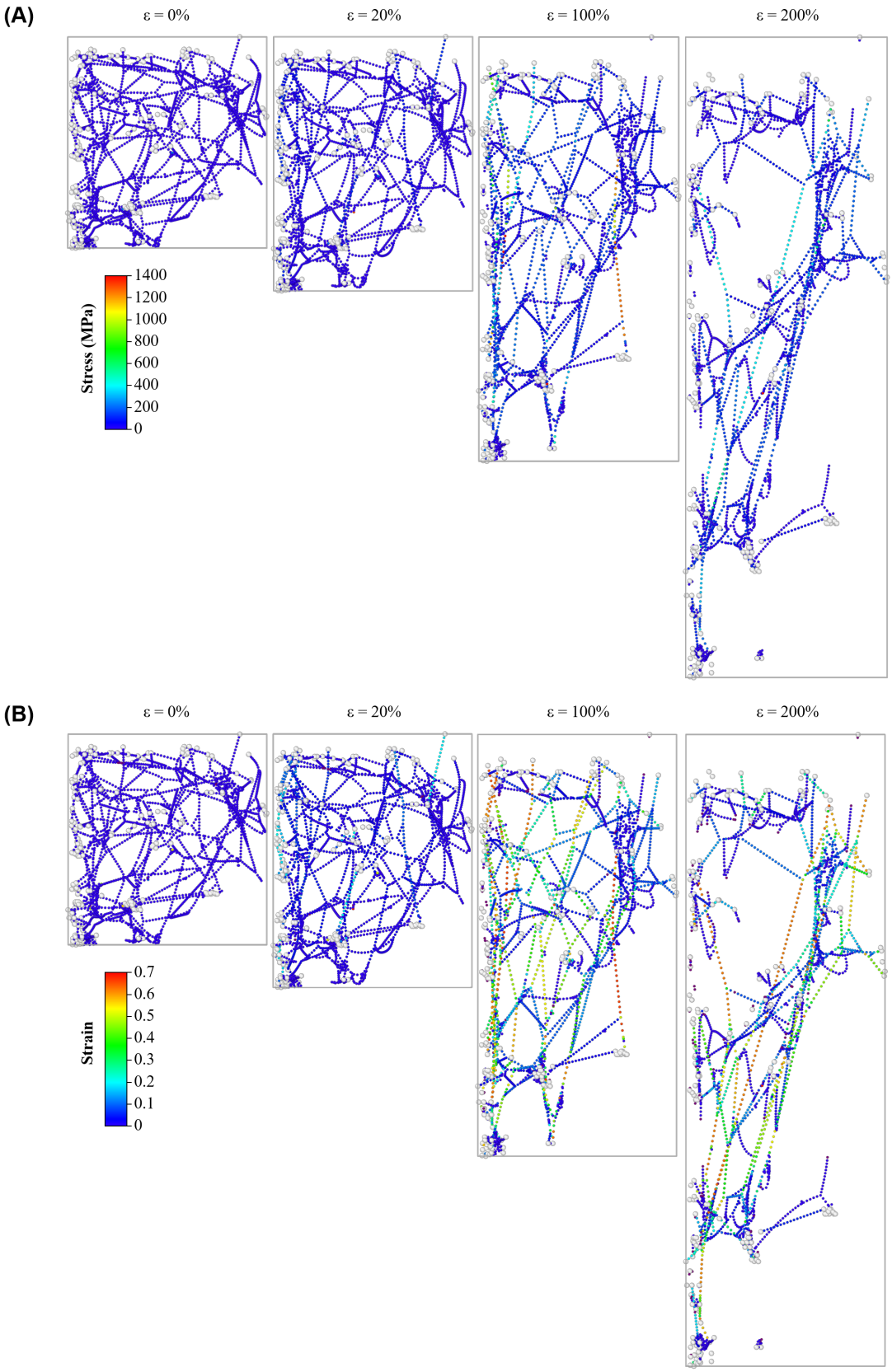

Figure 3-4: Snapshots of a web sample (density: 1.8×10^{-4} kg/m^3) under uniaxial stretching in the z-direction simulation. **(A)** Stress color-coded. **(B)** Strain color-coded.

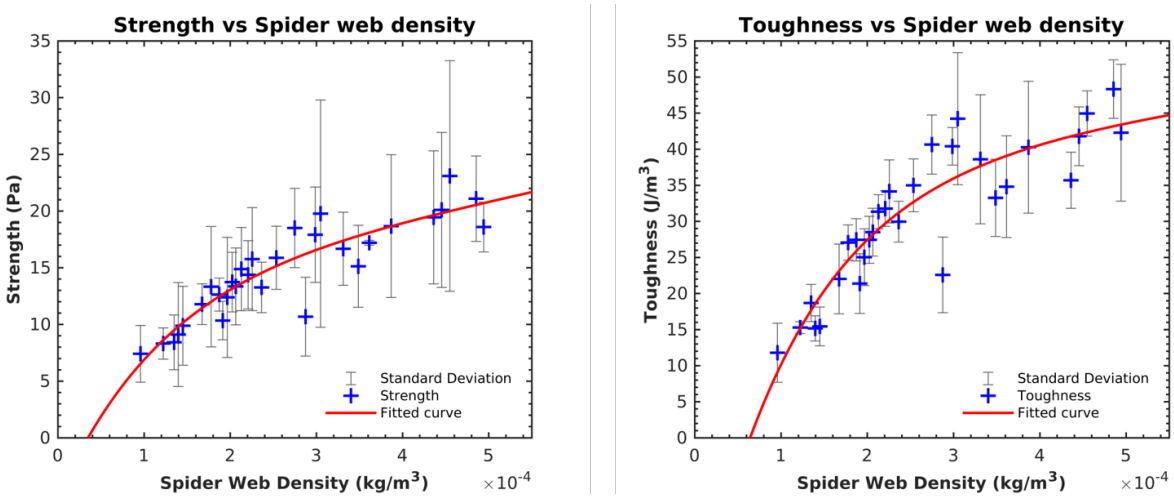

Figure 3-5: Variation of strength and toughness with web sample density.

3.3.2 Spider Web under Projectile Impact

We have shown that the interplay between nonlinear silk behavior and redundant 3D spider web architecture makes spider webs robust and resilient. Here, we investigate the role of silk and web architecture in prey catching and predator defense mechanisms. Two types of projectile are thrown in web samples of different densities and different impact velocities, which represent natural spider prey (fly) and predator (mud-dauber wasp) (Figure 3-2). Figure 3-6 shows the variation of projectile velocities for different impact velocities and web densities. All projectiles are thrown along the z-axis in the center, from above (Figure 3-6) and under the web sample. For all cases, the drops of projectile velocities indicate that it is hitting and slowed down by fibers. When the velocities become negative, the projectiles have bounced off the fibers and changed flying direction to opposite direction of impact. The impact velocities illustrated here are the estimated velocities of a fly (2 m/s), mud-dauber wasp (5 m/s) and an extreme case (20 m/s). For low density webs (Figure 3-6A), we observe that both the fly and the wasp exit the web with a slight deceleration after hitting and sliding through a few fibers. The web is too porous to stop the projectiles at those velocities because they only hit one fiber at a time, which is not enough to stop them. For intermediate web densities (Figure 3-6B), the velocities decrease more than for the porous web, but similarly all the projectiles exit the web. For the fly, the velocity drops are sharper than for the wasp, because the smaller fly is slowed down one fiber at a time, while the wasp is slowed down with a cooperation of fibers. Indeed, for extreme speed (20 m/s), we observe only one drop of velocity for the wasp, which confirms that multiple fibers absorb projectile impact. For the high-density web region, which includes the tent of the *Cyrtophora citricola* spider web (Figure 3-6C), both wasp and fly get caught by the web for natural velocities, as their velocity decreases greatly and becomes negative. They are caught by the silk net, which is where the spider is usually located [91]. For extreme impact speed, the tent region catches the fly projectile but fails against the high-speed wasp. For these projectile impact cases, only the high-density mesh can stop the flies and wasps for natural velocities, the tangle regions help decelerate projectile speed but filter them in.

The impact speeds and web densities also have a role in the structural integrity and

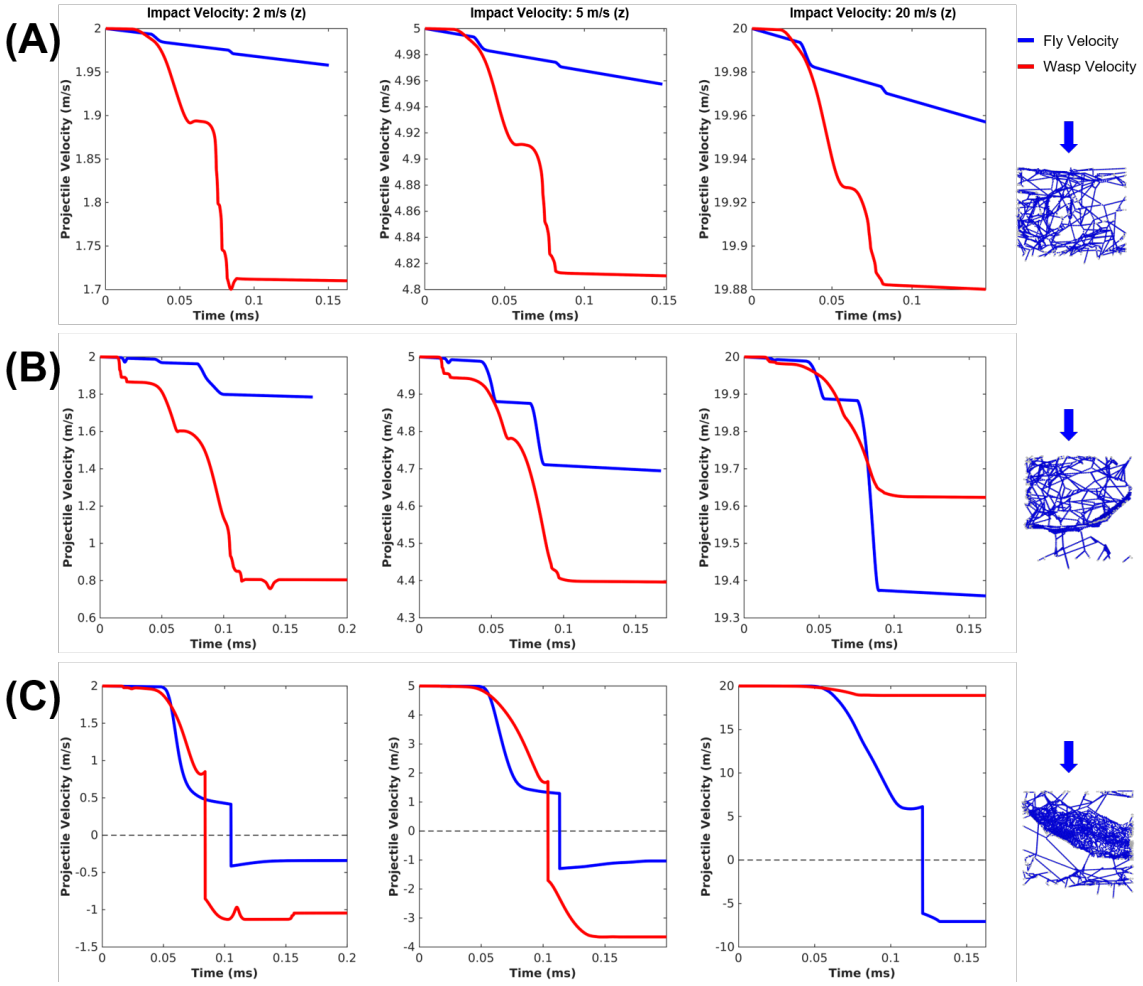

Figure 3-6: Variation of projectile velocities for different impact velocities and web densities. Densities: **(A)** 2.4×10^{-4} kg/m^3 , **(B)** 3.5×10^{-4} kg/m^3 , **(C)** 4.5×10^{-4} kg/m^3 .

failure of the web. Figure 3-7A shows the variation of a number of broken fibers with web sample densities for three different impact speeds. The fly projectile does not break any fibers for web densities lower than 3.0×10^{-4} kg/m^3, which belong to the tangle region of the web, for natural and extreme speeds. This is due to the small size of the fly projectiles, they just slide through the fibers. For higher densities, belonging to the tent region, the number of broken fibers increases with density and impact speed, but does not exceed ten broken fibers, which is a very small fraction of the fibers composing the web. For the wasp, the number of broken fibers is higher than the fly, because it is larger and heavier than the fly. We observe an increase of broken fibers with web density, because there are more fibers in the way of the projectile. This trend is not as clear for natural velocities because of the unique spider web sample geometry, each data point corresponds to one to two web samples.

In the case of the densest web sample (4.5×10^{-4} kg/m^3), the fly and wasp only break 0.14% and 0.55% of the web structure, respectively, at an extreme impact speed of 20 m/s, which is evidence of the web's robustness against fly and wasp impacts.

Spider webs are not only resistant to impact, they also help decelerate the natural prey and predators. Figure 3-7B describes the variation of ratio of projectile velocity after crossing the web over the impact velocity with the web density for different impact speeds. The ratio is lower than 1 when the projectile velocity decreases and negative when the projectile has been bounced in the opposite direction. For all impact speeds, all projectiles' velocity decreases while crossing through the web. These decelerations are greater with the web densities. For natural velocities, the fly will get caught in the highest density tent of the web, but not decelerate considerably in the tangle webs. The flies are filtered in through the tangle web to reach the tent where they are immobilized. As the tent is where the spider is located, the tangle region provides food to the spider by allowing prey to penetrate through. For wasps' estimated velocity (5 m/s) the density increase is not enough to stop them, except for one case for the highest density web. They decelerate slightly, for tangle regions. For slower impact velocity (2 m/s), wasps decelerate considerably more with web densities and are even stopped at the highest density tent. Those estimated natural impact velocities are still too fast for the tangle region to stop the wasp and protect the spider, but for slower natural velocities the wasp will get caught in the tangle region (Figure 3-8). For extreme velocities (Figure 3-7B), the flies and wasps hardly decelerate, except for the highest density web for the fly. The webs do not protect the spider at such speeds, but will only allow localized failure, as they break few fibers (Figure 3-7A).

Expanding to a wide range of impact speeds from 0.5 m/s to 20 m/s, we have summarized whether the fly and wasp projectile penetrates though or is immobilized in the webs in Figure 3-8. The interface line drawn is the impact velocity threshold under which the prey or predator projectile is captured in the web. For both flies and wasps, successful capture increases with web density (Figure 3-8), which is similar to what has been observed for tangle, sheet and orb webs [47]. The fly projectiles only get captured in the denser parts of the web, belonging to the tent region. The performance of the tent region to catch flies increases

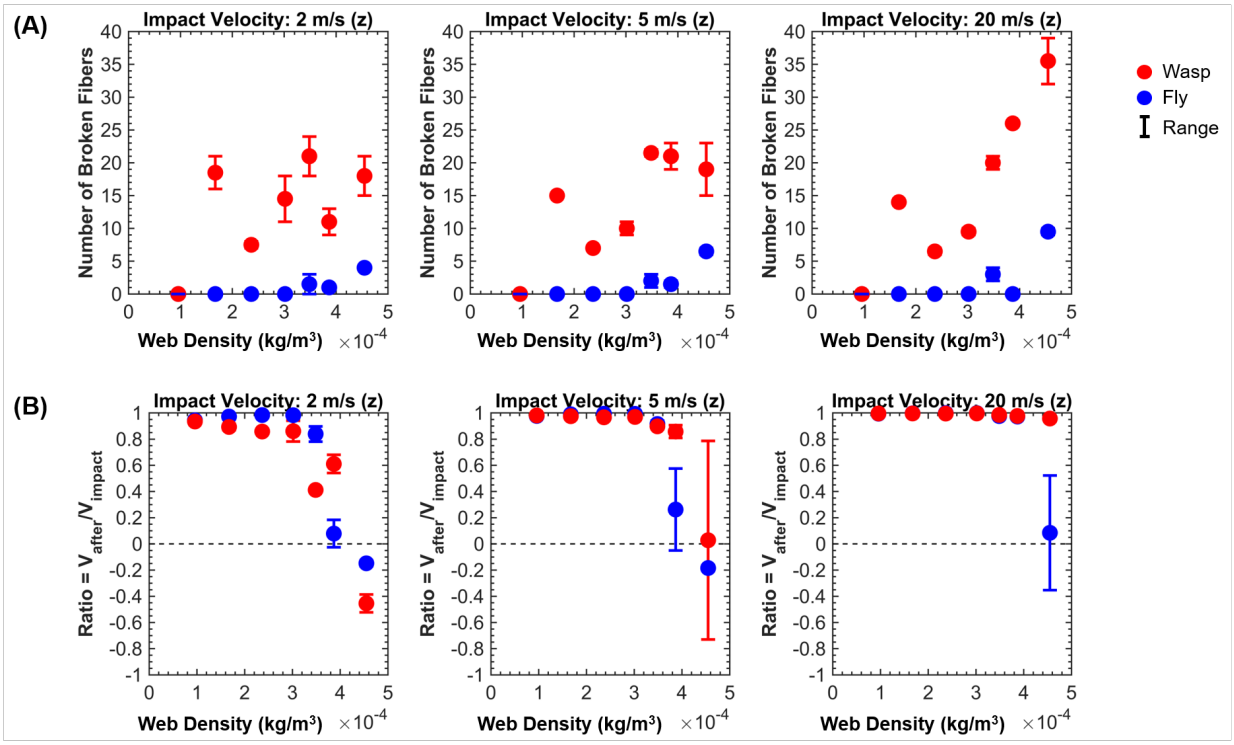

Figure 3-7: **(A)** Variation of number of broken fibers and **(A)** variation of ratio of projectile velocity after crossing the web over the impact velocity, with the web density for different impact speeds.

with density. The denser tent regions can capture flies that fly at higher flying speed than estimated natural velocities (2 m/s). The porous tangle regions allow the prey to reach the dense tent. On the other hand, the mud-dauber wasps get caught in the tangle region, with densities higher than 1.5×10^{-4} kg/m^3, for velocities under 1 m/s which is within the range of the flying speeds of the mud-dauber wasps' Order, but much lower than the estimated natural speed of a wasp (5 m/s). The chance for a wasp to get caught in the web increases with density. For estimated natural wasp velocities, the wasp is only caught in the densest region of the web, but not in the tangle regions. We derive that for low flying speeds, the role of the tangle region is to slow down and block the mud-dauber wasp predators from reaching the spider that is on the tent region. For high speeds ($>$ 5 m/s), the predators will slide or break through the webs without catastrophically failing the structure. In nature, *Cyrtophora citricola* spiders build webs within a colonial aggregation of other webs [91], so in this case, high-speed predators might get through the first spider web, but not the webs below. Indeed, prey capture is enhanced in *Cyrtophora citricola* spider colonies, which is

why large colonial spider web settle where insect prey are abundant [48].

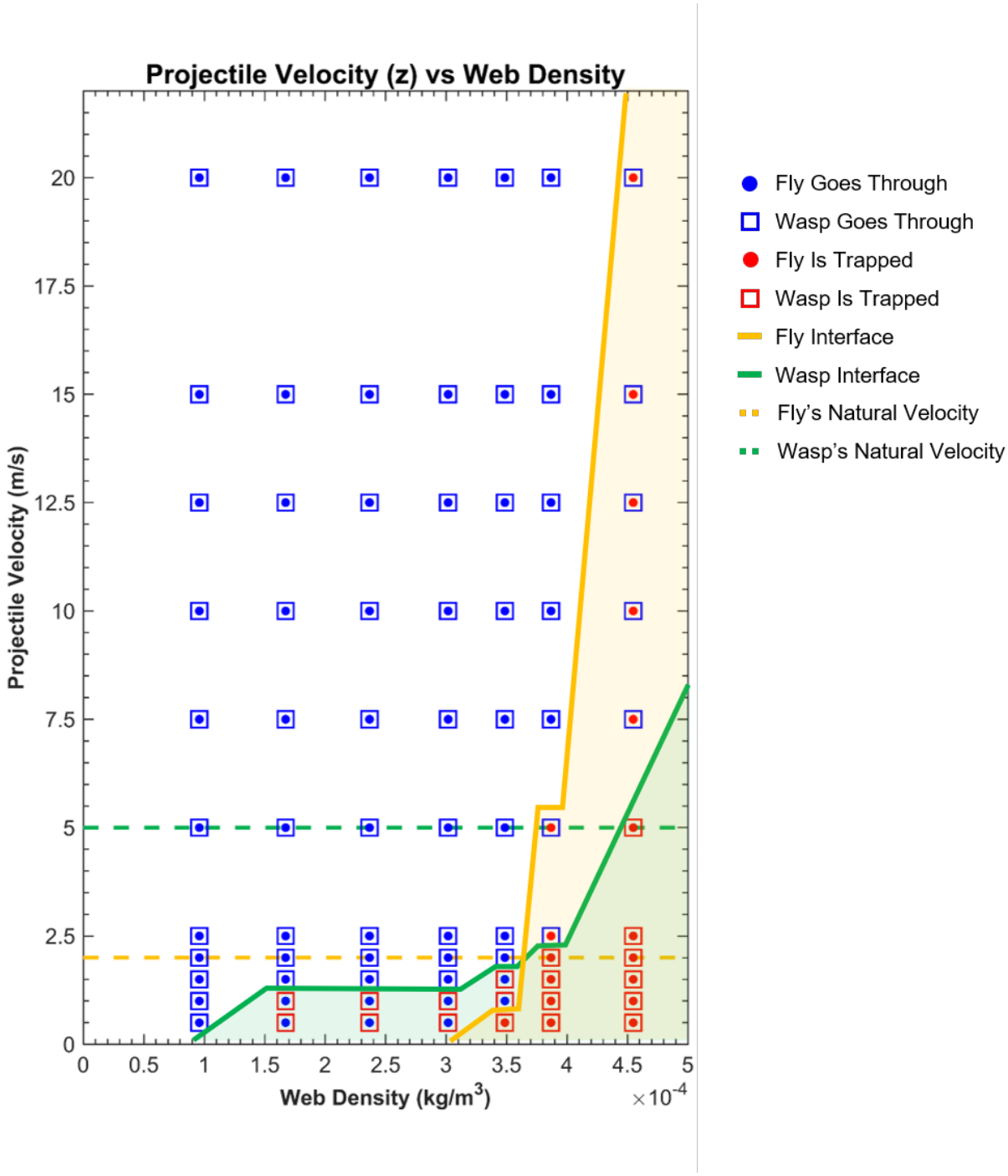

Figure 3-8: Summary graphs showing whether the flies or mud-dauber wasp penetrate though the web samples. As web sample density increases, the projectiles are more likely to be captured.

Here, we have demonstrated the crucial role of tangle regions that confine the tent region, where the spider eats and lives. It provides food by allowing the prey to fly through and reach the spider, but also protect the spider by preventing the larger predators, such

as mud-dauber wasps from penetrating through at flying speeds slower than 1 m/s. This also confirms that the tangle 3D barrier above and under the tent protect the spider, and may be the reason why 3D webs evolved from 2D webs, as it has been suggested in [23]. We also have shown that the 3D *Cyrtophora citricola* spider web is robust against projectiles at extreme impact speeds, by allowing localization of web failure. The spider can quickly repair small defects and the web retains its functions.

3.4 Conclusions

The study reported here presents the mechanical behavior of a real 3D *Cyrtophora citriola* spider web (shown in its entirety in Figure 3-1A) under uniaxial stretching and natural projectile impact. We used a method based on meso–scale bead- spring particle dynamics simulations on cubic samples of the real web, to investigate the role of web micro-architectures, especially densities as a characterizing approach to distinguish variations of geometry, on mechanical performance. The robustness and resilience of the web under uniaxial stretching rely on the interplay between nonlinear behavior of dragline silk and the complex redundant architecture of the spider web. The tangle region of the spider web acts as a filter: it allows prey to reach the tent where the spider is located while protecting it from predators.

Moving forward, we can use this method systematically and in an automated way for any type of 3D spider web architecture and mechanical loading. We can scan real webs, model them and use different loading for simulations, such as stretching, projectile impact, vibrations, and wind load. Because of this self-consistent method, we can use the web mechanics results and deep learning to design web-inspired architecture with specific functions. For example, in the case of projectile impacts, we could directly expand this study to a larger variety of projectile types, weights, and speeds and use deep learning to design web-inspired filters with varying fiber densities, allowing chosen projectiles to get in but not out, or safety nets that gradually slow down projectiles. We can also further take inspiration from the spider to design manufacturing, recycling and monitoring methods, as spiders and webs naturally and effectively perform those functions [53].

Chapter 4

Three-Dimensional Spider Web Construction and Mechanics

This research and review presented in this chapter will be published in:

- **Su I**, Narayanan N, Logrono MA, Bisshop A, Mühlethaler R, Saraceno T, Buehler MJ: "In-situ Three-Dimensional Spider Web Construction and Mechanics." Proc Natl Acad Sci (submitted)

4.1 Introduction

While completed 3D web construction patterns and topologies have been investigated in previous chapters, little is known about the mechanics of 3D spider webs during construction. In Chapter 3, we have investigated the mechanical behavior of *Cyrtophora citricola* 3D spider webs under uniaxial stretching and projectile impact. The interplay between the nonlinear behavior of dragline silk and the complex redundant architecture of the webs leads to robust and resilient webs under uniaxial stretching. The tangle web plays a crucial role in the functionality of the spider webs: it filters in prey and protects the spider from predators. In this chapter, we investigate the mechanical and functional behavior of a *Tidarren sisyphoides* spider web under construction. We use image processing and computational simulation methods to quantify and validate what has been observed in nature.

We describe the experimental and computational methods to obtain the topology of a 3D spider web during construction. We present the different topological and mechanical properties of the web under construction. Finally, we explore future applications of web-inspired structures and construction processes.

4.2 Materials and Methods

4.2.1 *Tidarren sisyphoides* Spider

Spiders of the genus *Tidarren* build tangle webs with aerial sheets [31]. In this study, we focus on the webs of *Tidarren sisyphoides* (Walckenaer, 1842) spiders (Figure 4-1C). They can be found from the US to Argentina [68]. We purchased female *Tidarren sisyphoides* spiders from Spider Pharm (www.spiderpharm.com) and fed them crickets from Premium Crickets (www.premiumcrickets.com). We chose to use female spiders for their web building behavior and their larger size compared to male *Tidarren* spiders [102].

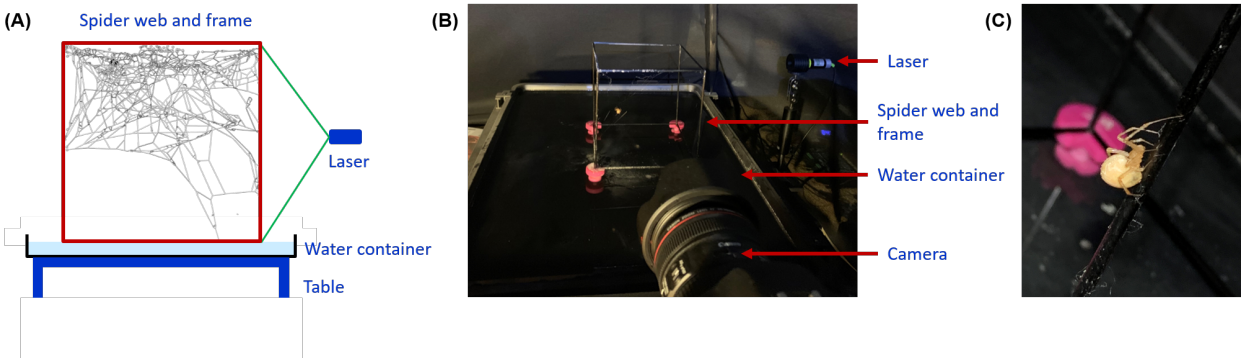

Figure 4-1: 3D spider web scanning setup. **(A)** Schematic of the scanning setup. **(B)** image of the scanning setup. The frame and the spider is placed on top of water filled container so the spider is forced to build in the frame. The camera takes high resolution images of slices illuminated by the sliding sheet laser. **(C)** *Tidarren sisyphoides* spider (female).

4.2.2 Spider Web Construction Scanning

We extended the experimental setup described in Chapter 2 to scan the 3D spider web during construction. The setup for scanning the static 3D spider web consisted of a raised table upon which the finished 3D spider web was placed and a supporting stand of a moving rail machine upon which the high-resolution camera and the sheet laser were placed

at a fixed distance. The camera's focus point was always aligned with the plane of the sheet laser; during scanning, the laser and the camera moved together along the depth of the spider web. The camera took high-resolution images of the slices of the web illuminated by the sheet laser (Chapter 2). While the previous scanning method was automatic, it required intermediate manual interventions, such as placing the spider web on the raised table, starting the camera shutter timer together with the movement on the rail controlling the computer, and importing the images from the camera to a computer for processing. Moreover, this previous method would only work for a spider-less completed web (Chapter 2). In order to follow web construction over time, we fixed a shallow water container on top of the raised table upon which an empty cubic 15.24 × 15.24 × 15.24 cm carbon fiber tube frame was placed. The frame was stabilized by four 3D-printed foot supports at the bottom corners of the frame, keeping the frame stable and above the water. After adding water in the container and positioning the frame, we placed a *Tidarren sisyphoides* on the frame. The spider had to build its web inside the frame as the water prevented it from escaping, and remained in the frame during scanning. Figure 4-1A,B illustrates the upgraded scanning setup. This new setup allows scanning of the web during web construction.

To improve to a fully remote and automatic setup, we used the microcontroller board Arduino UNO (www.arduino.cc) to automate and synchronize the movement of the laser on the rail, the illumination of the web, and picture capture (Figure 4-2A). All the images were saved directly to the computer from the camera using the software digiCamControl (www.digicamcontrol.com). Those images were instantaneously synced to the cloud through Dropbox (www.dropbox.com). This allowed us to start and monitor the scanning process remotely, which minimized light in the laboratory to preserve image quality. Figure 4-2B shows the scanning process sequence controlled by Arduino UNO. The laser stayed on for 20 min and was turned off for 1 min to minimize fire hazard. For each cycle, the laser and camera moved together 0.6 mm for 0.1 s, then after 3 s of stabilization, necessary to take a clear image, the camera took a picture with an exposure time of 2 s. To make sure that the picture had been saved in the computer, Arduino UNO ordered a waiting time of 2 s before the laser moved again. One cycle lasted 7.1 s. For the dimensions of the web frame, the web

scan lasted 34 min and was composed of 276 images of resolution 1669 $\times$ 1686 pixels. The gap between each image of the slices of the spider web was 0.6 mm. After finishing one scan, the laser and camera moved back to their initial position. Each of these parameters can be changed easily depending on the size of the web, quality of images, and scan frequency required. This upgraded setup with Arduino UNO allows remote control and monitoring of the web scanning without moving the frame and the spider.

Because of the long scanning time (34 min), we scanned the spider web once a day for seven consecutive days to minimize light disruption. We obtained eight scans of the web at different stages of construction. The scan at day zero was obtained 3 hours after the spider was placed on the frame. During the scan, the spider needed to stay immobile; otherwise blurry images would result. For this particular spider species, *Tidarren sisyphoides*, some fibers were invisible to the camera no matter the angle of view, so we added talcum powder loosely around the web every two days to make the fibers more visible.

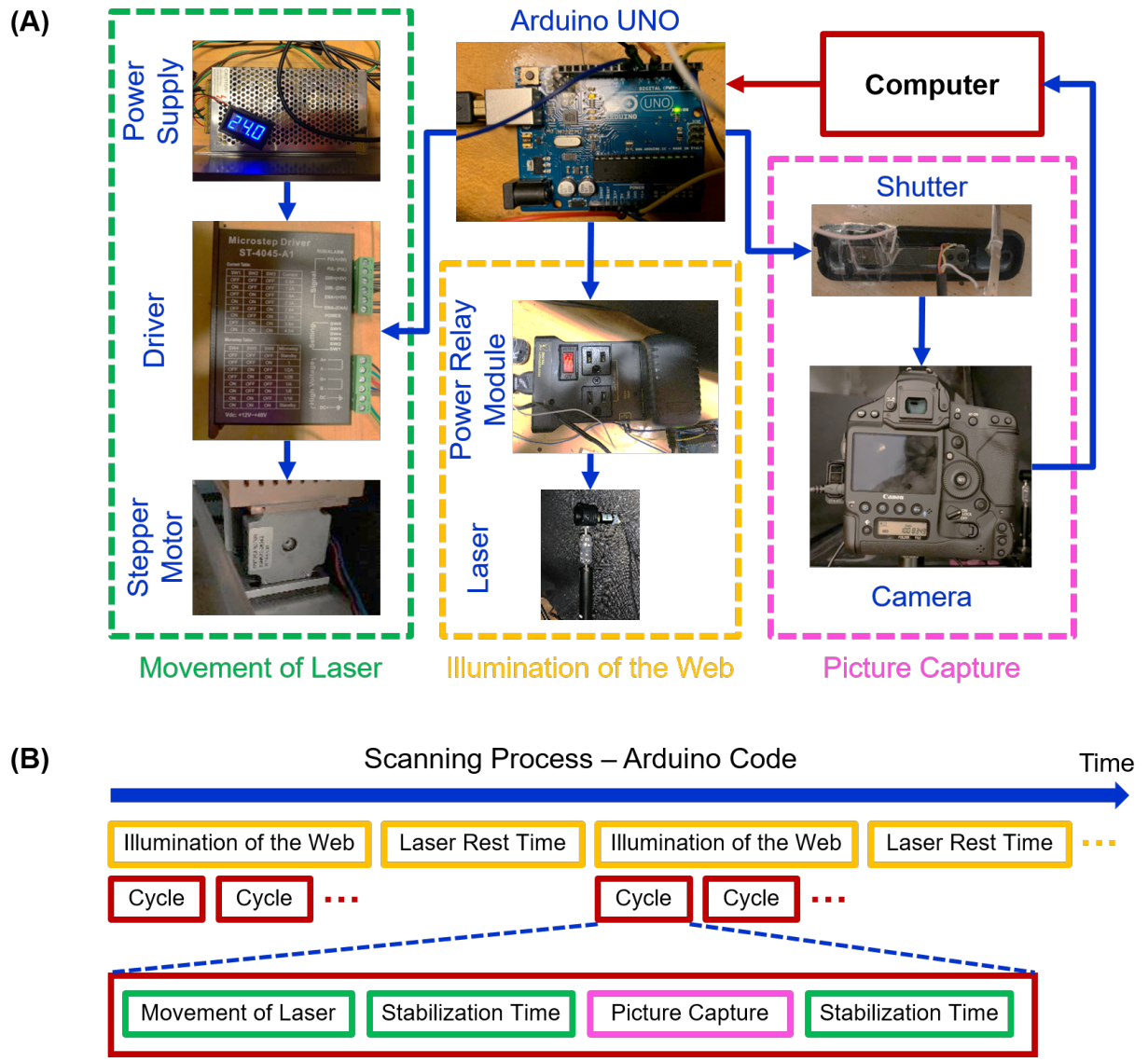

Figure 4-2: Arduino UNO implementation for synchronizing the laser scanning setup. **(A)** Schematic of the web scanning system used here. Arduino UNO is used to synchronize movement of the laser, illumination of the web, and camera. Using this upgraded method, the scanning timing is more precise, fully automatic, and can be monitored remotely. **(B)** Scanning sequence of the of the web scanning synchronized and controlled by Arduino UNO.

4.2.3 Spider Web Image Processing

We used image processing algorithms, based from [5, 103], to transform the 2D color images of slices of the web into a 3D model which consisted of a list of node coordinates (fiber connections) and a list of pairs of nodes (fibers). To reduce the image noise created by the laser hitting the metal frame, we superposed all the images from the eight web scans

and identified the 2D coordinates of the corners of the frame. Then, for all the images, we convert all the pixels outside of the four corners previously selected into black pixels using MATLAB (www.mathworks.com). After reducing image noise, we used the same image processing and line finding algorithms used in Chapter 2. We changed a few parameters such as image dilation, pixel size, and gap size between slices. As the spider was present during web scanning, we measured the coordinates of the spider location in the web from the 2D color images.

4.2.4 Computational Model of Silk and Spider Web

For each web model representing a stage of web construction, we built a meso-scale bead-spring model for particle dynamic simulation using LAMMPS (Large-scale Atomic/Molecular Massively Parallel Simulator) [93] from the 3D spider web network data (list of node coordinates and list of pair of linked nodes). Similar to the method described in Chapter 2, silk fibers were modeled as a chain of beads separated by springs that follow the nonlinear mechanical behavior of dragline silk. In particular, we used the dragline silk properties parameterized from [6, 7, 8]. We assumed that *Tidarren sisyphoides* web is uniquely composed of dragline silk as their webs do not have viscid threads in nature [31, 86]. 3D spider webs tend to be more permanent structures, so they need silks that age well and can endure repetitive and prolonged stresses, such as dragline silk [23]. Each bead described a dragline silk cylinder segment of length $r_0 = 1$ mm and diameter $d = 3$ μm, which was within the range of silk fiber diameters measured for *Latrodectus hesperus* spiders, belonging to the same family (*Theridiidae*) as the *Tidaren sisyphoides* spiders [96]. The modeled silk had density $\rho_{silk} = 1.3$ g/cm^3, which was the density of silk measured in [94]. This silk's bending stiffness, damping effects, and breaking strain were described in Chapter 2.

In addition to parameterizing the silk and web models, we also added a spherical bead that represented the spider at the location measured in the images. The bead had a diameter $d_{spider} = 6$ mm and weight $m_{spider} = 5.8 \times 10^{-2}$ g, which were the diameter and weight measured for *Tidarren sisyphoides* female spiders in [102]. Then, the fibers inside and passing through the spider bead were removed so that they were directly connected to the

spider bead surface. We defined four types of beads: the boundary, free, spider-center, and spider-surface beads. Boundary beads represented the ends of the silk fibers attached to the metal frame: they were fixed during the simulation. Free beads were the beads belonging to the silk fibers: they followed the mechanical properties of silk and were free to move. The spider-center was the bead representing the spider. Spider-surface beads were beads with silk properties that are attached to the surface of the spider bead. We used MATLAB to prepare the eight web models and simulation scripts. We used OVITO (Open Visualization Tool) [98] to render the visual representations of the model.

4.2.5 Spider Web Relaxation Simulations

The eight web models, of the web stages over seven days, were equilibrated during 10 s. The simulation timestep is 1×10^{-7} s.

4.2.6 Spider Web Stretching Simulations

We applied uniaxial stretching along the x, y, and z-axes at a rate of 0.1 m/s on the eight spider web models, resulting in 24 simulations. The simulations ended when the spider webs reached 900% strain. We output web stresses and web strain from the simulations.

4.2.7 Spider Web Projectile Simulations

Spider webs are subject to prey impacts which are a source of food for the spider. Flies impacting the web, as commonly occurs in nature, were represented as sphere projectiles. The projectile had a diameter of 7 mm and weight of 4.7 mg, which was calculated using the model in [99]. For each of the eight spider web construction stage models, sphere projectiles were thrown at the speed of 0.5 m/s, along the x, y, and z-axes following a 3D Cartesian 2 cm-spaced grid. The speed of 0.5 m/s was chosen from previous results from Chapter 3, it is the threshold over which the fly will get caught in the tent region of a *Cyrtophora citricola* spider web. For example, for one face of the spider web cube, the projectiles were thrown along the axis perpendicular to the face following a 2 cm-spaced grid. There were 36 different projectile impact locations for each face, which led to 1728 different locations for eight web

cubes. For each simulation, only one projectile was thrown. To save simulation time, we omitted impact locations where no fibers were in the way of the projectile's trajectory, resulting in 1504 projectile simulations. We output projectile position and velocity from the simulations. We used MATLAB to process and visualize the projectile impact results.

4.3 Results and Discussions

4.3.1 3D Spider Web Construction

We first investigate the different web architectures at different stages of construction. Under laser light and a restricted web building environment, the spider built a tangle web, which is similar to *Tidarren sisyphoides* spider webs found in nature [104, 86]; however, some *Tidarren sisyphoides* add aerial sheet elements to their webs, as described in [31, 105]. Figure 4-3 compares the web scans and models over time. The density increases from 0.07×10^{-5} to 3.56×10^{-5} kg/m^3 over seven days of construction. The scans and models show that the spider builds the foundation of the web geometry during the first two days of construction, after which the spider reinforces exiting network with limited expansion of the structure within the frame. The spider web construction progress is not linear, as the main structure of the web is built in the first two days. Indeed, the web density increases by 700% between day zero and day one, 400% between day one and day two, and only 9% between day two and day three. This behavior is similar to what has been described in [31], the *Tidarren sisyphoides* spiders use one to four nights to build complete and functional webs and then add silk threads to the web the following nights. V4-1 is a montage of the consecutive scans taken along the depth of the spider web, where each video frame is a superposition of all the scans over 7 days of one slice of the web. The days are color coded from dark blue to yellow. The video shows the changes in the 3D web structures over time. We observe that the nodes connecting the same fibers shifted position over time; otherwise, all the video frames would have the color of the last day (yellow). By adding silk structures to the web, the spider tunes web tension and fiber connection locations.

The construction behavior of the *Tidarren sisyphoides* spider can also be observed

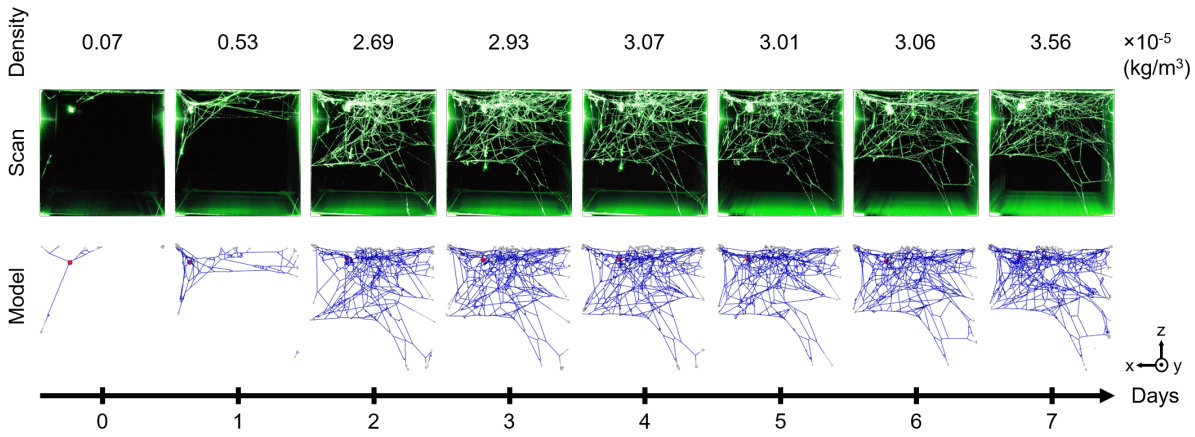

Figure 4-3: Comparison between scans and model of the 3D spider web under construction. (Top row) Each scan image is an image superposition of all the scans over depth. (Bottom row) 2D view of the 3D web model. The web density increases as the construction progresses.

through the fiber length distribution of the different web construction stages (Figure 4-4A). We observed that most fibers making the web are spun during the first two days of construction, after which, the number of fibers increases slowly over several days. From day zero to day one, the fiber length median increases from 2 mm to 3 mm. From day three of the construction the fiber length median is stable at 4 mm. This confirms, once again, that the main structure is built within the first two days, then, the structure is reinforced without expansion over the following days. The *Tidarren sisyphoides* spider web here follows a similar skewed fiber length distribution to the *Cyrtophora citricola* spider web described in Chapter 2. Moreover, the average fiber length of the *Cyrtophora citricola* web is of 3 mm (Chapter 2) which is comparable to the web described in this study. Figure 4-4B shows the node degree distribution of the different web construction stages. In graph theory, the degree of a node is the number of edges connected to a vertex [106], which in the case of the spider web means the number of fibers that are connected to a node. The node degree ranges from 1 to 16, but only 1 or 2 nodes have degree above 7. The high degree nodes could be artifacts from image processing on scans with higher laser light noise. Nodes of degree 1 and 2 are nodes that are attached to the frame, in which the spider spins the web. The fibers are considered straight, so there are no nodes of degree 2, unless they are attached to the boundary frame. Most nodes have a degree 3, which means that most fibers are attached to two other fibers. The degree distribution is very similar to *Cyrtophora citricola* spider web,

which also have most nodes with a degree 3 (Chapter 2). The number of nodes of degree 3 increases greatly in the first two days, which is consistent with what has been observed in the scans, models, and fiber length distribution.

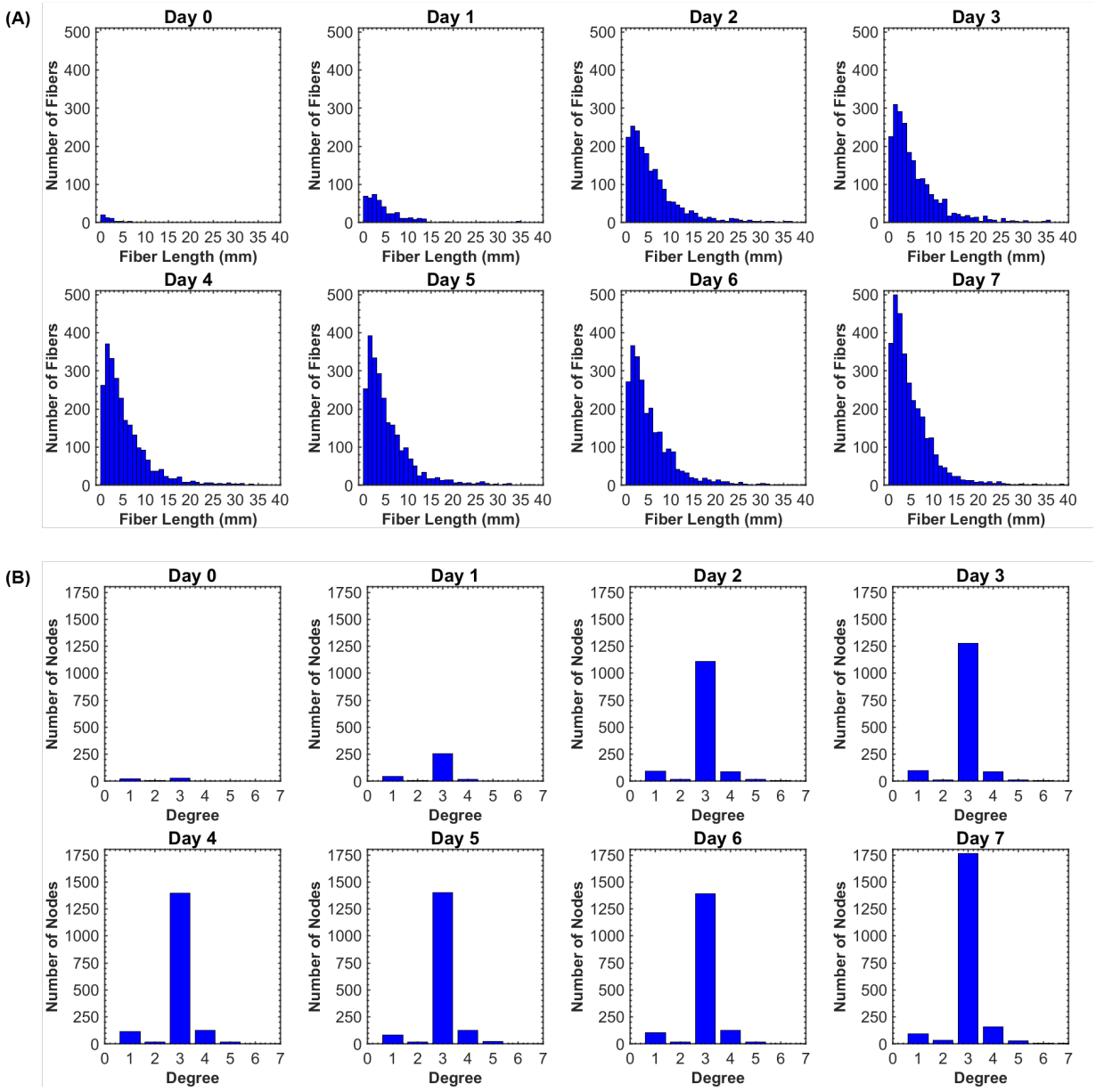

Figure 4-4: Fiber length and node degree distribution histograms over seven days of web construction. **(A)** The fiber lengths follow a skewed distribution, as most fibers are shorter than 4 mm. As the construction progresses, the fiber length median increases within the first two days then is stable after the third day of construction. **(B)** The node degree is the number of fibers that are connected together at a node. Nodes of degree 1 and 2 are fiber extremities that are attached to frame boundary. Most nodes are of degree 3, which is consistent with what has been derived for the *Cyrtophora citricola* spider web [5]

The upgraded, remote, and automatic method for scanning and modeling spider webs

can be used efficiently for tracking stages of construction of a spider web and it can be used consistently for different types of spider species. However, there is a trade-off between web imaging frequency and quality. High-quality images of a spider web require the spider not to move excessively, as this can disturb the web structure and lead to blurry images over the duration of the whole web scan (34 min). A higher scanning speed lowers the chance of the spider moving, but leads to lower resolution web images. *Tidarren sisyphoides* spiders, belonging to the Theridiidae family, usually build their webs at night as they are sensitive to light which could disrupt web construction [31, 86]. Increasing the web scanning frequency would show more details of the construction over time; however, more laser scans would likely slow down or even stop web construction. As an opportunity for future work, the current experimental setup could be improved by adding infrared light and a camera that could record the position of the spider over time without the need for visible light. With an infrared component, we would be able to follow the position of the spider which would help with deriving the fiber placement and reinforcement sequence.

4.3.2 Spider Web under Stretching

In nature, spider webs that are attached to moving supports, such as tree branches, sliding windows, and cupboard doors, are being constantly stretched. Under those natural stretching conditions, spiders are able to build strong and resilient webs that are functional and repairable. To understand whether the web can withstand stretching during construction, even before being fully complete, we investigate the mechanical performance of 3D spider web construction stages over time under uniaxial stretching. The composite stress-strain curves of the spider web over seven days of construction under uniaxial stretching along the x, y, and z-axes are shown in Figure 4-5A. The stress-strain curves show that the spider webs first follow a linear elastic behavior, then a nonlinear stiffening until the failure of the first fiber, after which the web is subject to continuous fiber failures. The nonlinear behavior and failure of individual silk fibers can be found within the composite stress-strain curve of the web. Indeed, the spikes coincide with individual fibers breaking. After the fiber bearing the load reaches its failure stress and breaks, the load is transferred to its connecting

fibers. Because of redundancy in the structure and nonlinear behavior of dragline silk, the spider web does not fail catastrophically at any stage of construction. A similar behavior can be found for the tangle regions of a *Cyrtophora citricola* spider web, which is more than ten times denser, under uniaxial stretching [107]. In addition, web strength increases with web density, which increases as the construction progresses. Denser webs have a higher strength because more fibers contribute to carrying the load generated by the uniaxial stretching of the web. In particular, web strength increases greatly in the first two days of construction, which is when the main web structure is built. After the second day of construction, the web strengthens slowly, as the spider reinforces its web without expansion.

Using non-destructive uniaxial stretching simulations of the different stages of web construction, we show that the spider first focuses on building the main structure within only a few days, which is strong and resilient. Even at the early stages of construction the web avoids catastrophic failure, as sequential fiber failure distributes the loads to the connected fibers via the combination between web redundancy and nonlinear dragline silk. This allows the spider to repair the existing web without needing to build a new one. From this strong web foundation, the spider adds silk to reinforce the web on subsequent days, increasing web density and consequently web strength. The spider's construction method consists of prioritizing a fast build of the structure followed by slow structural reinforcement, while using only silk as material and keeping the structure stable and functional throughout construction. This approach could inspire more sustainable fiber structure construction methods that are stable, functional, repairable, and always reinforceable.

Web strength and toughness increase with density, which increases with construction time, as is summarized in Figure 4-5B. The increase of web strength and toughness has also been described for a *Cyrtophora citricola* spider web in [107]. Web strength and toughness variations with web density are fitted using the equations:

$$\sigma_x = d \times 2.929 \times 10^4 + 0.2096 \tag{4.1}$$

$$T_x = d \times 5.923 \times 10^4 + 0.09969 \tag{4.2}$$

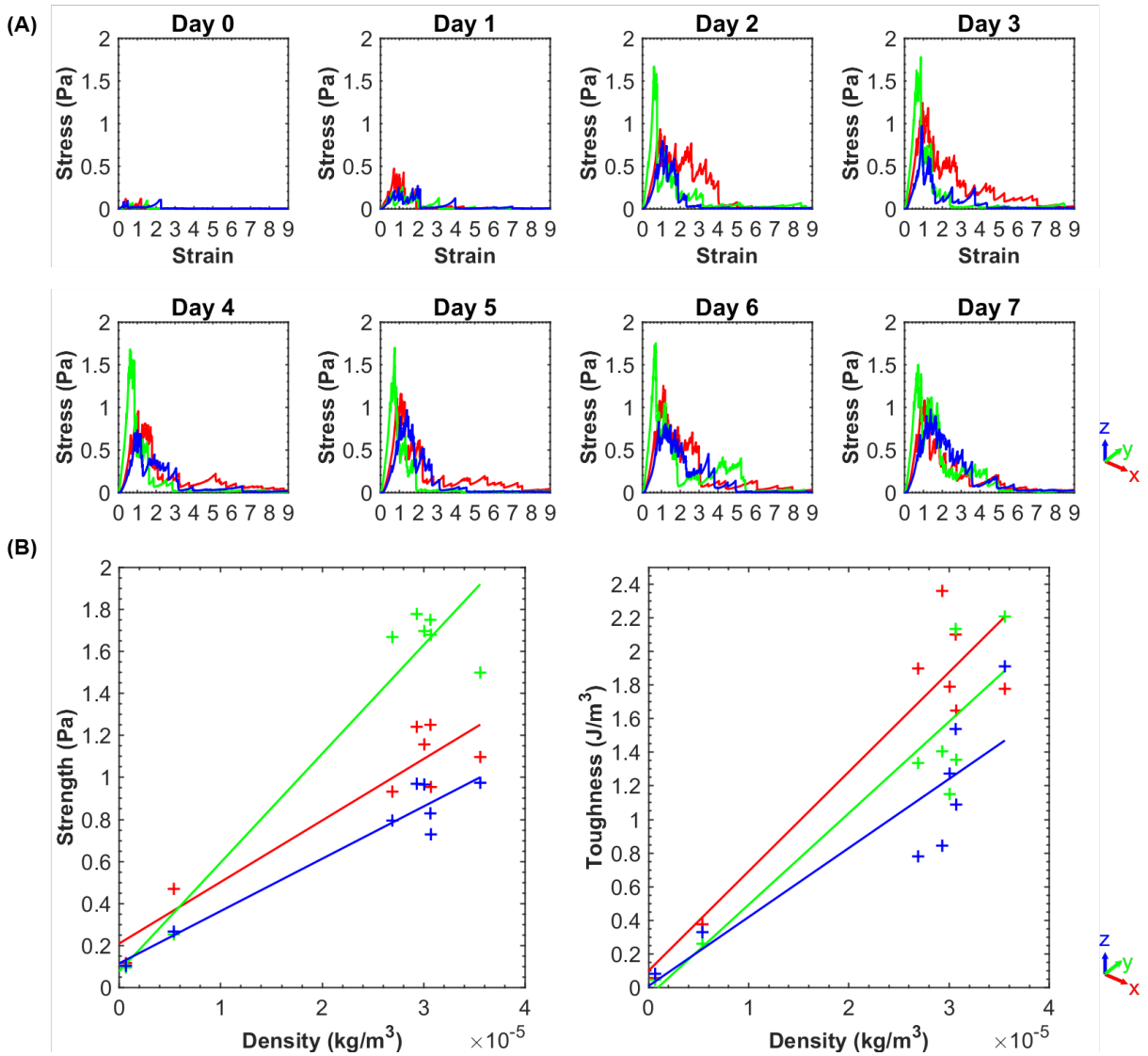

Figure 4-5: Web strength and toughness increase with density which increasing over building time. **(A)** Stress-strain curves of 3D spider webs at different construction stages under uniaxial stretching along the x, y, and z-axes. **(B)** Variation of strength and toughness with web sample density. Web strength and toughness increases with density which increases as web construction progresses.

$$\sigma_y = d \times 5.18 \times 10^4 + 0.07719 \tag{4.3}$$

$$T_y = d \times 5.445 \times 10^4 - 0.05103 \tag{4.4}$$

$$\sigma_z = d \times 2.491 \times 10^4 + 0.115 \tag{4.5}$$

$$T_z = d \times 4.109 \times 10^4 + 0.008784 \tag{4.6}$$

With σ and T, web strength and toughness along the x, y and z-axes, and d den-

sity. The web strength increases more with density along the y-axis, because more fibers are aligned in the y-direction. Web toughness increases with density because of the web redundancy; the uniaxial stretching load is transferred to one or a few fibers at the time, which is transferred to other fibers once they break.

Uniaxial stretching simulations are a non-destructive method to measure the strength and toughness of the *Tidarren sisyphoides* spider web throughout construction. Through web visualization (Figure 4-3) and an analysis of mechanical properties (Figure 4-5), we show that most of the web's structure and mechanical performance is realized between day one and day two of construction. Taking inspiration from the mechanics of webs during construction could lead to lightweight and high-performance network composites with stable architecture and tunable properties throughout construction.

4.3.3 Spider Web under Projectile Impact

Spider webs are naturally subject to projectile impact from prey, predators, and debris, which is why webs are rarely found intact in nature. Here, we investigate the prey catching performance of the *Tidarren sisyphoides* under different stages of construction to test the hypothesis that spider webs are functional throughout construction. Projectiles, representing a fly prey, are thrown at a velocity of 0.5 m/s, into the different locations of the web. Each simulation consists of one projectile thrown into the web under construction at one location. Figure 4-6 shows the projectile deceleration map, where the ratio of speed after impact over the speed at impact is colored from red to dark blue, for high deceleration to no deceleration, respectively. The maps are mostly blue, which means that the velocity ratio remains high for most impact locations. The spider web lets most of the flies through without slowing them down because of the very low density of this spider web. Most projectiles would hit one or a few fibers and slide through the web. While most prey escape the web, we can identify a few locations where the projectile will considerably slow down each day of the construction from day one. The locations where the projectiles greatly decelerate are the areas where prey has a higher chance to get caught by the spider. After one day of web construction, the spider is able to catch food if the prey enters the web at a specific

location. At each stage of web construction, the location of high prey deceleration changes, demonstrating that the spider tunes its fiber architecture over time, although the foundation of the structure remains the same. While the *Tidarren sisyphoides* spider used in this study did not create aerial sheet elements, some spiders of this species add an aerial sheet to their webs [31, 105]. This allows the spider to sense prey entering the tangle web as it drops onto the sheet, allowing the spider to then attack [31]. Similarly, the tangle region of the *Cyrtophora citricola* web would help filter and slow down the prey entry into the tent region where the spider waits [107]. Here, we have shown that the web can efficiently decelerate prey projectiles. Consequently, the web increases the probability of catching prey at very specific locations in the web and after only one day of construction.

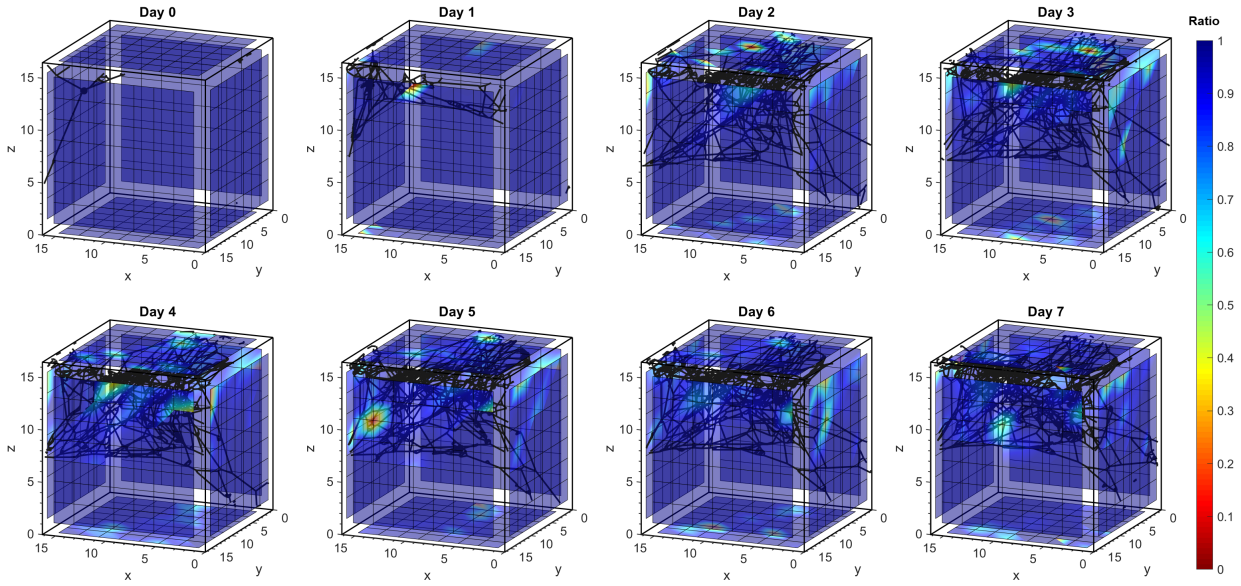

Figure 4-6: Projectile impact deceleration map. The color map represents the ratio of the speed after web impact over speed at impact (0.5 m/s). (Units in cm). Most prey projectiles fly through the web because of its high porosity. After the first day of construction, the web can decelerate prey projectiles at very specific locations and consequently increase its capture.

4.4 Conclusions

This study presents novel insights on into the mechanical and functional performance of a 3D spider web during construction. In particular, we focused on the tangle web of the *Tidarren sisyphoides* spider. We advanced our existing web scanning method, which previously could only be used for completed webs, into a fully automatic and remotely monitored

scanning setup for spider webs under construction. Using image processing algorithms, we transformed 2D images of slices of the web into a 3D fiber network. The scans and web models showed that the *Tidarren sisyphoides* spider built most of the web structure in the first two days of construction, after which it used silk to reinforce and tune the structure without expansion. We used meso-scale bead-spring particle dynamic simulations of the web at different construction stages to investigate its mechanical behavior under uniaxial stretching and prey projectile impact. We found that web strength and toughness increased with web density, which increased over construction time. Throughout web construction, the *Tidarren sisyphoides* spider web is robust and resilient; it avoids catastrophic failure because of its complex architecture and the nonlinear mechanical behavior of dragline silk. The spider can then repair defects to maintain web functionality such as decelerating and catching prey. We then simulated prey projectiles being thrown at the spider web at hundreds of different locations per construction stages. Due to the web's high porosity, most prey passed through the web. At very specific locations, starting from one day of construction, the spider web could cause considerable deceleration of the prey, thus increasing the capture rate. Learning from and improving on the spider's construction process could lead to innovative assembly method for stable, functional, repairable, and reinforceable fiber structures.

In nature, *Tidarren sisyphoide*s spiders build tangle webs [104, 86], with some adding aerial sheet elements [31, 105]. In the artificial environment created in this study, the *Tidarren sisyphoides* spider did not add any aerial sheet components. This may be as result of a number of environmental and biological factors, such as diet, age, light sensitivity, and space constraints. Spiders adopt behavioral plasticity to change their silk-spinning and web-building behaviors in response to selective pressures [84]. Indeed, web geometry could depend on the energy level of the spider; in one study, starved western black widow *Latrodectus hesperus* spiders designed their webs to catch prey more efficiently than fed spiders [84]. Using the automated and non-destructive imaging, modeling, and simulation methods reported in this chapter, we now have a way to study the effects of those parameters. For example, we can quantify the change of web construction behavior under external stimuli such as minimal substrate, expanding, vibrating, and long-span supports. Investigating how spiders

adapt their web-building behavior to artificial environmental stimuli, may lead to flexible and adaptable 3D network structures and assembly methods in complex environmental conditions.

Moving forward, we can use these imaging methods and computational simulations to investigate the architectural and mechanical properties of webs built by different spider species in different artificial environments. Computational simulations are essential for studying the web over time without disturbing the spider and destroying the web. The scanning, imaging, and simulations can be used in an automated and systematic way. Using this consistent method, we can investigate webs built by different species and generate more geometrical, construction, and mechanical web properties that can be used for deep-learning to design spider and web-inspired architectures, material assembly methods, and mechanical properties for specific functions. To obtain even more details on the fiber assembly sequence, we can add infrared lights and cameras to the experimental setup to minimize light disruption and follow spider movements during construction. This could lead to efficient spider-inspired fabrication sequences for complex fiber structures. Expanding our knowledge of spiders' web construction, silk recycling, web monitoring, and repair methods could inspire novel self-sufficient, self-repairable, and self-monitored smart structures.

Chapter 5

Sonification of a 3-D Spider Web

This research and review presented in this chapter will be published in:

- **Su I**, Qin Z, Bisshop A, Mühlethaler R, Saraceno T, Ziporyn E, Buehler MJ: "Sonification of a 3D Spider Web and Reconstitution into Musical Composition using Granular Synthesis." *Comput Music J.* 2021 (accepted)

5.1 Introduction

In the previous chapters, we derived the topologies and mechanics of 3D spider web, completed and under construction. We made possible the visualization of the 3D spider web with image processing and visualization software. However, because of the complex structure of the webs, finding features would require manipulating the web model or carrying out a computational analysis. For example, we need to rotate and zoom a 3D physical model to derive its information [58]. Adding sonification, a visualization method through sound, would complement the visualization, and add another perspective for understanding the model and natural spider webs, and identifying key web features.

By using the correlations between music and silk, we propose a parameter mapping sonification of 3D spider web data that enables a more holistic comprehension of the complex geometric features. This work presents a new way to aurally perceive the intricate architectures of 3D spider web, which could open new pathways for musical expression and creative

instrument design.

5.2 Materials and Methods

5.2.1 3D Spider Web Topology Data

The spider web topology was obtained using the automatic laser scanning and image processing protocol defined in Chapter 2. A 35.6 × 35.6 × 24.4 cm 3D web was built by a *Cyrtophora citricola* spider and scanned by capturing images of planes illuminated by a sheet laser moving automatically through the web. From each of the scans, the web topology was derived using image processing tools and line finding algorithms (Chapter 2). The *Cyrtophora* web is composed of a tent region sandwiched between two tangle regions. The tangle region above the tent is denser than the tangle region under the tent [5]. The 3D spider web data was described with a list of node coordinates, with each node connecting intersecting fibers, and a list of pairs of nodes that represented the end points of each fiber. In this study, we focused on the complex tangle region of the web. We chose to focus our study on the tangle region, instead of the tent region which is mostly horizontal, in order to explore an irregular and complex 3D fiber architecture through sound. We chose to sonify two different 76 mm cube samples of the dense and porous web, extracted from above and below the tent region and with different volume fractions of 2.0×10^{-7} and 1.1×10^{-7}, respectively.

The volume fraction was calculated by dividing the fiber volume in the cube by the volume of the cube (439 cm^3). The dense sample was 1.7 more dense than the porous sample. We estimated the thickness of the fibers to be 4.34 μm [79].

5.2.2 Parameter Mapping Sonification

In these two web sonifications, we aimed to derive a true reflection of the 3D spider web data in the form of sound. We used the parameter mapping method, often used to describe multivariable data [58], to map the three-dimensional web data into audio. Parameter mapping sonification consists of mapping the data into a sonic event through acoustic characteristics [58, 57]. In this study, from numerous possible acoustic characteristics we used

pitch, amplitude, time, and release to map the spider web data, reducing the dimensionality of the data and facilitating data perception. The sonification of such a complex spider web structure resulted in a polyphonic piece, in which the data blend and overlap in ways that cannot be easily mapped back to the original data by our human perceptual faculties.

5.2.3 Sonification Rules

To sonify the spider web data, we chose a set of rules that select only the essential data for visualization and interpretation through sound. For each web, we sonified the data in the form of slices along x, y and z-directions, what we term in this paper the sonification direction. We only described rules for a z-direction sonification, the x and y-direction sonifications were obtained by rotating the web sample so that what was previously the z-axis was aligned to the x or y-axis. The z-axis passes through the center of each slice of the web sample, and was interpreted as a function of time. This means that sound appearing early in the resulting sonification describes fibers that have low z-coordinates, and sound appearing later in the sonification corresponds to fibers with high z-coordinates (Figure 5-1A). Each fiber was assigned a note whose pitch depended on the distance between the center of the fiber and the z-axis. The distances to the fiber centers represent the fibers' average distance from the z-axis. The fibers whose center was closer to the z-axis had a higher pitch than those located farther from the z-axis. The note or sound corresponding to each fiber began and ended at the time points corresponding to the z-coordinate of the first and second extremity, respectively. The duration of the sound of each fiber directly correlated with the length of the projection of the fiber to the z-axis (Figure 5-1A). Long fibers were assigned a longer sound release duration. The envelope of the sound was described by a short attack followed by a linearly decreasing release, such that the amplitude of the sound increased very quickly for 0.02 s, then decreased linearly to 0 at the end of the fiber. Short attacks were added to avoid clicking sounds from the series of notes produced. Assigning a release time allowed us to hear and visualize the specific region of the fiber being described at a specific time. If the amplitude of a sound was high, this sound corresponded to the beginning of a fiber, and if the amplitude was low, the sound described the terminus of the fiber (Figure 5-1B). The connectivity of one node was described by the initial amplitude of the note: if a

given node was connected to multiple fibers, the initial amplitude was higher than a node connected to only one or two other fibers (Figure 5-1C). By superposing all the notes from the fibers, we were able to hear the density of the web: if the music sounds busy, the web that it described was dense in fibers; if listeners were able to aurally distinguish only a few sounds, the web was porous –as only a few fibers were sonified. The important parameters of the web captured by the sonification rules were: web density, fiber location, fiber length, and connectivity distribution.

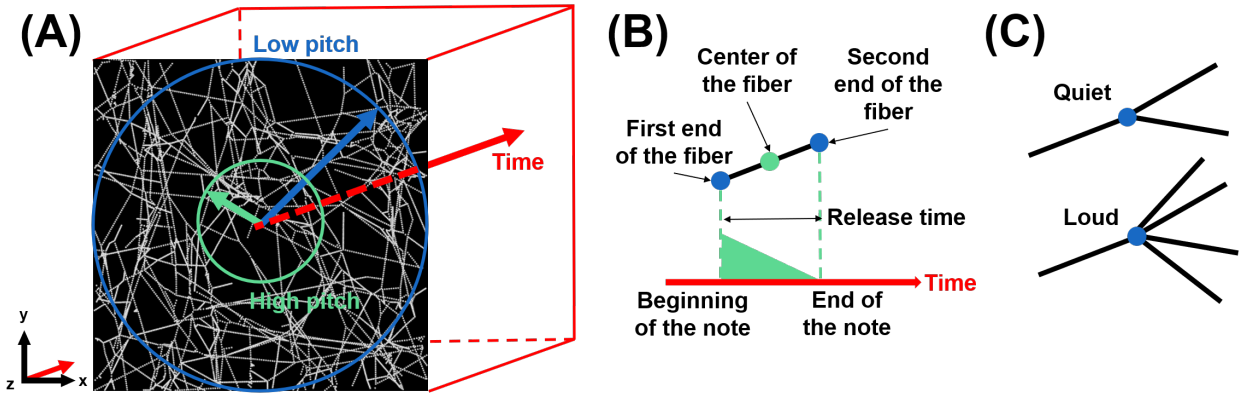

Figure 5-1: Schematics describing the parameter mapping sonification rules. **(A)** 3D spider web model and its translation into music. Each fiber was assigned one sound, determined by the xyz-coordinates of its middle point. The z-coordinates of the fibers corresponded to the temporal position in the musical composition. The higher the z-coordinate, the later the sound attributed to a fiber occurs. The distance of each fiber was translated into pitch; the closer the fiber was to the z-axis, the higher the pitch. **(B)** Correlation between fiber length and note length. Each note began and ended at time points corresponding to the z-coordinates of the first and second end points of the fiber, respectively. The longer the fiber, the longer the duration of the note. The release time of the note allowed the audience to locate themselves in the length of the fiber. **(C)** Correlation between connectivity and note amplitude. The more fibers linked from a connection, the louder the amplitude.

5.2.4 Musical Coding for Sonification

The web data sonification was carried out using the free software Sonic Pi (available at https://sonic-pi.net/), a computer program for coding music. The sound used for each web fiber was a pure sine wave, chosen for representing the simplest sonic building block. The combination of the simultaneous sine waves representing multiple fibers resulted in a more complex sound. The pitch varied from 15.49 to 135.08 in MIDI (Musical Instrument Digital Interface) notes, which corresponds to a range of 20 Hz to 20,000 Hz in frequency [108], the

described upper and lower audible frequency thresholds of the human ear [109]. The pitches were linearly assigned so that the highest pitch corresponded to the fiber whose center was located farthest from the z-axis, and the lowest pitch corresponded to fibers closest to the z-axis. The duration of all sonified music pieces was 76 s for the dense and porous webs, and in the x, y, z-directions, respectively. This duration was chosen so that the resulting musical pieces were short, but still long enough that the different sounds made by individual fibers could be audibly distinguishable. Indeed, the melodies should not be too long, as auditory temporal memory is not as efficient as visual memory [59].

The z-length of the cube was 76 mm, such that 1 mm of the web corresponded to 1 s of sonified music. The duration of the release and the temporal start of the notes were derived from these scaling rules. The connectivity of one node was defined by the number of fibers attached to each node, and was described by the amplitude of the corresponding note. The lowest amplitude was attributed to nodes that were connected to only one web fiber (free-end fibers), and the highest amplitude value assigned to the node with the largest number of connections. Sonic Pi was used to synthesize the sonification music and to save the resulting audio.

5.2.5 Visualizations

Data sonification was combined with data visualization to explore a holistic comprehension of the 3D spider web data. Using OVITO [98] and MATLAB [77], the data was transcribed into animations that coordinated with the sonification melody (Videos V5-1, V5-2, V5-3, V5-4, V5-5, and V5-6. Using the data from Chapter 2, we created a 3D model of the web: each fiber was constructed with a chain of beads separated by 0.1 mm. In addition, for the web sonification along the z-axis, we complemented the animations with a sequence of real spider web scans from Chapter 2 (V5-3 and V5-6), the scans of which the sonification and the model is based on. The scans are images of the web illuminated by a sheet laser sliding along the z-axis. The scan sequence animation is also synchronized to the sonification. The animations are composed of 760 frames, using ten frames per second.

One second in time corresponded to a 1 mm slice for both the dense and porous

webs. The animation videos are 76 s in duration, which corresponds to the duration of the sonification pieces. To better illustrate the music throughout the animation, the beginning of each fiber/note are represented with a larger red bead. Fibers/notes that have not reached their end extremities and thus are still an active part of the melody, are assigned colors as a function of their distances to the central sonification axis, ranging from yellow (close) to blue (far). Fibers/notes that have already been visualized and sonified are shown in white. With these animations, we can obtain a better understanding of the web data and data sonification (Figure 5-2B). Additionally, for the z-direction sonification we paired the music with an actual video of the laser scanning of the *Cyrtophora* web, to illustrate its accord with the sonified web (Figure 5-2A).

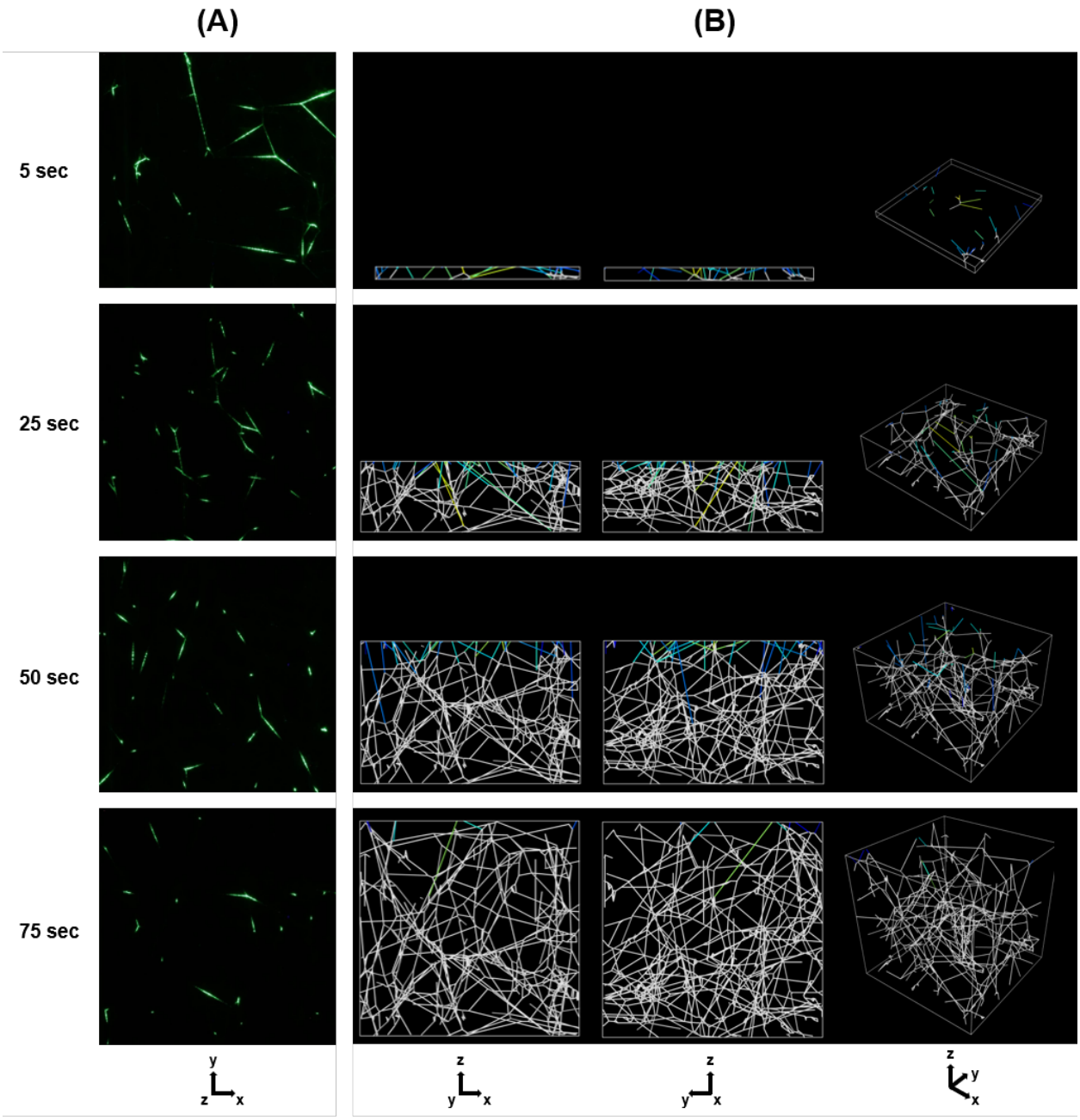

Figure 5-2: Snapshots of video (V5-3) at time 5, 25, 50 and 75 s (from a total duration of 76 s). **(A)** Spider web laser scan video from which the 3D model was derived. **(B)** Animations from model created by 3D spider web laser scan. Color code: in white the fibers/notes that have already been sonified. In yellow to blue, the fibers/notes still active in the sonification.

5.2.6 Spectrograms

To analyze the musically relevant features and consequently the spider web's key topological features, we created a spectrogram representing the audio data in the frequency

spectrum for each musical piece (Figure 5-3), using Sonic Visualiser [9]. In particular, we used a melodic range spectrogram, which has a logarithmic frequency scale (linear scale for perceived musical pitch). The linear color scale shows the loudness of the important frequencies. For example, frequencies with a higher amplitude (louder sounds) are represented in yellow, and frequencies with a lower amplitude (quieter sounds) in blue.

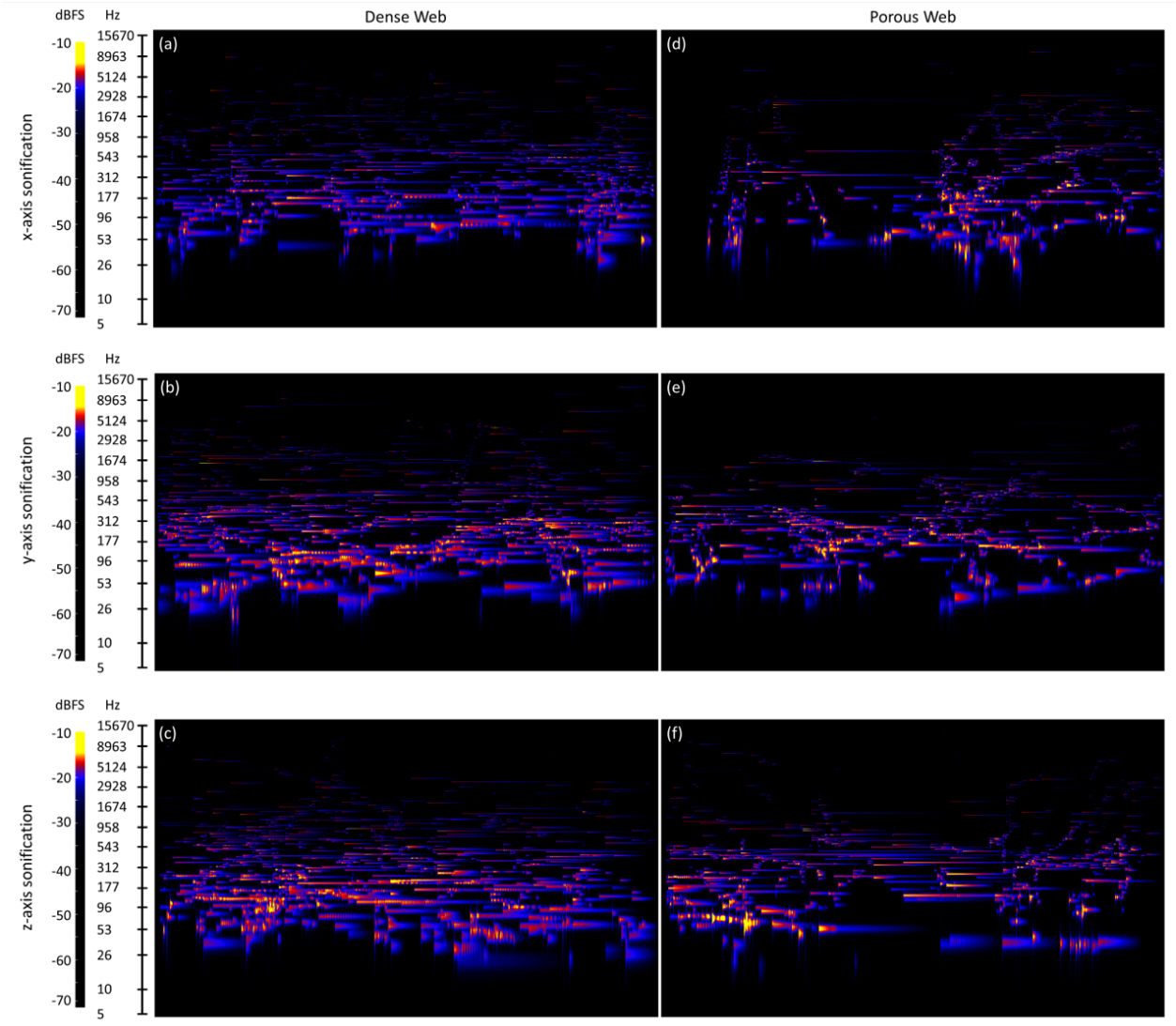

Figure 5-3: Melodic range spectrograms (produced using Sonic Visualiser [9]) of the dense and porous webs (columns) sonified in the x, y, z direction (rows), offering a visual comparison between the audio signals corresponding to the two types of web structure, and between the different sonification axes. The vertical axis represents frequencies ranging from 5 Hz to 15670 Hz. The horizontal axis is the time ranging from 0 s to 76 s (duration of all the pieces). The color scale represents the loudness of the notes, ranging from the quiet notes in blue to the loud notes yellow.

5.3 Results and Discussion

We first create six musical pieces from 3D web data sonifications (M5-1, M5-2, M5-3, M5-4, M5-5, and M5-6) paired with video animations (V5-1, V5-2, V5-3, V5-4, V5-5, and V5-6).

M5-1: busy music, sonification of the dense web along x-axis

M5-2: busy music, sonification of the dense web along y-axis

M5-3: busy music, sonification of the dense web along z-axis

M5-4: less busy music, sonification of the porous web along x-axis

M5-5: less busy music, sonification of the porous web along y-axis

M5-6: less busy music, sonification of the porous web along z-axis

Each of the musical pieces is 76 s in duration, for sonifications of both dense and porous webs. By analyzing the sonification musical compositions and comparing them to the web architectures, we derived interesting insights into web properties such as porosity, fiber length, and connectivity. For each of the musical pieces, we were able to hear superposition of continuous sine wave sounds at different amplitudes and different pitches, and at an irregular tempo.

To interpret the melodies, the audience must immerse themselves in the web. It is as if the audience are moving along a track that follows the sonification axis (x, y or z-axis) inside a physical spider web over time. As the music plays, the audience travel along this axis, and hear a sonic representation of the fibers located in the slice orthogonal to the sonification axis (and thus the audience's position on the sonification axis). In this way, we might think of the auditory perception of this piece in terms of passive radar – a process of aurally detecting the spatial features of fibers, including their distance to the audience (pitch), length (duration of the notes), and connectivities (amplitude). For each of the musical pieces, four relationships apply: first, the higher the pitch, the closer the fiber is to the audience; second, the louder the start of the notes, the more fibers are connected to the starting node; third, the longer the sound, the longer the fiber; and fourth the more sounds overlap, the denser the web.

We used the melodic range spectrograms (Figure 5-3) to discern and analyze the key

topological features of the webs. The fibers, sonified as frequencies, are clearly represented by horizontal color line segments. For the dense webs (Figure 5-3), the spectrograms show a comparatively uniform distribution of the notes/lines over time and frequencies, which suggests that the dense web also has a uniform distribution of fibers along the sonification axis. On the other hand, for the porous webs (Figure 5-3), the note distribution is not uniform: there are time intervals where only a few fibers can be seen (in the spectrograms) and heard (in the recordings), which correspond to regions of the webs with fewer fibers.

Similarly, when we listen to the recordings, the sonification of the dense web has a fast tempo with many overlapping notes. The audience hears fast, short notes with slow, long notes in the background, which means that the dense web has long fibers with numerous short fiber branches. The recordings of the porous web have intervals similar to those of the dense web, but also contains intervals where the audience hears only several long notes, with fewer overlapping notes, and in which the tempo slows. When comparing the dense web and porous web pieces, the denser web sonifications contain more overlapping notes, such that the sounds are almost undistinguishable for some parts of the audio. The spectrograms (Figure 5-3) show that the porous web is not as musically busy as the dense web, as there is less overlap of sounds. The porous web is globally quieter than the dense music, which confirms that this web has fewer highly connective nodes and less branching out of fibers. Using sonification, we can store, interpret and find new patterns in the complex 3D spider web data. Without using visual representation, the audience is able to listen to and grasp the density, location, connectivity, fiber length of the web.

With the set of rules implemented in this study, we can transcribe the 3D spider web data into a musical piece. However, it is not possible to easily reverse engineer this sonification to 3D web data. Indeed, during the sonification process, the dimensionality of the web was reduced to a few parameters (pitch, amplitude, release) in order for it to become interpretable and perceivable by the audience. For example, the z-axis sonification did not contain information about the xy-location of the fibers, in particular the first and second end nodes of each fiber, as our sonification rules illustrated only the distance of the middle of the fiber to the z-axis. One way to solve this reversibility limitation would be to assign

pitch to one dimension (x), assign an instrument or discrete timbre to the other dimension (y), and let the notes of the fibers vary along their length (time). For example, one fiber parallel to the x-z plane (constant y) will have one continuous pitch glide with and one timbre. Fibers aligned in the y-z plane (constant x) will have the same pitch played by different instrument or timbre over time. This set of rules could preserve the xyz-location of all the fibers. Nevertheless, it would generate discontinuities of the sonic representation of individual fibers, as the timbre could change along the length of each fiber. A partial solution would be to map the distance to the fiber continuously to pitch instead of mapping the average fiber distance to the center. This would result in more direct sonification based on glissandi, however the fiber coordinates would remain unknown. Another possible solution would be to assign pitch to x, y, and z so that the length of a fiber produces an interval rather than a single pitch. However, this solution might make it difficult for an untrained audience to interpret a more complex musical piece.

There are a number of other possible methods to sonify the spider web data, such as model-based sonification where the data is analogous to an instrument that a user can play interactively [58]. Understanding these connections between the web architecture and its translation in music through sonification offers the audience another perspective by which to interpret the data, and eventually find new patterns, which may be difficult to visualize through vision alone. Moreover, making the sonification reversible could lead to new and improved spider web-inspired structural designs generated from both existing and new musical pieces.

5.4 Conclusions

This study presents a 3D spider web data sonification as a method for interpreting, finding new patterns, and storing the complex 3D architecture of webs. A simple set of rules translates the 3D data into sound using a set of rigorously defined parameters: pitch, amplitude, and release time. Through parallel sonic and visual explorations of this data, the audience can virtually immerse themselves in the 3D web. They are able to perceive and understand length, distance, connectivity of web fibers, and web density.

We note that the process by which the data sonification works is not unique, the objective of this approach is not to demonstrate the uniqueness of the mapping exercise, but to illustrate the mapping.

Understanding this two-way translation represents a novel approach to designing and improving spider silk and web-inspired material and structure through music.

Chapter 6

Exploration of a hierarchical spider web structure with sound

This research and review presented in this chapter will be published in:

- **Su I**, Hattwick I, Southworth C, Ziporyn E, Bisshop A, Mühlethaler R, Saraceno T, Buehler MJ: "Interactive exploration of a hierarchical spider web structure with sound." *J Multimodal User Interfaces.* (revision)

6.1 Introduction

Sonification is an excellent tool for data exploration [58] as the human ear is well-suited to the perception of temporal changes and pattern identification, allowing for the identification of interesting data patterns in large and complex datasets [110, 67, 111]. Combined with a visual representation, data sonification provides a more holistic experience of the data and can deepen our understanding of it, especially when the data is difficult to interpret with sight only [112, 58].

Depending on the application and the interactivity of the system, a specific sonification technique may be used. Parameter-mapping sonification is the most commonly used method, and consists of translating data into sonic events and assigning variables to a variety of acoustic characteristics, such as pitch, amplitude, time, and envelope [112, 58]. A

more recent method is model-based sonification: the data is transformed into a dynamic model, which generates sound through user excitation [58]. Interacting with this dynamic model is similar to tuning and playing a musical instrument [113], since in both cases the user is able to adjust and excite the model. Aside from observation, humans primarily learn through interaction with the physical world [114], which explains how effective interactive sonification can be. Sonification for scientific applications such as data mining or exploration requires accuracy, while sonification for musical applications needs to be aesthetically pleasing. Nevertheless, accuracy and aesthetics often work together in sonification, both for art and science. Aesthetics helps the user stay focused on the sonification piece [115]. Accuracy conserves data precision and prevents introduction of human artifacts [115]. Using interactive sonification, the user can decide which aspect of the sonification to prioritize, and tune the parameters to find a suitable balance between accuracy and aesthetics for a particular application [115].

The hierarchical architectures of spider webs and music have many similarities. Spider webs' hierarchical structure ranges from silk protein, to micrometer-sized fibers, to cm-scale spider webs [116, 117, 11, 53]. Similarly, music is organized at its lowest scale in sine wave building blocks, which can be assembled to design richer timbres. At its highest scale, musical compositions are created from a combination of timbres [112, 60, 61]. Spiders use vibrations to communicate and sense prey, predators, and environment [64, 63]. A spider web can also be compared to a musical instrument as the spider tunes and plays its web for communicating, foraging and protecting [49, 65]. The correspondence between spider webs and musical instruments (and the spider as "musician") was previously explored artistically by Saraceno et al. [118] through the scientific framework of biotremology (vibrational communication).

In Chapter 5, we proposed a non-interactive sonification approach that requires the listeners to know and understand the sonification rules in order to analyze the piece and derive insights from the web [112]. As humans already intuitively interact with real-world objects, their environment, and other humans [58], adding an interactive aspect to spider web sonification can improve users' experience and allow them to navigate through and manipulate the complex 3D fiber network data more efficiently [67, 113]. An interactive

3D web holistic exploration audiovisual tool can help researchers, musicians, artists, and any listeners to locate essential features and patterns of the web. Understanding 3D spider topology can lead to a better comprehension of its role, with silk, in carrying the functions of the webs.

Using model-based sonification and the analogy between spider webs and music, we propose and implement an interactive sonification model of the 3D spider web. We describe how this model can be used as a musical instrument for art performances, as done through the Spider's Canvas/Arachnodrone project (arachnodrone.com). We discuss how we can use this model for exploring spider web architecture and finding key topological features. Finally, we explore future applications of this data exploration musical instrument for data mining, arts, and 3D network holistic experiences.

6.2 Materials and Methods

6.2.1 Spider Web Sonification Model

Contrarily to parameter-mapping sonification, where data is mapped to sound with acoustic characteristic (which offers limited interactivity and freedom), model-based sonification (MBS) is a sonification technique that translates the data into a dynamic model which produces sound with user excitation [58, 114]. It is by definition an interactive sonification. The model generates sound with user interaction in real time [58, 114], just as a musical instrument would respond to user action [113], and here, the data or the model is the instrument. Sounds rendered by the sonification model should be independent of the data [58], and the model is reusable for other data. A MBS model is configured following the six stages of model setup, dynamics, excitation, initialization, parameters, and listener characteristics [58, 114]. The sonification model is summarized in Figure 6-1.

Model Setup

The setup stage consists in connecting data to the dynamic model [58]. The spider web sonification model is based on fiber topology data of a real 3D *Cyrtophora citricola*

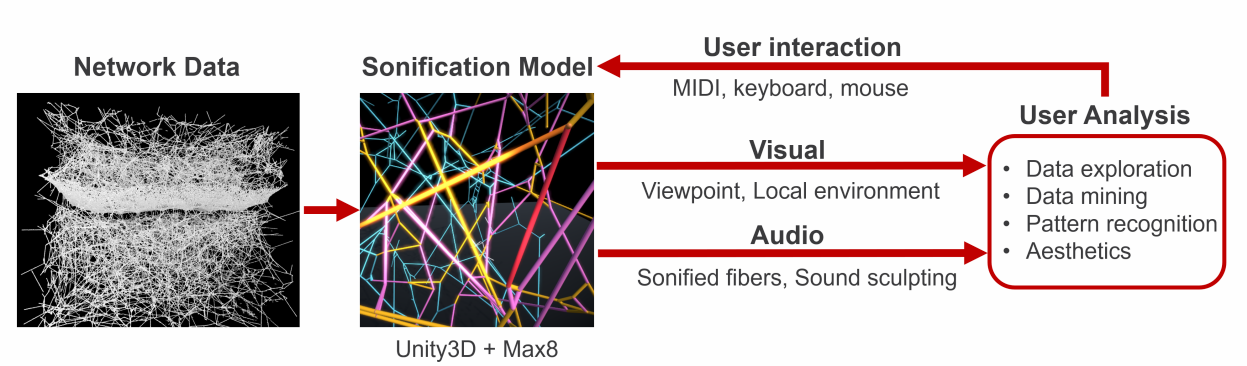

Figure 6-1: Schematic of the interactive sonification process of the 3D spider web. We load the network data, here, the 3D spider web structure, to the sonification model, built on Unity3D and Max 8. The user interacts with the model by sending commands through MIDI messages, keyboard and computer mouse. The sonification model produces audiovisuals that the user can use for data exploration, pattern recognition, and arts

spider web contained in a 35.6 × 35.6 × 24.4 cm frame, that we scanned and modeled in Chapter 2. The spider web is a network composed of nodes (connections) and links (fibers). The network data is composed of a list of nodes with their xyz-coordinates in space and a list of links with their two extremity nodes. The data has been normalized so that the longest edge of the frame is 1, to facilitate calculations. Here, the data space is the same as the model space, except their dimensions; the model is also a spider web network. The user in the model space is modeled as a capsule (virtual body) and a camera (virtual eyes).

Model Dynamics

The model dynamics configuration stage determines how data under analysis will produce sound [58]. The user of the spider web exploration tool controls what they look at in the modeled web. For example, they can decide whether to look at a cluster of fibers or not. The fibers in their field and within an adjustable hearing radius produce sound, or else they stay silent. Those rules are illustrated in Figure 6-2. The user can also choose to pluck a fiber that will produce sound and excite the neighboring fibers that may produce sound as well. The sound propagation time depends on the length of the neighboring fibers. The user can also produce plucking when their virtual body in model space touches a fiber.

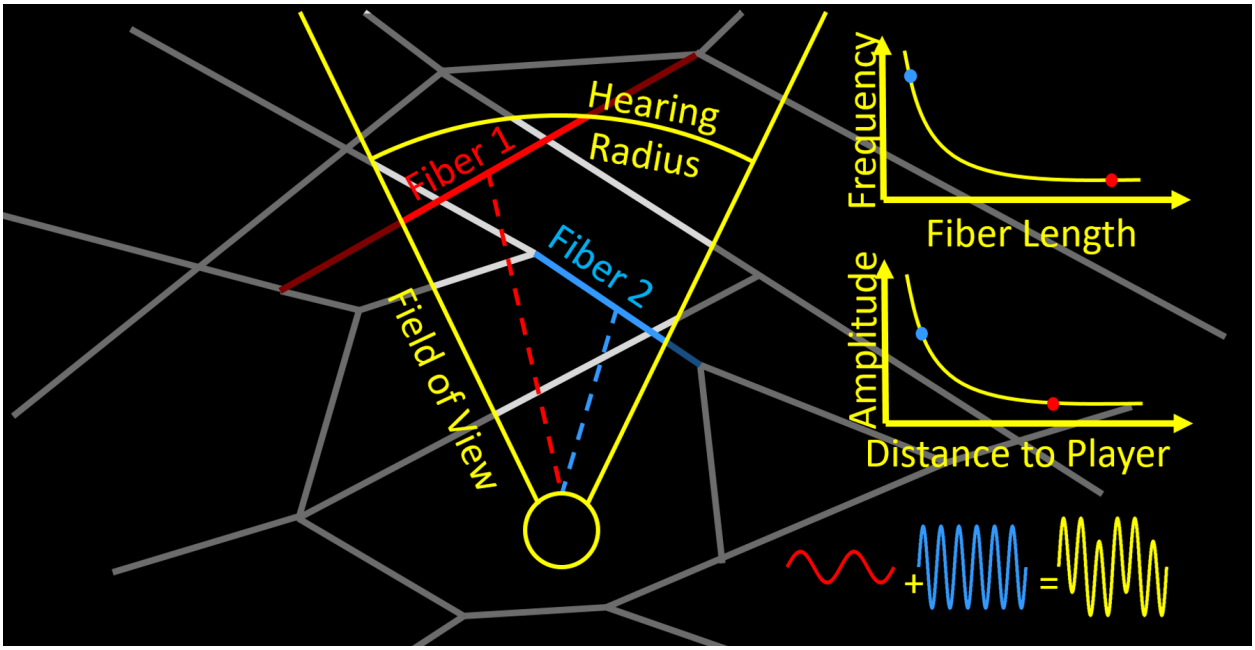

Figure 6-2: Schematic of the sonification rules. The frequencies and amplitudes are inversely proportional (default) to the fiber lengths and distances to the player, respectively. The fibers inside of the user's field of view and within a chosen hearing radius are sonified with sine waves. In white the fibers that are sonified, and grey the silent ones. The superposition of simple sine waves create a new waveform, and consequently a more complicated timbre.

Model Excitation

The model excitation setup defines the interplay between the user and the model [58]. The user plays by choosing their field of view, the hearing radius and which fibers to pluck, and tunes the model by changing the parameters. The user uses a mouse or MIDI (Musical Instrument Digital Interface) continuous controllers to change the direction of their field of view and the hearing distance. For example, if the user's field of view is an area of the model space with no fibers the model stays silent, but if they move it toward fibers, they will be sonified and produce sound if they are within the hearing radius set by the user. The user also can move its field of view using a virtual reality (VR) headset (HTC vive), intensifying the immersive experience. By physically moving their head, they can navigate in the spider web. The user can also choose to pluck a fiber by using the MIDI keyboard to send a command. The user can also tune many more parameters that can change the sound synthesized by controlling frequency assignment, frequency modification, frequency range, frequency filter, fiber colors, and others. In this sonification model, the user manually

sends commands through MIDI controls, computer, VR headset and controllers, keyboard and mouse: they have a direct interaction with the model.

Model Initialization

Initialization is the status of the model immediately after setup [58]. After setup, the user is placed at the origin of the model space and the hearing radius is set to 0. Whether there are fibers or not in the field of view of the user, they will not be sonified, as they are considered to be not within the hearing radius.

Model Parameters

This stage explains the rules that transforms data into sound [58]. The principal parameters that the user can adjust are summarized in Table 6.1. Each sonified fiber is a sound source and produces a simple sine wave, the frequency of which is determined by the length of that fiber. For default, the frequency of the fiber is inversely proportional to the fiber length, which is the case for string vibration. Indeed, the resonance frequencies of a string under tension and fixed at its extremities for a given mode n are:

$$f_n = \frac{1}{L}\left(\frac{n}{2}\sqrt{\frac{T}{\mu}}\right) \tag{6.1}$$

With μ the mass density, T the tension, and L the length of the string [119, 120]. For simplicity, we choose the fundamental harmonic (n=1). We choose this fiber length-frequency relationship as the model's default setting because we are already intuitively accustomed to this rule. For example, if we look at the strings of a harp, we expect the shorter string to have a higher pitch than the longer fiber string. The user can also choose to assign frequencies linearly to the fiber lengths or even personalize their own fiber length-frequency relationship (Figure 6-2). The fiber frequencies can also undergo frequency modification such as frequency rounding, low resonance frequency filtering, frequency shifting by addition, and frequency modification through adding a percentage. The frequency ranges to the limits of human hearing frequencies, from 20Hz to 20,000Hz. To get a richer and more complex

timbre, those extremities are adjustable.

Table 6.1: Principal parameters for data exploration, personalization, and artistic creation

Parameters	Description	Usage
Frequency	Relationship between fiber length and frequency	
Amplitude	Relationship between fiber distance-to-user and amplitude	Data
Movement and speed	Navigate in space and control movement speed	exploration
Field of view	Control of the camera movement in the virtual environment	
Frequency shifting by addition	Shift all the frequencies by a adding a value or a percentage	
Frequency rounding	Round all the frequencies by an integer	
Low resonance filter	Filter all the frequencies that are not a multiple or factor of a chosen value	Personalization and
Fiber colors and textures	Colors/rendering texture of the sonified and silent fibers	Artistic Creation
Spatialization	Choose a spatialization grid	
Fiber Plucking	Choose a frequency and pluck the fiber is sonified at this frequency	

The amplitude of the sound produced by the fibers is related to their distance from the user. The fiber distance is defined as the distance between the center of the fiber and the user's virtual body in the model space (Figure 6-2). Similar to the fiber-frequency relationship, for default, the amplitude is inversely proportional to the distance, which is the case for sound waves. The user has the option to change this relation to linear or to free-hand draw a relation. The user has infinite ways to optimize and tune the relationships between fiber length-frequency or fiber distance-amplitude.

The plucked fibers follow the same fiber length-frequency and distance-amplitude relationships as the fibers in the user's field of view. To distinguish them from the sound produced by the static fibers, the user can change the plucked fibers' amplitude envelope (attack, decay, sustain, release) and the amplitude dissipation factor. The envelope will define how fast the sound will reach its highest amplitude, how long it will decay and sustain, and how slowly the amplitude will drop to zero. The amplitude dissipation factor measures the loss of amplitude as the plucking propagates to neighboring fibers.

Model Listener Characteristics

The listener characteristics describe the relation between the user/listener and the sound sources (fibers), and how fiber locations, orientations, and distances influence the user's perception of sound [58]. In our model, the user is in a virtual world where they are surrounded by a fiber network – here, the 3D spider web. In this world, the user's body is modeled as a 2 m capsule and their eyes are a virtual camera placed at 1.58 m from the bottom of the capsule (feet). The user has the option for the capsule to have a rigid body,

in which case it allows collisions to trigger fiber plucks. They either have free movement inside of the space (including flying), or they are placed in a predefined adjustable path. On the path, the user controls their speed and path direction. It allows them to focus only on looking (moving their field of view) and finding interesting parts of the data, while still allowing movement to explore the whole network. Because the user only hears what is in front of them, and needs to move their head to explore the data, our spatial model does not require a multi-channel audio system; however, with more speakers, the user receives insightful information on fiber location and distribution. The user can adjust the number of output channels (default 1). For a multi-channel setup, the rectangular field of view is divided into a grid whose row and column numbers are defined by the user. A grid cell represents one channel output. Only cells containing fibers output sound. When a fiber crosses multiple grid cells, its amplitude is distributed across the associated channels following this law:

$$A_{Channel} = \left(\frac{1}{N}\right)^{0.75} A \tag{6.2}$$

with $A_{Channel}$ being the amplitude of the fiber that is produced by the channel assigned to the cell containing the fiber, N is the number of cells the fiber is seen in, and A being the amplitude of the fiber related only to the distance to the user.

6.2.2 Implementation and Code Development

The sonification model is implemented in Unity3D (unity3d.com) and Max 8 (cycling74.com) (Figure 6-3). We use the game engine Unity3D to navigate inside a virtual spider web environment, to compute the basic sonification parameters based on the virtual model, and to create visuals to aid the interpretation of the sonification. We use Max 8, a programming software for music and multimedia applications, for sound synthesis and the creation of a user interface. Max 8 and Unity3D communicate through OSC (Open Sound Control) message using UDP (User Datagram Protocol) packets. Instead of using only Unity3D to create the sonification model, we use two communicating software packages because Max 8 provides richer support for sound synthesis and for creating user interfaces independent of the visualization of the web.

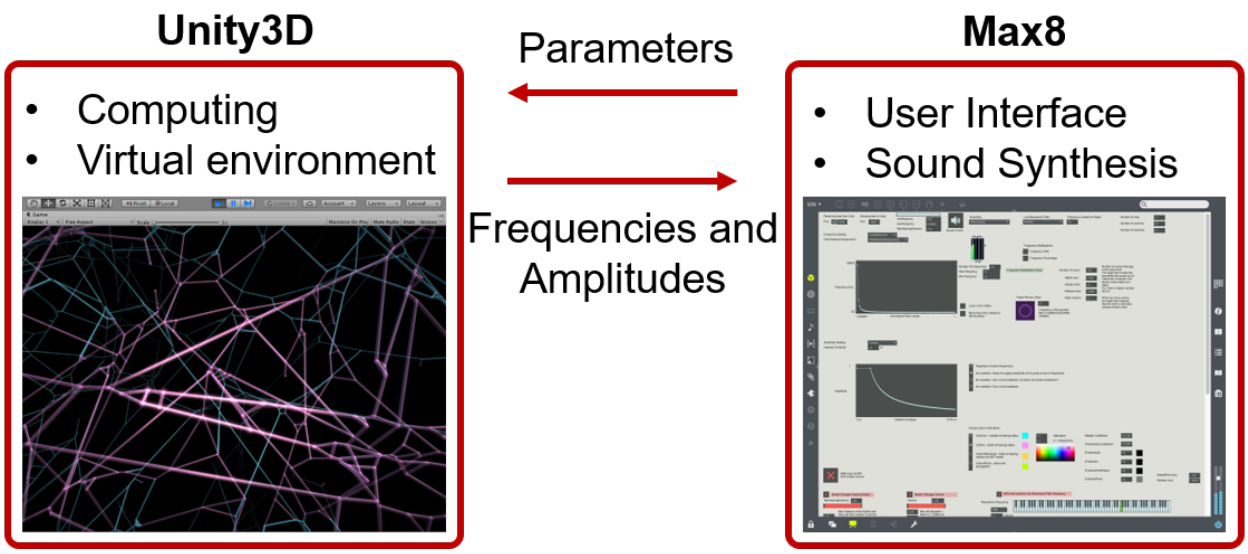

Figure 6-3: Simplified schematic of the sonification model's implementation using Unity3D and Max 8

Unity3D

Unity3D renders the 3D spider web network from a list of point coordinates and a list of pairs of points that need to be linked. For each point and link on the lists, the program generates a 0.1 m diameter sphere and cylinder, respectively. We use Unity3D to create a first-person game where all the graphics are rendered from the user's point of view. The user navigates through the web by moving the mouse or their head with VR headset, the positions of which are tracked and translated in camera direction. The virtual camera renders the user's field of view. For each fiber, rendered by a cylinder, in the field of view of the user, if the distance between the center of the fiber and the user is shorter than the chosen hearing radius, then we compute the frequency and amplitude of the sonified fiber according to the fiber length-frequency and fiber distance-amplitude relations chosen. A list of frequency-amplitude pairs, corresponding to the sonified fibers, per audio channel is sent to Max 8, where the sound synthesis happens. To aid user interpretation, the visuals respond to the sonification by changing the colors and textures of the spheres and cylinders that are in the field of view and within the hearing radius, corresponding to sonified fibers. The user can visually distinguish the fibers that produce sound and the fibers that are silent.

Several user-controllable parameters allow for manipulating the frequency and ampli-

tude associated with a fiber.Several, such as the number of columns and rows (described in section 6.2.1) and data thinning options, are typically set before interaction begins. Others can be changed dynamically to affect the output of the system.

The most pertinent parameters that will affect which fibers are sonified are the view of the player in Unity (player position and orientation) and the hearing radius. Only fibers within the view of the player are processed; and the amplitude of a fiber is correlated to its location between the players location and the hearing radius.

Other parameters allow for controlling the frequencies assigned to the fibers. The minimum and maximum frequency (i.e. the frequency assigned to the longest and shortest fiber, respectively) can be set with a variety of frequency distributions available, ranging from linear to user-defined transfer functions. In addition, an arbitrary rounding frequency can be chosen. This defines the "fundamental frequency" of the web, and the frequency for each fiber is quantized to the closest integer multiple of this fundamental.

Max 8 implementation

Lists of frequency-amplitude pairs are sent to Max when an animation frame is rendered in Unity3D, with one list being sent for each audio channel. These lists are used as parameters for multiple instances of an additive synthesis algorithms The output of each instance is the sum of a bank of sine wave oscillators, one oscillator for each frequency-amplitude pair.

Each new set of values is assigned to an additive synthesis instance with an attack-decay amplitude envelope. The use of multiple synthesis instances, each with their own envelope, prevents audible discontinuities when new sets of frequency-amplitude pairs are received, and the overlap of instances smooths the transition between new parameter values.

The output of the synthesis instances are then further processed and sculpted, and each channel is sent to a dedicated output of a multi-channel audio interface.

We also used Max 8 to create a simple user interface to sends commands and parameters to Unity3D. This interface provides access to all of the Unity parameters.The user

interface also allows for the use of standard MIDI controllers for control of parameters for both Unity and Max.

6.2.3 Application: Spider's Canvas/Arachnodrone

The spider web interactive sonification model was used as a creative platform for live performance and art installations, where the composer and audience are immersed into a multimedia experience inside of a complex 3D spider web. Inspired and commissioned by Studio Tomás Saraceno (STS), in the context of Saraceno's carte blanche exhibition, ON AIR, at the Palais de Tokyo, Paris (2018), Spider's Canvas/Arachnodrone is a multimedia live performance in which the sonification of the fibers of the spider web are used as a virtual spider web musical instrument. The premiere of Spider's Canvas/Arachnodrone was performed by Isabelle Su and Ian Hattwick on the spider web instrument, Evan Ziporyn on the EWI (Electronic Wind Instrument), and Christine Southworth on the guitar and EBow (Electronic Bow) (Figure 6-4A,B,C). The composers, performers and audience travel together sonically through the intricate architecture of the *Cyrtophora citricola* 3D spider web. Following its premiere at the Palais de Tokyo in November 2018 for Saraceno's public program, "ON AIR live with ...", the Spider's Canvas/Arachnodrone was performed on three subsequent occasions at the MIT Theater, on several popup peformances (Figure 6-4D,E) at MIT.nano in February 2019, and at the Central Square Theatre in September 2020. The videos V6-1 and V6-2 are excerpts of the performances at Palais de Tokyo, Paris and the MIT Theatre, respectively. The Spider's Canvas/Arachnodrone also was also exhibited as an immersive environment at MIT.nano, where the virtual spider web sonification model musical instrument runs automatically (Figure 6-4F).

Sound Sculpting and Performance

The MBS methodology described in section 6.2.1 allows the spider web data to be perceptible through sound. We added additional synthesis functionality in Max and designed a user interface that controls both Max and Unity. During the performance, Su and Hattwick shared the control of Spider Web instrument. Su controlled the the field of view within

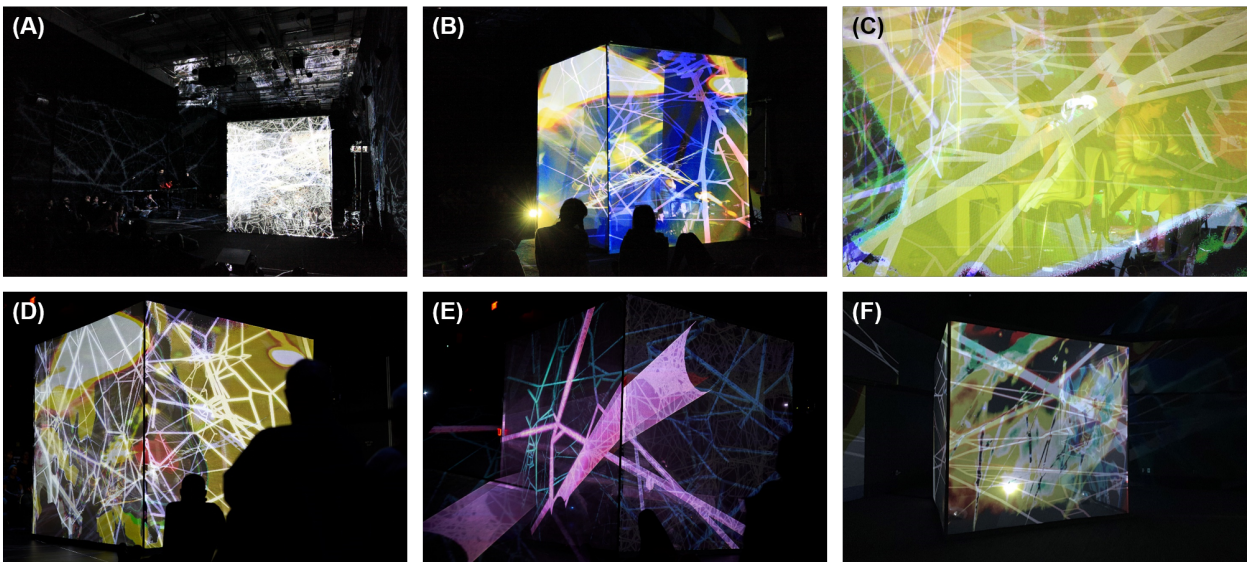

Figure 6-4: Spider's Canvas/Arachnodrone performed by Isabelle Su and Ian Hattwick on the spider web instrument, Evan Ziporyn on the EWI (Electronic Wind Instrument), and Christine Southworth on the guitar and EBow (Electronic Bow). **(A,B,C)** Premiere of the Spider's Canvas/Arachnodrone performance at the Palais de Tokyo, Paris (2018). The performance was commissioned by Studio Tomás Saraceno (STS), in the context of Saraceno's carte blanche exhibition, ON AIR. **(D,E)** Spider's Canvas/Arachnodrone performances at MIT Theatre (February 2019). **(F)** Spider's Canvas/Arachnodrone installation at MIT.nano (February-June 2019). The installation runs automatically and autonomously. (A,B,C) Credit: Aurelie Cenno/Palais de Tokyo. (D,E) Credit: Leon Yim/MIT. (F) Credit: Isabelle Su/MIT

Unity and the speed of the avatar on a predefined path. Hattwick controlled the sound sculpting parameters determining the overall sonic output of the web sonification. The sound sculpting and the performance are described in more detail in [121].

Installation

Following the concert series at MIT Spider's Canvas/Arachnodrone was installed as a multimedia installation at MIT.nano, on MIT's campus. We built a 10' × 10' × 10' aluminum frame, three of the four vertical sides of the cube are covered with grey shark tooth scrim, with three projectors projecting through each side. The installation was first used for the performances and reused for the art installation. For this installation, a fixed trajectory and player orientation was set to repeat within Unity, and a procedural function was created to morph between snapshots of audio parameters within Max 8. While the exact trajectory within the audio parameter space was non-deterministic, the overall character of the visual

and audio parameters was set to repeat every 15 minutes. We create a video montage of photographs of local Lexington, MA spider webs mixed with scans and model images of the spider web used for the sonification. Inspired by STS' multi-species hybrid spider webs [71], we project on the three screens the video montage overlapped with the spider web instrument user's viewpoint. Just as the spider plays inside the web, the performers play inside the cube, creating the illusion that they are inside a large-scale and dynamic spider web (Figure 6-4).

6.3 Results and Discussion

The spider web sonification model could be used not only as an artistic creative platform but also as a scientific research tool for visualizing, exploring, and understanding complex and large network datasets. Here, we use the model for identifying and locating key topological features of a *Cyrtophora citricola* 3D spider web, such as its fiber length distribution and web density. This particular spider web is composed of a dense mesh-like region sandwiched between more porous tangle regions. We choose to investigate a 76 mm cube sample of the web, belonging to the tangle region. The spider web network is scaled up so that its size is 30 m, making the 2 m tall user fully immersed in the structure. For the data exploration analysis, we restrict the interactivity to these parameters: field of view, movement, and hearing radius.

The user has complete control of their viewpoint (V6-3) and hearing radius (V6-4): they decide which fiber regions to look and therefore hear. Novice users can start learning how to use the sonification tool by assigning a short hearing radius (for example, 2 m), allowing them to hear one to a few fibers at a time when fibers are in their field of view. Using the default inversely proportional fiber length-frequency relationship, if the user hears a high pitch or a low pitch sine wave, it would mean that the sonified fiber in front them is very short or very long, respectively. The user can adjust and personalize the fiber length-frequency parameters to their needs. For example, if they cannot hear very high frequencies, they can decrease it to a hearing level. The video V6-5 is an example on how to use the spider web instrument model with VR headset and controllers.

As the user gets familiar with the tool, they can increase the hearing radius to include more sonified fibers. They hear a complex sound produced by a superposition of simple sine waves of different frequencies and amplitudes, corresponding to different fiber lengths and distances, respectively. The user is facing a high-density region of the web where they can distinguish numerous different sine waves and a more porous web region where they only hear a few different sine waves. Similarly, if they hear many high frequencies, they are in front of a region of short fibers, or long fibers if they hear low frequencies. The user can differentiate high or low fiber density regions and determine the distribution of fiber lengths.

One effective method to use the model for data exploration is to start with a larger hearing radius to locate fiber regions of interest, then slowly zoom in by decreasing the hearing radius so only a few fibers are heard, and observe the details of the structure. By adjusting the hearing radius, we can also clearly conceptualize, both through sight and hearing, the hierarchical structure of the spider web.

The sonification model and rules are set up so that if the user closes their virtual eyes (no fiber rendering), they should hear exactly what is in front of them. However, visualization is useful for aiding the comprehension of the sonification and helping the user grasp web features more in detail, especially for beginners. By assigning different color and texture to the sonified and silent fibers, users can visualize which fibers they are hearing. After using sonification to quickly hear and locate web density and fiber distribution, users can use sight to recognize the heard fibers and carry out a deeper analysis. As the sonification does not provide fiber orientation or connectivity information, visualizing through sight provides more insight into web architecture. With only visuals, we would need to rotate and zoom in and out of the web to capture the web characteristics. Paired with interactive sonification, users have a more complete holistic experience of the data. They can use sonification to have a quick overview of all the data (large hearing radius) while preserving its complexity.

6.3.1 Future Applications

The intuitive and interactive aspects of this spider web sonification instrument are two of its most compelling features. Users can tune and personalize parameters of the

model such as hearing radius, viewpoint, and movement, for a specific purpose, dataset, or personal comfort. Not only can we use the spider web data visualization tool for creative and scientific purposes, we can also apply it for any type of network datasets, including 2D spider orb webs, transportation, social, and many more types of networks. For a social network, where the length of a link between two nodes describes the relationship strength between two individuals, hearing a region of high frequencies (short link) would describe a group of close acquaintances, while low frequencies (long link) would represent a weak connection between individuals. The model's intuitive and tunable parameters allow anybody to use the tool, ranging from novice to expert users. Novices can limit their movements and the number of heard fibers and experts can simultaneously play with all the parameters to construct complex sounds.

This intuitive and interactive data exploration musical tool shows promising future applications in the field of arts, data mining, and holistic experience of 3D network data. For example, we can use it as a dancing platform, where the performers' movement would be tracked and translated into user movements inside of the virtual environment. The dance would not follow the music – but dancing would generate it [113, 122]. We can also use this network visualization method for aiding visually impaired persons to explore data without using their sight [123]. They can travel inside of a virtual 3D space data and aurally conceptualize the lengths and location of the network links directly in front of them. Adding 3D sound, with HRTF (Head-Related Transfer Function), would allow users to locate spatial data more precisely [124].

While this data visualization tool is an innovative and effective method to obtain insights of complex static structures, it does not provide any mechanical information of the spider web. Because rendering and physics features on Unity3D and data processing on Max 8 of large datasets are computationally expensive, we limited our study to static and smaller spider web architectures. In the future, we plan to add real-time mechanics to the method, allowing users to pluck fibers and hear the actual sound propagation in the web or to stretch a fiber and hear its sonified frequency changing with fiber length and its effect on the neighboring fibers. The user will have a more holistic and immersive experience, through

touch, sight, and hearing. New mechanical and pattern insights could be derived from using this tool.

6.4 Conclusions

The work reported in this paper reported a novel interactive method to visualize, through sight and sound, a 3D spider web architecture that can be used as a data exploration tool or a creative platform. We use model-based sonification to transform data into a model that produces sound with real-time user interaction. In other words, we created a spider web virtual musical instrument, where the data is the musical instrument. We use the game engine Unity3D and the multimedia program Max 8 to create a virtual spider web environment where the user is immersed in the network.

Fibers, if in the field of view of the user and within a chosen hearing radius, are sonified with sine waves, the frequencies and amplitudes of which are determined by fiber lengths and fiber-to-user distances, respectively. Overlapping multiple simple sine waves create a complex timbre, which reflects the hierarchical structure of the spider web, ranging from simple silk threads to an intricate 3D fiber network.

This tool can be used as a musical instrument but also a method to recognize spider web topological features. The method's intuitive and interactive aspects make it multi-purpose and accessible for everyone. It provides a new way to understand data and find interesting patterns that would be difficult to comprehend with sight only.

Chapter 7

Conclusions and Future Work

Parts of the review presented in this chapter have been/will be published in:

- **Su I**, Qin Z, Saraceno T, Krell A, Mühlethaler R, Bisshop A, Buehler MJ: "Imaging and analysis of a three-dimensional spider web architecture." *J R Soc Interface* 2018, 15.

- **Su I**, Jung GS, Narayanan N, Buehler MJ: "Perspectives on 3D printing of self-assembling materials and structures." *Curr Opin Biomed Eng* 2020,

- **Su I**, Buehler MJ: "Mesomechanics of a Three-Dimensional Spider Web." *J Mech Phys Solids* 2020,

- **Su I**, Qin Z, Bisshop A, Mühlethaler R, Saraceno T, Ziporyn E, Buehler MJ: "Sonification of a 3D Spider Web and Reconstitution into Musical Composition using Granular Synthesis." *Comput Music J.* 2021 (accepted)

- **Su I**, Hattwick I, Southworth C, Ziporyn E, Bisshop A, Mühlethaler R, Saraceno T, Buehler MJ: "Interactive exploration of a hierarchical spider web structure with sound." *J Multimodal User Interfaces.* (revision)

- **Su I**, Narayanan N, Logrono MA, Bisshop A, Mühlethaler R, Saraceno T, Buehler MJ: "In-situ Three-Dimensional Spider Web Construction and Mechanics." Proc Natl

Acad Sci (submitted)

7.1 Conclusions

The objective of this research was to develop a systematic experimental and computational framework for investigating 3D spider webs, quantifying, and validating what arachnologists have observed in nature. Our methods can be used systematically and provide the foundation for understanding the geometries, mechanics, construction, and visualization through sound of 3D spider webs. This was accomplished by developing the first automatic, remote, and in-situ imaging and modeling methods for quantifying natural 3D spider webs, completed webs and webs under construction, using image processing on high-resolution images of slices of the web illuminated by a sliding sheet laser. Using the web model, we carried out meso-scale particle dynamic simulations to investigate the mechanical and functional properties of webs at different stages of construction. We also explored visualization methods for intuitiely and interactively finding web features and patterns using sonification. Detailed findings, contributions, and impacts of the imaging method, mechanics, construction, and sonification of 3D spider webs are summarized below.

Imaging of a 3D spider web architecture: We developed an innovative experimental method to directly capture the complete digital 3D spider web architecture with micron-scale resolution. We built an automatic segmentation and scanning platform to obtain high-resolution 2D images of individual cross-sections of the web that were illuminated by a sheet laser. The web was obtained by letting a *Cyrtophora citricola* spider builds its web inside a hollow frame for a few days. We then developed image processing algorithms to reconstruct the digital 3D fibrous network by analyzing the 2D images. This digital network provides a model that contains all of the structural and topological features of the porous regions of a 3D web with high fidelity, and when combined with a mechanical model of silk materials, will allow us to directly simulate and predict the mechanical response of a realistic 3D web under mechanical loads. Our work is the first consistent and automatic method that can be used to capture the architecture of sophisticated 3D spider web, that could lead to studies of the relation between architectural, material, and biological functions for numerous

3D spider web applications. For example, our imaging and modeling methods could help gaining new insights on the influence of spider species and environmental conditions on web architectures.

Mechanics of a 3D spider web: we investigate the mechanical behavior of highly complex *Cyrtophora citricola* 3D spider web, the architecture of which has been digitally modeled with micron-scale details from images of full-scale laboratory experiments (Chapter 2), under stretching and projectile impact, using coarse-grain bead-spring simulations. We show that the interplay between the nonlinear behavior of spider silk and the redundancy of complex 3D spider web structures is crucial for the robustness and resilience of spider webs. The tangle region of the spider web allows prey to fly through and be caught in the dense tent web region, providing food to the spider. It also filters out predators at low impact velocity, and consequently protects the spider located in the tent region. Understanding the role of the interplay between silk mechanics and 3D web structure in webs' evolutionary fitness could lead to high-performance and lightweight fiber network composite for structural, material, and biomedical engineering. Our work provides a basis for systematic computational methods that can be used to generate data for deep learning design [125].

Construction of a 3D spider web: We investigate the structure and mechanics for a *Tidarren sisyphoides* spider web at varying stages of construction. This is accomplished by imaging, modeling, and simulations throughout the web-building process to capture changes in the natural web geometry and the mechanical properties. The foundation of the web geometry, strength, and functionality is created during the first two days of construction, after which the spider reinforces the existing network with limited expansion of the structure within the frame. Our computational tools can be used to investigate how spiders adapt their web-building behavior to artificial environmental stimuli, which may lead to flexible and adaptable 3D network structures and assembly methods in complex environmental conditions

Parameter-mapping sonification of a 3D spider web: We translate complex 3D data from the original web model into music, using data sonification. We map the spider web data into audio parameters such as pitch, amplitude, and envelope. Paired with a visual

representation, the resulting audio allows a unique and holistic immersion into the web that can describe features of the 3D architecture (fiber distance, lengths, connectivity and overall porosity of the structure) as a function of spatial location in the web. We provide a holistic and intuitive way to conceptualize complex 3D spider web architectures through sound.

Model-based sonification of a 3D spider web: We propose an intuitive and interactive way to explore and visualize a 3D *Cyrtophora citricola* spider web geometry. We use model-based sonification to translate the web architecture into sound, allowing for aural perception and interpretation of its essential topological features. We implement this sonification using Unity3D and Max 8 to create an interactive spider web environment in which a user travels through a virtual spider web. Each silk fiber in their field of view is sonified using different sine waves. Together, the sonified fibers create new and more complex timbres that reflect the architecture of 3D spider webs. These concepts are implemented into a spider web-based instrument for live performances, art installations and data exploration. It provides an unprecedented and creative way to immerse the composer, audience, and user in an multimedia experience generated by the complexity of a 3D spider web. Our model-based sonification is reusable, tunable, and can be used for any type of network data. Furthermore, adding real-time mechanics would help to intuitively understand spider webs' architecture and mechanics.

7.2 Opportunities for Future Research

The development of an experimental and computational framework for 3D spider web imaging and deriving mechanical properties opens many possibilities for future exploration. Our consistent and automated non-destructive in-situ imaging, mechanical computational simulations, and sonification of 3D spider webs can be applied to understand and visualize the influence of biological, environmental, and artificial stimuli on 3D spider web architecture, construction, and functions for designing web-inspired complex systems.

7.2.1 Effect of Environmental and Human Pressures

Our imaging and computational simulation methods for quantifying 3D spider web architectures and their mechanics, whether they are completed webs or webs under construction, can be used to investigate the many natural and artificial factors that could impact web architectures, mechanics, construction, and functions. Indeed, the work presented here was applied to *Cyrtophora citricola* and *Tidarren sisyphoides* spider webs, that were built in an artificial environment free of human intervention. Our computational tools can be used for other types of spider species and different web-building environments. For example, we could explore the effects of environmental and human factors, such as attachment availability, spider diet, wind, pollution, noise, and vibration, on the web structure, performance, construction, and functions. Understanding how spiders adapt and thrive in the presence of many environmental and human pressures could lead to adaptable, high-performance 3D spider web-inspired fiber structures.

7.2.2 *De novo* Spider Web-inspired Designs

Moreover, because our methods can be used systematically and automatically, they can be applied to generate data for machine learning purposes such as predicting spider web properties. For instance, Buehler et al. [125] have developed Webnet, a machine learning model trained on *Cyrtophora citricola* uniaxial stretching simulations and augmented data to predict complex biomateriomical mechanics of spider webs. Further machine learning opportunities also include generating spider web scan-like images with deep learning for building a *de novo* 3D spider web.

7.2.3 Spider Web Mechanics Sonification

In addition to quantifying 3D spider web structures and mechanics, we also developed an intuitive, interactive, and holistic sonification platform for spider web data exploration. We hope that future advances in computational performance would allow the addition of real-time real silk mechanics into the current VR sonification model. This would allow a fully immersive experience, through sight, sound, and touch where users interact with the virtual

silk fibers and hear the stress distribution from the mechanical load applied. For example, sonified fiber frequency would increase with fiber stress, which is similar to chord instruments. This way, novice users would intuitively discern stress distribution and fiber failure sequence. This opens doors for many opportunities in complex data visualization, exploration, and learning, as well as creative exploration.

7.2.4 Spider Web-like 3D Printer

Finally, we anticipate exciting opportunities beyond the scope of silks and webs, in the field of spider web-inspired sustainable and multi-functional construction.

Additive manufacturing, or 3D printing, can fabricate complex geometries from the micro-scale to macro-scale directly from computer-aided design instructions [116, 126]. In addition, 3D printing allows a variety of benefits, which include cost-effective and fast prototyping, freedom of design, mass customization, lower shipping cost, and reduction of waste [126]. It has led to the development of innovative and performant structures in numerous fields such as building construction, biomedical devices, bioinspired composite materials, and aerospace. Although polymers are the most used material, a wide variety of nontraditional materials are also used for 3D printing such as metals, ceramics, concrete, and silk protein, which are used for aerospace [126], scaffolds [126], buildings [126], and biomedical applications [10], respectively. In particular, Mu et al. [10] have recently developed a method for 3D printing silk fibroin in an ambient and aqueous environment to mimic hierarchical assembly of natural silk spinning. The combination of the biological properties of silk and the versatility of 3D printing could lead to production of multifunctional, biocompatible, and strong biomedical devices for drug delivery or surgical implants [10]. Spiders can be considered as analogous to 3D printers, where the spinning dope or the stored spider silk protein solution is the printing ink, the spider's silk spinning apparatus is the printer head, and the spider's body is a mobile 3D printer that moves along its 3D printed fibers (Figure 7-1). Future research on spider-inspired 3D printing can increase the complexity of silk architectures while maintaining the advantageous biological and mechanical properties of silk. With a portable and mobile spider-like 3D printer, wasteful support material scaffolding will no longer be

necessary to 3D print a fiber network architecture, and such structures can be built directly on site.

Constructing artificial 3D spider webs is not as simple as it appears to be for the spider. STS was the first to build a 16.7:1 scale 3D spider web, the geometry of which was obtained through laser scanning [14]. Although spiders only require silk and a few days to build webs, the large-scale spider web installation was built manually and required intensive planning and thousands of nylon threads, tapes, and hooks for construction. On the other hand, Yablonina built an intricate 3D web-like structure manually inside a cube frame by carefully planning the fabrication sequence using a fiber wrapping effector tool and scaffolding threads [40]. Huang et al. [127] demonstrated the importance of sequence and motion planning in 3D printing to construct complex structures. Using mobile spider-like 3D printer robots that move along its printed fiber to build a 3D web-inspired structure would reduce construction time and the need for construction artifacts. Although such a robot has not yet been developed, recent advances in mobile 3D printing show promise. Hunt et al. [128] have created a flying 3D printing robot that can produce simple polyurethane structures for repairing damaged structures.

Other researchers have developed the Siemens Spiders; they are terrestrial spider robots with 3D printers [129, 130]. They move, communicate, and work together like social spiders but also print plastic 3D structures [129, 130]. Terrestrial and aerial autonomous 3D printers could provide some freedom of construction on inaccessible sites, such as the moon, radioactive land, or earthquake sites [128, 129, 130]. Lightweight, long span, and tensile fiber structures can also be built without 3D printing, with the help of unmanned aerial vehicles transporting fibers and controlling their tension [131, 132]. This method has been used for constructing a leaf miner moth-inspired pavilion [131] and a suspension footbridge [132]. Similarly, wall climbing communicating robots can also build human-scale 3D fiber structures [133]. Mobile 3D printing and mobile robots for fiber structure construction technologies combined with silk-like materials could revolutionize large-scale, high-performant, and self-repairable construction. The autonomous 3D printing spider-like robot would travel along its printed fibers and consequently deform the fiber structure during construction. In addition

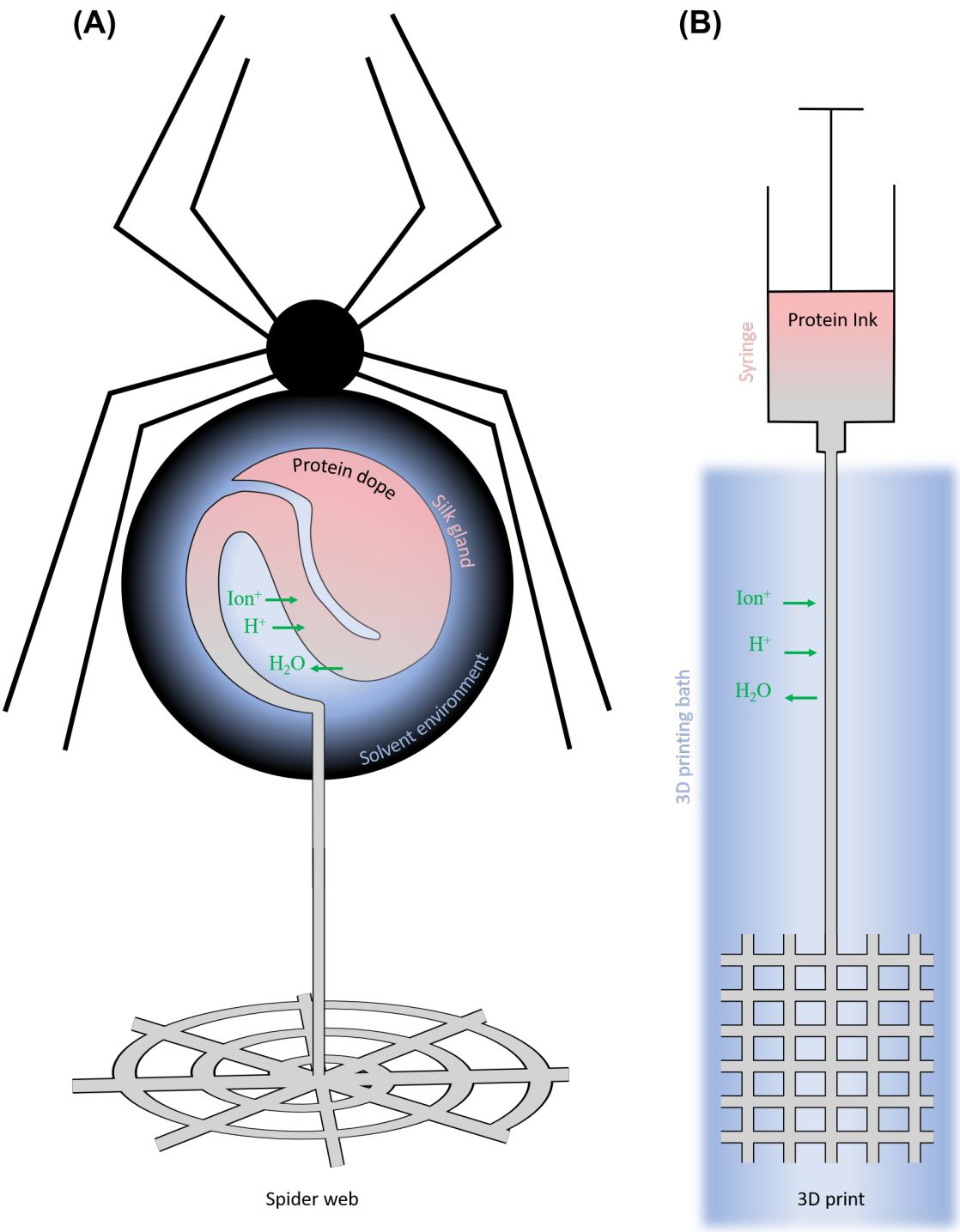

Figure 7-1: Schematic of comparing spider's natural spinning process to build webs and bioinspired 3D printing of 3D silk fibroin structures. The schematic was inspired by a study by Mu et al. [10]. **(A)** Natural silk spinning process in the silk gland. Silk fibers used for web structures originates from protein dope undergoes shear stress, ion exchange, and acidification [11, 10]. **(B)** Spider-inspired 3D printing of silk fibroin structures. Inspired by the natural silk spinning process, fibers are spun in aqueous salt bath that controls silk fibroin assembly [10].

to printing fibers, it has to be able to tune fiber tension, detect damages, and recycle loose fibers to fully be autonomous and self-sufficient.

Building a complex and performant large-scale structure is not sufficient. Often, structural health monitoring is necessary to predict when a structure deteriorates and determine the location of possible damages. Analyzing data obtained by sensors placed on the structure not only prevent the catastrophic failure of a structure but also help extend the structure's life span and reduce maintenance cost [134]. Although structures need to be monitored, the inverse is also possible –structures can monitor and locate building occupants with footsteps through induced vibration and wave propagation [135]. Similarly, spiders carry out structural health monitoring of their webs but also differentiate prey from predators, or communicate with mates within their webs through vibration [112].

Spider and web-inspired 3D printing methods could revolutionize the future of low environmental impact construction. Indeed, spider-like robots would only use protein, the properties of which we can tune by changing the amino acid building blocks, to print strong and tough fibers to build any designed fiber architecture. In case of damage, just like spiders in nature, the robots would quickly make life-saving repairs and consequently prevent disastrous failure of the structure. They would also be able to locate and monitor the health of their occupants. Finally, because the fibers are easily recyclable, the life cycle of such a structure is truly sustainable and environmentally friendly. Spiders and webs are a self-sufficient, self-monitored, and self-reparable system that could lead to more sustainable complex structures (Figure 7-2).

Although such technology does not exist yet, current advances in proteinaceous printing, mobile additive manufacturing, mobile robots for fibers construction, and structural and human health monitoring technologies show promising future for sustainable structures and construction.

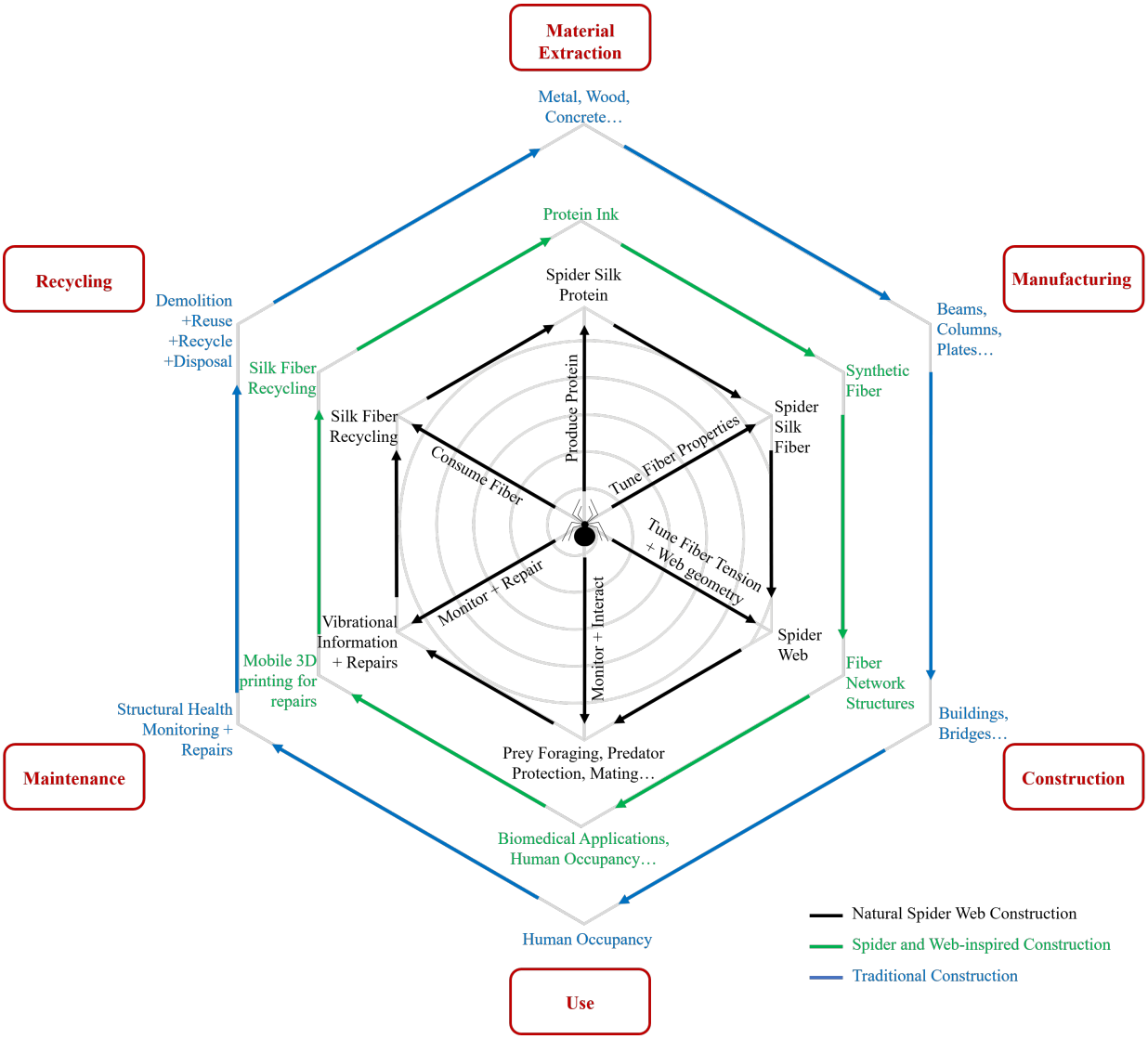

Figure 7-2: Schematic of the life cycle of a spider and web-inspired sustainable and resilient structures. In black is the natural spider web construction cycle. In green, the suggested spider and web-inspired construction cycle. In blue, the traditional construction cycle. Taking inspiration from spiders and web construction and traditional construction could lead to self-sufficient, self-monitored, self-reparable, complex and high-performant bioinspired structures.

References

[1] Anna Tarakanova and Markus J Buehler. A Materiomics Approach to Spider Silk: Protein Molecules to Webs. *JOM*, 64(2):214–225, 2012. doi: 10.1007/s11837-012-0250-3. URL https://doi.org/10.1007/s11837-012-0250-3.

[2] Steven W Cranford and Markus J Buehler. *Biomateriomics*, volume 165. Springer Science & Business Media, 2012. ISBN 9400716117.

[3] Tristan Giesa, Melis Arslan, Nicola M Pugno, and Markus J Buehler. Nanoconfinement of Spider Silk Fibrils Begets Superior Strength, Extensibility, and Toughness. *Nano Letters*, 11(11):5038–5046, nov 2011. ISSN 1530-6984. doi: 10.1021/nl203108t. URL https://doi.org/10.1021/nl203108t.

[4] William Humphrey, Andrew Dalke, and Klaus Schulten. {VMD} – {V}isual {M}olecular {D}ynamics. *Journal of Molecular Graphics*, 14:33–38, 1996.

[5] Isabelle Su, Zhao Qin, Tomás Saraceno, Adrian Krell, Roland Mühlethaler, Ally Bisshop, and Markus J. Buehler. Imaging and analysis of a threedimensional spider web architecture. *Journal of the Royal Society Interface*, 15(146), 2018. ISSN 17425662. doi: 10.1098/rsif.2018.0193. URL http://rsif.royalsocietypublishing.org/content/royinterface/15/146/20180193.full.pdf.

[6] Steven W. Cranford, Anna Tarakanova, Nicola M. Pugno, and Markus J. Buehler. Nonlinear material behaviour of spider silk yields robust webs. *Nature*, 482(7383):72–76, 2012. ISSN 00280836. doi: 10.1038/nature10739. URL http://dx.doi.org/10.1038/nature10739http://www.nature.com/nature/journal/v482/n7383/pdf/nature10739.pdf.

[7] Sinan Keten, Zhiping Xu, Britni Ihle, and Markus J. Buehler. Nanoconfinement controls stiffness, strength and mechanical toughness of beta-sheet crystals in silk. *Nature Materials*, 9(4):359–367, 2010. ISSN 14764660. doi: 10.1038/nmat2704.

[8] Sinan Keten and Markus J. Buehler. Nanostructure and molecular mechanics of spider dragline silk protein assemblies. *Journal of the Royal Society Interface*, 7(53):1709–1721, dec 2010. ISSN 17425662. doi: 10.1098/rsif.2010.0149.

[9] Chris Cannam, Christian Landone, and Mark Sandler. Sonic visualiser: An open source application for viewing, analysing, and annotating music audio files. In *Proceedings of*

the 18th ACM international conference on Multimedia, pages 1467–1468. ACM, 2010. ISBN 1605589330.

[10] Xuan Mu, Yu Wang, Chengchen Guo, Yamin Li, Shengjie Ling, Wenwen Huang, Peggy Cebe, Huan-Hsuan Hsu, Fabio De Ferrari, Xiaocheng Jiang, Qiaobing Xu, Alessandra Balduini, Fiorenzo G. Omenetto, and David L. Kaplan. 3D Printing of Silk Protein Structures by Aqueous Solvent-Directed Molecular Assembly. *Macromolecular Bioscience*, page 1900191, aug 2019. ISSN 1616-5187. doi: 10.1002/mabi.201900191. URL `https://onlinelibrary.wiley.com/doi/abs/10.1002/mabi.201900191`.

[11] Isabelle Su and Markus J. Buehler. Nanomechanics of silk: The fundamentals of a strong, tough and versatile material. *Nanotechnology*, 27(30):302001, 2016. ISSN 13616528. doi: 10.1088/0957-4484/27/30/302001.

[12] Nicole L Garrison, Juanita Rodriguez, Ingi Agnarsson, Jonathan A Coddington, Charles E Griswold, Christopher A Hamilton, Marshal Hedin, Kevin M Kocot, Joel M Ledford, and Jason E Bond. Spider phylogenomics: untangling the Spider Tree of Life. *PeerJ*, 4:e1719, 2016.

[13] Charu Vepari and David L Kaplan. *Silk as a biomaterial*, volume 32. 2007. ISBN 0079-6700.

[14] S Arrhenius, H Granström, P Jäger, J Kastner, H.-U. Obrist, and T Saraceno. 14 Billions (working title). Skira Editore, Milano, 2011. ISBN 885720857.

[15] Jin Kim and Kanggeun Park. The Design Characteristics of Nature-inspired Buildings. *Civil Engineering and Architecture*, 6(2):88–107, 2018. doi: 10.13189/cea.2018.060206. URL `http://www.hrpub.org`.

[16] Yuqiang Jin, Haocheng Yuan, Jin Le Lan, Yunhua Yu, Yuan Hua Lin, and Xiaoping Yang. Bio-inspired spider-web-like membranes with a hierarchical structure for high performance lithium/sodium ion battery electrodes: The case of 3D freestanding and binder-free bismuth/CNF anodes. *Nanoscale*, 9(35):13298–13304, sep 2017. ISSN 20403372. doi: 10.1039/c7nr04912a.

[17] Fiorenzo G Omenetto and David L Kaplan. A new route for silk. *Nature Photonics*, 2(11):641–643, 2008. doi: 10.1038/nphoton.2008.207. URL `https://search.ebscohost.com/login.aspx?direct=true{&}db=a9h{&}AN=34995805{&}site=eds-live{&}scope=site`.

[18] Olena Tokareva, Matthew Jacobsen, Markus Buehler, Joyce Wong, and David L Kaplan. Structure–function–property–design interplay in biopolymers: Spider silk. *Acta biomaterialia*, 10(4):1612–1626, 2014.

[19] Markus J Buehler. Tu (r) ning weakness to strength. *Nano Today*, 5(5):379–383, 2010.

[20] Periklis Papadopoulos, Jan Sölter, and Friedrich Kremer. Hierarchies in the structural organization of spider silk—a quantitative model. *Colloid and Polymer Science*, 287 (2):231–236, 2009. ISSN 1435-1536. doi: 10.1007/s00396-008-1968-x. URL https://doi.org/10.1007/s00396-008-1968-x.

[21] Marine Wojcieszak, Aline Percot, Sylvie Noinville, Gwénaël Gouadec, Bernard Mauchamp, and Philippe Colomban. Origin of the variability of the mechanical properties of silk fibers: 4. Order/crystallinity along silkworm and spider fibers. *Journal of Raman Spectroscopy*, 45(10):895–902, 2014. doi: https://doi.org/10.1002/jrs.4579. URL https://onlinelibrary.wiley.com/doi/abs/10.1002/jrs.4579.

[22] Zhao Qin, Brett G Compton, Jennifer A Lewis, and Markus J Buehler. Structural optimization of 3D-printed synthetic spider webs for high strength. *Nature communications*, 6, 2015.

[23] Aaron M T Harmer, Todd A Blackledge, Joshua S Madin, and Marie E Herberstein. High-performance spider webs: integrating biomechanics, ecology and behaviour. *Journal of The Royal Society Interface*, 2010. doi: 10.1098/rsif.2010.0454.

[24] Todd A Blackledge, Jonathan A Coddington, and Rosemary G Gillespie. Are three-dimensional spider webs defensive adaptations? *Ecology Letters*, 6(1):13–18, 2003. doi: 10.1046/j.1461-0248.2003.00384.x. URL https://search.ebscohost.com/login.aspx?direct=true{&}db=egh{&}AN=8665328{&}site=eds-live{&}scope=site.

[25] Sean J Blamires, Chueh Hou, Lin-Fei Chen, Chen-Pan Liao, I Min Tso, J Blamires Sean, Hou Chueh, Chen Lin-Fei, Liao Chen-Pan, and I Min Tso. Three-dimensional barricading of a predatory trap reduces predation and enhances prey capture. *Behavioral Ecology and Sociobiology*, 67(5):709, 2013. doi: 10.1007/s00265-013-1493-x. URL https://search.ebscohost.com/login.aspx?direct=true{&}db=edsjsr{&}AN=edsjsr.23500376{&}site=eds-live{&}scope=sitehttps://link.springer.com/article/10.1007{%}2Fs00265-013-1493-xhttps://doi.org/10.1007/s00265-013-1493-x.

[26] Samuel Zschokke, Yann Hénaut, Suresh P. Benjamin, and J. Alvaro García-Ballinas. Prey-capture strategies in sympatric web-building spiders. *Canadian Journal of Zoology*, 84(7):964–973, jul 2006. ISSN 0008-4301. doi: 10.1139/z06-074. URL http://www.nrcresearchpress.com/doi/10.1139/z06-074.

[27] Todd A Blackledge and Jacquelyn M Zevenbergen. Condition-dependent spider web architecture in the western black widow, Latrodectus hesperus. *Animal Behaviour*, 73 (5):855–864, 2007. doi: http://dx.doi.org/10.1016/j.anbehav.2006.10.014. URL http://www.sciencedirect.com/science/article/pii/S0003347207000528.

[28] Todd A Blackledge, John E Swindeman, and Cheryl Y Hayashi. Quasistatic and continuous dynamic characterization of the mechanical properties of silk from the cobweb of the black widow spider Latrodectus hesperus. *Journal of Experimental Biology*, 208 (10):1937–1949, 2005.

[29] Cecilia Boutry and Todd A Blackledge. Biomechanical variation of silk links spinning plasticity to spider web function. *Zoology*, 112(6):451–460, 2009.

[30] Ingi Agnarsson, Cecilia Boutry, and Todd A Blackledge. Spider silk aging: initial improvement in a high performance material followed by slow degradation. *Journal of Experimental Zoology Part A: Ecological Genetics and Physiology*, 309(8):494–504, 2008.

[31] Ruth Madrigal-Brenes and Gilbert Barrantes. Construction and function of the web of Tidarren sisyphoides (Araneae: Theridiidae). *Journal of Arachnology*, 37(3):306–311, 2009. doi: 10.1636/Sh09-16.1. URL https://doi.org/10.1636/Sh09-16.1.

[32] UTCT University of Texas. Resolution and Size Limitations. URL http://www.ctlab.geo.utexas.edu/about-ct/resolution-and-size-limitations/.

[33] Jean-Paul Saint Martin, Simona Saint Martin, Susanne Bolte, and Didier Néraudeau. Spider web in Late Cretaceous French amber (Vendée): The contribution of 3D image microscopy. *Comptes Rendus Palevol*, 13(5):463–472, 2014. doi: http://dx.doi.org/10.1016/j.crpv.2014.03.005. URL http://www.sciencedirect.com/science/article/pii/S1631068314000554.

[34] Micro Photonics Inc. Micro-CT Center . URL https://www.microphotonics.com/products/micro-ct.

[35] C Wulff. Zu Hause bei der Schwarzen Witwe oder das letzte Projekt mit Rolf-Dieter Düppe. *Festschrift anlässlich der Pensionierung von Dr.-Ing. Rolf-Dieter Düppe nach 36 Jahren am Institut für Photogrammetrie und Kartographie; Schriftenreihe / Fachrichtung Geodäsie*, 30:8, 2010.

[36] T Luhmann. *Nahbereichsphotogrammetrie, Errata.* . Wichmann Verlag, Heidelberg, 2017. URL http://iapg.jade-hs.de/nbp/errata3.pdf.

[37] T Luhmann. *3D-Rekonstruktion von Spinnennetzen.* Wichmann Verlag, Heidelberg, 2010.

[38] T Saraceno and P Jäger. Unser Kosmos ist (fast) wie ein Spinnennetz. . *Natur Forschung Museum*, 142(5/6), 2012.

[39] Studio Tomás Saraceno. 3D Spider Web Scan. URL http://tomassaraceno.com/projects/3d-spider-web-scan/.

[40] Maria Yablonina. Portfolio, 2013. URL https://www.mariayablonina.com/spider-research-new.

[41] Eleanor R Tew, Alex Adamson, and Thomas Hesselberg. The web repair behaviour of an orb spider. *Animal Behaviour*, 103:137–146, 2015. doi: https://doi.org/10.1016/j.anbehav.2015.02.016. URL http://www.sciencedirect.com/science/article/pii/S0003347215000780.

[42] J.M. Gosline, P.A. Guerette, C.S. Ortlepp, and K.N. Savage. The mechanical design of spider silks: from fibroin sequence to mechanical function. *Journal of Experimental Biology*, 202(23), 1999.

[43] Gustavo V. Guinea, Manuel Elices, José Ignacio Real, Sara Gutiérrez, and José Pérez-Rigueiro. Reproducibility of the tensile properties of spider (Argiope trifasciata) silk obtained by forced silking. *Journal of Experimental Zoology Part A: Comparative Experimental Biology*, 303(1):37–44, jan 2005. ISSN 0022104X. doi: 10.1002/jez.a.111. URL http://www.ncbi.nlm.nih.gov/pubmed/15612009.

[44] Hui Yu, Jialing Yang, and Yuxin Sun. Energy absorption of spider orb webs during prey capture: A mechanical analysis. *Journal of Bionic Engineering*, 12(3):453–463, sep 2015. ISSN 1672-6529. doi: 10.1016/S1672-6529(14)60136-0. URL http://link.springer.com/10.1016/S1672-6529(14)60136-0.

[45] J Wesley Burgess. Social Spiders. *Scientific American*, 234(3):100–107, 1976. ISSN 00368733, 19467087. URL http://www.jstor.org/stable/24950309.

[46] George W. Uetz. The "ricochet effect" and prey capture in colonial spiders. *Oecologia*, 81(2):154–159, oct 1989. ISSN 00298549. doi: 10.1007/BF00379799.

[47] Ann L. Rypstra. Building a better insect trap; An experimental investigation of prey capture in a variety of spider webs. *Oecologia*, 52(1):31–36, jan 1982. ISSN 00298549. doi: 10.1007/BF00349008. URL http://link.springer.com/10.1007/BF00349008.

[48] Ann L. Rypstra. Foraging flocks of spiders - A study of aggregate behavior in Cyrtophora citricola Forskål (Araneae; Araneidae) in West Africa. *Behavioral Ecology and Sociobiology*, 5(3):291–300, sep 1979. ISSN 03405443. doi: 10.1007/BF00293677.

[49] B Mortimer, A Soler, C R Siviour, R Zaera, and F Vollrath. Tuning the instrument: sonic properties in the spider's web. *Journal of The Royal Society Interface*, 13(122), 2016. doi: 10.1098/rsif.2016.0341. URL http://rsif.royalsocietypublishing.org/content/royinterface/13/122/20160341.full.pdf.

[50] B. Mortimer, A. Soler, L. Wilkins, and F. Vollrath. Decoding the locational information in the orb web vibrations of Araneus diadematus and Zygiella x-notata. *Journal of The Royal Society Interface*, 16(154): 20190201, may 2019. ISSN 1742-5689. doi: 10.1098/rsif.2019.0201. URL https://royalsocietypublishing.org/doi/10.1098/rsif.2019.0201.

[51] B Mortimer, A Soler, C R Siviour, and F Vollrath. Remote monitoring of vibrational information in spider webs. *The Science of Nature*, 105(5):37, 2018. doi: 10.1007/s00114-018-1561-1. URL https://doi.org/10.1007/s00114-018-1561-1.

[52] M A Landolfa and F G Barth. Vibrations in the orb web of the spider Nephila clavipes: cues for discrimination and orientation. *Journal of Comparative Physiology A*, 179(4):493–508, 1996. doi: 10.1007/bf00192316. URL https://doi.org/10.1007/BF00192316.

[53] Isabelle Su, Gang Seob Jung, Neosha Narayanan, and Markus J Buehler. Perspectives on three-dimensional printing of self-assembling materials and structures. *Current Opinion in Biomedical Engineering*, 15:59–67, 2020. ISSN 2468-4511. doi: https://doi.org/10.1016/j.cobme.2020.01.003. URL http://www.sciencedirect.com/science/article/pii/S2468451120300040.

[54] M Jörger Katharina and G Eberhard William. Web Construction and Modification by Achaearanea tesselata (Araneae, Theridiidae). *The Journal of Arachnology*, 34(3): 511, 2006. URL https://search.ebscohost.com/login.aspx?direct=true{&}db=edsjsr{&}AN=edsjsr.4149964{&}site=eds-live{&}scope=site.

[55] Suresh P Benjamin and Samuel Zschokke. Untangling the tangle-web: web construction behavior of the comb-footed spider Steatoda triangulosa and comments on phylogenetic implications (Araneae: Theridiidae). *Journal of Insect Behavior*, 15(6):791–809, 2002.

[56] Jose Carrasco Hortal, Salvador Serrano Salazar, and Francesc Morales Menárguez. Sequences, Tracks and Footprints: Graphic Lessons Gathered from Swarm and Spider Web Robotics. pages 633–643. Springer, Cham, jun 2020. doi: 10.1007/978-3-030-47983-1_56.

[57] Thomas Hermann. Taxonomy and definitions for sonification and auditory display. In *Proceedings of the 14th International Conference on Auditory Display (ICAD 2008)*, 2008.

[58] Thomas Hermann, Andy Hunt, and John G Neuhoff. *The sonification handbook*. Logos Verlag Berlin, 2011. ISBN 3832528199.

[59] Gregory Kramer, Bruce Walker, Terri Bonebright, Perry Cook, John H. Flowers, Nadine Miner, and John Neuhoff. Sonification Report: Status of the Field and Research Agenda. *University of Nebraska - Lincoln University of Nebraska - Lincoln*, 444, 2010. URL https://digitalcommons.unl.edu/psychfacpubhttps://digitalcommons.unl.edu/psychfacpub/444.

[60] Tristan Giesa, David Spivak, and Markus Buehler. Reoccurring Patterns in Hierarchical Protein Materials and Music: The Power of Analogies. *BioNanoScience*, 1(4): 153, 2011. URL https://search.ebscohost.com/login.aspx?direct=true{&}db=edo{&}AN=ejs26047057{&}site=eds-live{&}scope=site.

[61] Joyce Y Wong, John McDonald, Micki Taylor-Pinney, David I Spivak, David L Kaplan, and Markus J Buehler. Materials by design: Merging proteins and music. *Nano Today*, 7(6):488–495, 2012. doi: https://doi.org/10.1016/j.nantod.2012.09.001. URL http://www.sciencedirect.com/science/article/pii/S1748013212001041.

[62] Martin Rohrmeier. Towards a generative syntax of tonal harmony. *Journal of Mathematics and Music*, 5(1):35–53, mar 2011. ISSN 1745-9737. doi: 10.1080/17459737.2011.573676. URL http://www.tandfonline.com/doi/abs/10.1080/17459737.2011.573676.

[63] Peggy S M Hill and Andreas Wessel. Biotremology. *Current Biology*, 26(5):R187–R191, 2016.

[64] Beth Mortimer. Biotremology: Do physical constraints limit the propagation of vibrational information? *Animal Behaviour*, 130:165–174, 2017. doi: https://doi.org/10.1016/j.anbehav.2017.06.015. URL http://www.sciencedirect.com/science/article/pii/S0003347217301902.

[65] B Mortimer, S Gordon, D Drodge, C R Siviour, J Windmill, C Holland, and F Vollrath. Sonic properties of silks. *XIV International Conference on Invertebrate Sound and Vibration - ISV 2013*, page 43, 2013.

[66] Ute Meta Bauer and Anca Rujoiu. Tomás Saraceno: Arachnid Orchestra. Jam Sessions, 2017.

[67] P Papachristodoulou, A Betella, and PFMJ Verschure. Sonification of Large Datasets in a 3D Immersive Environment: A Neuroscience Case Study. In *ACHI2014: The Seventh International Conference on Advances in Computer-Human Interactions*, pages 35–40, 2014.

[68] World Spider Catalog. World Spider Catalog (2020), 2020.

[69] Leslie Brunetta and Catherine Lee Craig. *Spider silk : evolution and 400 million years of spinning, waiting, snagging, and mating.* New Haven, Conn. ; London : Yale University Press, 2012., 2012. ISBN 9780300181463 0300181469. URL https://search.ebscohost.com/login.aspx?direct=true{&}db=cat00916a{&}AN=mit.002123003{&}site=eds-live{&}scope=site.

[70] Todd A Blackledge, Nikolaj Scharff, Jonathan A Coddington, Tamas Szüts, John W Wenzel, Cheryl Y Hayashi, Ingi Agnarsson, and Thomas W Schoener. Reconstructing Web Evolution and Spider Diversification in the Molecular Era. *Proceedings of the National Academy of Sciences of the United States of America*, (13):5229, 2009. doi: 10.1073/pnas.0901377106. URL https://search.ebscohost.com/login.aspx?direct=true{&}db=edsjsr{&}AN=edsjsr.40455178{&}site=eds-live{&}scope=site.

[71] Sasha Engelmann. Social spiders and hybrid webs at Studio Tomás Saraceno. *cultural geographies*, 24(1):161–169, 2016. doi: 10.1177/1474474016647371. URL https://doi.org/10.1177/1474474016647371.

[72] McMaster-Carr. URL https://www.mcmaster.com/.

[73] Bugs In Cyberspace. URL http://www.bugsincyberspace.com/.

[74] Samuel Zschokke and Marie E Herberstein. Laboratory methods for maintaining and studying web-building spiders. *Journal of Arachnology*, 33(2):205–213, 2005.

[75] Mach3. URL http://www.machsupport.com/software/mach3/.

[76] Michael Kerschnitzki, Philip Kollmannsberger, Manfred Burghammer, Georg N Duda, Richard Weinkamer, Wolfgang Wagermaier, and Peter Fratzl. Architecture of the osteocyte network correlates with bone material quality. *Journal of bone and mineral research*, 28(8):1837–1845, 2013. URL http://onlinelibrary.wiley.com/store/10.1002/jbmr.1927/asset/jbmr1927.pdf?v=1{&}t=j935rud8{&}s=876c6c659684effaf001e74abb9f0c4eafeded80.

[77] MATLAB. *9.6.0.1099231 (R2019a)*. The MathWorks Inc., Natick, Massachusetts, 2019.

[78] Fritz Vollrath, Mike Downes, and Sven Krackow. Design Variability in Web Geometry of an Orb-Weaving Spider. *Physiology & Behavior*, 62(4):735–743, 1997. doi: https://doi.org/10.1016/S0031-9384(97)00186-8. URL http://www.sciencedirect.com/science/article/pii/S0031938497001868.

[79] Hans M Peters. Functional organization of the spinning apparatus of Cyrtophora citricola with regard to the evolution of the web (Araneae, Araneidae). *Zoomorphology*, 113(3):153–163, 1993. doi: 10.1007/BF00394856. URL https://doi.org/10.1007/BF00394856.

[80] Markus Heim, David Keerl, and Thomas Scheibel. Spider Silk: From Soluble Protein to Extraordinary Fiber. *Angewandte Chemie International Edition*, 48(20):3584–3596, 2009. doi: 10.1002/anie.200803341. URL http://dx.doi.org/10.1002/anie.200803341.

[81] Albert-László Barabási. Scale-Free Networks: A Decade and Beyond. *Science*, 325(5939):412–413, 2009. doi: 10.1126/science.1173299. URL http://science.sciencemag.org/content/sci/325/5939/412.full.pdf.

[82] B Y ALBERT-LÁSZLÓ Barabási and Eric Bonabeau. Scale-free. *Scientific American*, 288(5):50–59, 2003.

[83] T Saraceno, C Wulff, D Steineck, P Jäger, and S Zschokke. Spider webs in science, art and space - an interdisciplinary project on 3D-visualisation, 2010.

[84] Jacquelyn M Zevenbergen, Nicole K Schneider, and Todd A Blackledge. Fine dining or fortress? Functional shifts in spider web architecture by the western black widow Latrodectus hesperus. *Animal Behaviour*, 76(3):823–829, 2008. doi: http://dx.doi.org/10.1016/j.anbehav.2008.05.008. URL http://www.sciencedirect.com/science/article/pii/S0003347208002182.

[85] Matjaž Kuntner and Ingi Agnarsson. Web gigantism in Darwin's bark spider, a new species from Madagascar (Araneidae: Caerostris). *Journal of Arachnology*, 38(2):346–356, 2010. doi: 10.1636/B09-113.1. URL https://doi.org/10.1636/B09-113.1.

[86] Suresh P Benjamin and Samuel Zschokke. Webs of theridiid spiders: construction, structure and evolution. *Biological Journal of the Linnean Society*, 78(3):293–305, 2003.

[87] T A Blackledge, M Kuntner, and I Agnarsson. The form and function of spider orb webs: evolution from silk to ecosystems. *Advances in Insect Physiology*, 41:175–262, 2011. URL https://search.ebscohost.com/login.aspx?direct=true{&}db=lah{&}AN=20123221181{&}site=eds-live{&}scope=sitehttp://www.sciencedirect.com/science/article/pii/B9780124159198000045.

[88] Silvio A Bedini. Along Came a Spider—Spinning Silk For Cross-Hairs. *The American Surveyor*, (March/April 2005):7, 2005.

[89] Anthoula Lazaris, Steven Arcidiacono, Yue Huang, Jiang-Feng Zhou, François Duguay, Nathalie Chretien, Elizabeth A Welsh, Jason W Soares, and Costas N Karatzas. Spider Silk Fibers Spun from Soluble Recombinant Silk Produced in Mammalian Cells. *Science*, 295(5554):472–476, 2002. doi: 10.1126/science.1065780.

[90] Bogdan Andrei Demian. Structural and mechanical analysis of the black widow spider web subjected to stretching, expansion and wind, 2014.

[91] GB Edwards. Cyrtophora Citricola (Araneae: Araneidae): A Colonial Tentweb Orbweaver Established in Florida. 2006.

[92] Carmen Viera and Marcelo O Gonzaga. *Behaviour and Ecology of Spiders: Contributions from the Neotropical Region*. Springer, 2017. ISBN 3319657178.

[93] Steve Plimpton. Fast Parallel Algorithms for Short-Range Molecular Dynamics. *Journal of Computational Physics*, 117(1):1–19, 1995. ISSN 0021-9991. doi: https://doi.org/10.1006/jcph.1995.1039. URL http://www.sciencedirect.com/science/article/pii/S002199918571039Xhttp://lammps.sandia.gov.

[94] Lin Römer and Thomas Scheibel. The elaborate structure of spider silk: structure and function of a natural high performance fiber., 2008. ISSN 1933690X.

[95] Zhao Qin and Markus J Buehler. Impact tolerance in mussel thread networks by heterogeneous material distribution. *Nature communications*, 4:2187, 2013. doi: 10.1038/ncomms3187https://www.nature.com/articles/ncomms3187#supplementary-information. URL https://doi.org/10.1038/ncomms3187.

[96] Todd A. Blackledge, Richard A. Cardullo, and Cheryl Y. Hayashi. Polarized light microscopy, variability in spider silk diameters, and the mechanical characterization of spider silk. *Invertebrate Biology*, 124(2):165–173, jun 2005. ISSN 10778306. doi: 10.1111/j.1744-7410.2005.00016.x. URL http://doi.wiley.com/10.1111/j.1744-7410.2005.00016.x.

[97] Kristie J Koski, Paul Akhenblit, Keri McKiernan, and Jeffery L Yarger. Non-invasive determination of the complete elastic moduli of spider silks. *Nature Materials*, 12(3):262–267, 2013. ISSN 1476-4660. doi: 10.1038/nmat3549. URL https://doi.org/10.1038/nmat3549.

[98] Alexander Stukowski. Visualization and analysis of atomistic simulation data with OVITO-the Open Visualization Tool. *MODELLING AND SIMULATION IN MATERIALS SCIENCE AND ENGINEERING*, 18(1), jan 2010. ISSN 0965-0393. doi: 10.1088/0965-0393/18/1/015012.

[99] S R Ganihar. Biomass estimates of terrestrial arthropods based on body length. *Journal of biosciences*, 22(2):219–224, 1997. doi: 10.1007/BF02704734. URL `https://doi.org/10.1007/BF02704734`.

[100] T J Dean. Fastest flyer. *Book of insect records*, 2003.

[101] Todd A. Blackledge and Jacquelyn M. Zevenbergen. Mesh Width Influences Prey Retention in Spider Orb Webs. *Ethology*, 112(12):1194–1201, dec 2006. ISSN 0179-1613. doi: 10.1111/j.1439-0310.2006.01277.x. URL `http://doi.wiley.com/10.1111/j.1439-0310.2006.01277.x`.

[102] Margarita Ramos, Duncan J. Irschick, and Terry E. Christenson. Overcoming an evolutionary conflict: Removal of a reproductive organ greatly increases locomotor performance. *Proceedings of the National Academy of Sciences of the United States of America*, 101(14):4883–4887, apr 2004. ISSN 00278424. doi: 10.1073/pnas.0400324101.

[103] Philip Kollmannsberger, Michael Kerschnitzki, Felix Repp, Wolfgang Wagermaier, Richard Weinkamer, and Peter Fratzl. The small world of osteocytes: Connectomics of the lacuno-canalicular network in bone. *New Journal of Physics*, 19(7):073019, jul 2017. ISSN 13672630. doi: 10.1088/1367-2630/aa764b.

[104] Hank Guarisco. Three cobweb spider genera (Anelosimus, Tidarren, and Thymoites) and Argyrodes fictilium (Araneae:Theridiidae) recently discovered in Kansas. *Journal of the Kansas Entomological Society*, 73(3):155–163, 2000. ISSN 0022-8567. doi: 10.2307/25085960.

[105] William G Eberhard, Ingi Agnarsson, and Herbert W Levi. Web forms and the phylogeny of theridiid spiders (Araneae: Theridiidae): chaos from order. *Systematics and Biodiversity*, 6(4):415, 2008. doi: http://dx.doi.org/10.1017/S1477200008002855. URL `https://search.proquest.com/docview/221943811?accountid=12492https://sfx.mit.edu/sfx{_}local?url{_}ver=Z39.88-2004{&}rft{_}val{_}fmt=info:ofi/fmt:kev:mtx:journal{&}genre=article{&}sid=ProQ:ProQ{%}253Aagricenvironm{&}atitle=Web+forms+and+the+phylogeny+of+theridiid+spiders+`.

[106] Albert-László Barabási and Others. *Network science*. Cambridge university press, 2016.

[107] Isabelle Su and Markus J. Buehler. Mesomechanics of a Three-Dimensional Spider Web. *Journal of the Mechanics and Physics of Solids*, 144:104096, jul 2020. ISSN 00225096. doi: 10.1016/j.jmps.2020.104096.

[108] G Tzanetakis and P Cook. Musical genre classification of audio signals. *IEEE Transactions on Speech and Audio Processing*, 10(5):293–302, 2002. doi: 10.1109/TSA.2002.800560.

[109] Edward Givelberg and Julian Bunn. A comprehensive three-dimensional model of the cochlea. *Journal of Computational Physics*, 191(2):377–391, 2003.

[110] Stratos Idreos, Olga Papaemmanouil, and Surajit Chaudhuri. Overview of Data Exploration Techniques, 2015.

[111] Chi Hua Yu, Zhao Qin, Francisco Martin-Martinez, and Markus J Buehler. A self-consistent sonification method to translate amino acid sequences into musical compositions and application in protein design using AI. *ACS Nano*, 13(7):7471–7482, 2019.

[112] Isabelle Su, Zhao Qin, Ally Bisshop, Roland Mühlethaler, Tomás Saraceno, Evan Ziporyn, and Markus J Buehler. Sonification of a 3D Spider Web and Reconstitution into Musical Composition using Granular Synthesis. *Computer Music Journal*, .

[113] Myounghoon Jeon, Michael T Smith, James W Walker, and Scott A Kuhl. Constructing the Immersive Interactive Sonification Platform (iISoP). In Norbert Streitz and Panos Markopoulos, editors, *Distributed, Ambient, and Pervasive Interactions*, pages 337–348, Cham, 2014. Springer International Publishing. ISBN 978-3-319-07788-8.

[114] Till Bovermann, Thomas Hermann, and Helge Ritter. Tangible data scanning sonification model. Georgia Institute of Technology, 2006.

[115] Natasha Barrett. Interactive Spatial Sonification of Multidimensional Data for Composition and Auditory Display. *Computer Music Journal*, 40(2):47–69, 2016. doi: 10.1162/COMJ_a_00358. URL `https://www.mitpressjournals.org/doi/abs/10.1162/COMJ{_}a{_}00358`.

[116] Grace X Gu, Isabelle Su, Shruti Sharma, Jamie L Voros, Zhao Qin, and Markus J Buehler. Three-dimensional-printing of bio-inspired composites. *Journal of biomechanical engineering*, 138(2):21006, 2016.

[117] Isabelle Su and Markus J Buehler. Spider silk: Dynamic mechanics. *Nature materials*, 15(10):1054–1055, 2016. doi: 10.1038/nmat4721. URL `http://dx.doi.org/10.1038/nmat4721`.

[118] Tomás Saraceno, Ally Bisshop, Adrian Krell, and Roland Mühlethaler. Arachnid Orchestras: Artistic Research in Vibrational Interspecies Communication. In *Biotremology: Studying Vibrational Behavior*, pages 485–509. Springer, 2019.

[119] Thomas D Rossing and Andrew Morrison. *The science of string instruments*. Springer, 2010. ISBN 1441971092.

[120] William Ralph Bennett and Christy K Holland. *The Science of Musical Sound*. Springer, 2018. ISBN 3319927949.

[121] Isabelle Su, Ian Hattwick, Christine Southworth, Evan Ziporyn, Ally Bisshop, Roland Mühlethaler, Tomás Saraceno, and Markus J. Buehler. Interactive exploration of a hierarchical spider web structure with sound. *Journal on Multimodal User Interfaces*, .

[122] PerMagnus Lindborg. Interactive Sonification of Weather Data for The Locust Wrath, a Multimedia Dance Performance. *Leonardo*, 51(5):466–474, 2018.

[123] Zhao Haixia, B K Smith, K Norman, C Plaisant, and B Shneiderman. Interactive sonification of choropleth maps. *IEEE MultiMedia*, 12(2):26–35, 2005. doi: 10.1109/MMUL.2005.28.

[124] D Y N Zotkin, J Hwang, R Duraiswaini, and L S Davis. HRTF personalization using anthropometric measurements. In *2003 IEEE Workshop on Applications of Signal Processing to Audio and Acoustics (IEEE Cat. No.03TH8684)*, pages 157–160, 2003. doi: 10.1109/ASPAA.2003.1285855.

[125] Eric L. Buehler, Isabelle Su, and Markus J. Buehler. WebNet: A biomateriomic three-dimensional spider web neural net. *Extreme Mechanics Letters*, 42:101034, jan 2021. ISSN 23524316. doi: 10.1016/j.eml.2020.101034.

[126] Tuan D. Ngo, Alireza Kashani, Gabriele Imbalzano, Kate T.Q. Nguyen, and David Hui. Additive manufacturing (3D printing): A review of materials, methods, applications and challenges. *Composites Part B: Engineering*, 143:172–196, jun 2018. ISSN 1359-8368. doi: 10.1016/J.COMPOSITESB.2018.02.012. URL `https://www.sciencedirect.com/science/article/pii/S1359836817342944`.

[127] Yijiang Huang, Caelan R. Garrett, and Caitlin T. Mueller. Automated sequence and motion planning for robotic spatial extrusion of 3D trusses. *Construction Robotics*, 2 (1-4):15–39, dec 2018. ISSN 2509-811X. doi: 10.1007/s41693-018-0012-z. URL `http://link.springer.com/10.1007/s41693-018-0012-z`.

[128] Graham Hunt, Faidon Mitzalis, Talib Alhinai, Paul A Hooper, and Mirko Kovac. 3D printing with flying robots. In *2014 IEEE International Conference on Robotics and Automation (ICRA)*, pages 4493–4499. IEEE, may 2014. ISBN 978-1-4799-3685-4. doi: 10.1109/ICRA.2014.6907515. URL `http://ieeexplore.ieee.org/document/6907515/`.

[129] Hasan Sinan Bank. A software framework for an agile manufacturing system. 2015. doi: https://doi.org/doi:10.7282/T3C24ZC7.

[130] Peter Jeffrey. Watch These Spiderbots Train to Build a City on the Moon - Bloomberg, 2016. URL `https://www.bloomberg.com/news/articles/2016-11-25/watch-these-spiderbots-train-to-build-a-city-on-the-moon`.

[131] ICD/ITKE Research Pavilion 2016-17 | Institute for Computational Design and Construction. URL `https://icd.uni-stuttgart.de/?p=18905`.

[132] Ammar Mirjan, Federico Augugliaro, Raffaello D'Andrea, Fabio Gramazio, and Matthias Kohler. Building a Bridge with Flying Robots. In *Robotic Fabrication in Architecture, Art and Design 2016*, pages 34–47. Springer International Publishing, Cham, 2016. doi: 10.1007/978-3-319-26378-6_3. URL http://link.springer.com/10.1007/978-3-319-26378-6{_}3.

[133] MARIA YABLONINA, MARSHALL PRADO, EHSAN BAHARLOU, TOBIAS SCHWINN, and ACHIM MENGES. MOBILE ROBOTIC FABRICATION SYSTEM FOR FILAMENT STRUCTURES. In *Fabricate 2017*, pages 202–209. UCL Press, apr 2017. doi: 10.2307/j.ctt1n7qkg7.32. URL http://www.jstor.org/stable/10.2307/j.ctt1n7qkg7.32.

[134] James Long and Oral Büyüköztürk. Decentralised one-class kernel classification-based damage detection and localisation. *Structural Control and Health Monitoring*, 24(6): e1930, jun 2017. ISSN 15452255. doi: 10.1002/stc.1930. URL http://doi.wiley.com/10.1002/stc.1930.

[135] Mostafa Mirshekari, Shijia Pan, Jonathon Fagert, Eve M. Schooler, Pei Zhang, and Hae Young Noh. Occupant localization using footstep-induced structural vibration. *Mechanical Systems and Signal Processing*, 112:77–97, nov 2018. ISSN 0888-3270. doi: 10.1016/J.YMSSP.2018.04.026. URL https://www-sciencedirect-com.libproxy.mit.edu/science/article/pii/S0888327018302280?